NOVEL TECHNIQUES IN HYPERSPECTRAL DATA ANALYSIS FOR ENDMEMBER EXTRACTION, CHANGE DETECTION AND CLASSIFICATION

Thesis

Submitted in Partial Fulfilment of the Requirements for the Degree of

DOCTOR OF PHILOSOPHY

by

PALLA PARASURAM YADAV

Under the Guidance of

Dr. A. V. NARASIMHADHAN
Dr. B. S. RAGHAVENDRA
Dr. AMBA SHETTY

Department of Electronics and Communication Engineering
NATIONAL INSTITUTE OF TECHNOLOGY KARNATAKA
SURATHKAL, MANGALORE - 575 025
January, 2024

NATIONAL INSTITUTE OF TECHNOLOGY KARNATAKA, SURATHKAL

DECLARATION

I hereby *declare* that the Research Thesis entitled **"Novel Techniques in Hyperspectral Data Analysis for Endmember Extraction, Change Detection and Classification"** which is being submitted to the ***National Institute of Technology Karnataka, Surathkal*** in partial fulfilment of the requirements for the award of the Degree of ***Doctor of Philosophy*** in ***Electronics and Communication Engineering***, is a *bonafide report of the research work carried out by me*. The material contained in this Research Thesis has not been submitted to any University or Institution for the award of any degree.

P. Parasuram Yadav.

PALLA PARASURAM YADAV
Register No.: 165014/EC16F07
Electronics & Communication Engineering
National Institute of Technology Karnataka
Surathkal, Mangalore - 575025

Place: NITK, Surathkal
Date: 31-01-2024

NATIONAL INSTITUTE OF TECHNOLOGY KARNATAKA, SURATHKAL

CERTIFICATE

This is to *certify* that the Research Thesis entitled "**Novel Techniques in Hyperspectral Data Analysis for Endmember Extraction, Change Detection and Classification**" Submitted by **Mr. PALLA PARASURAM YADAV** (Register Number: **165014/EC16F07**) as the record of the Research work carried out by him, is *accepted* as the *Research Thesis submission* in partial fulfillment of the requirements for the award of degree of ***Doctor of Philosophy***.

Dr. A. V. Narasimhadhan	**Dr. B. S. Raghavendra**	**Dr. Amba Shetty**
Research Guide	Research Guide	Research Guide
Associate Professor	Associate Professor	Professor
Dept. of E&C	Dept. of E&C	Dept. of WROE
NITK Surathkal - 575025	NITK Surathkal - 575025	NITK Surathkal - 575025

06/2/24

Chairperson - DRPC

Dept. of E&C

NITK Surathkal

(Signature with Date and Seal)

प्राध्यापक एवं विभागाध्यक्ष/PROF & HEAD
इ. एवं सी. विभाग / Department of E & C
एन.आई.टी.के. सुरत्कल/NITK Surathkal
मंगलूर / MANGALURU - 575 025

Statements of Contribution

1. This thesis is based on the following published articles.

   - Palla, P.Y., Shetty, A., Raghavendra, B.S. and Narasimhadhan, A.V., 2020. Subtractive clustering and phase correlation similarity measure for endmember extraction. Infrared Physics Technology, 110, p.103452. https://doi.org/10.1016/j.infrared.2020.103452
   - Yadav, Palla Parasuram, Amba Shetty, B. S. Raghavendra, and A. V. Narasimhadhan. "Similarity measures in generating spectrally distinct targets." In 2020 IEEE India Geoscience and Remote Sensing Symposium (InGARSS), pp. 221-224. IEEE, 2020. https://doi.org/10.1109/InGARSS48198.2020.9358963
   - Yadav, Palla Parasuram, Amba Shetty, B. S. Raghavendra, and A. V. Narasimhadhan. "Influence of the Darkest Pixel on Endmembers Initialization." In 2021 IEEE International Geoscience and Remote Sensing Symposium IGARSS, pp. 3845-3848. IEEE, 2021. https://doi.org/10.1109/IGARSS47720.2021.9553178
   - Yadav, Palla Parasuram, Amba Shetty, B. S. Raghavendra, and A. V. Narasimhadhan. "Effectiveness of phase correlation spectral similarity measure in distinguishing target signatures for hyperspectral data analysis." In 2020 IEEE 17th India Council International Conference (INDICON), pp. 1-5. IEEE, 2020. https://doi.org/10.1109/INDICON49873.2020.9342448
   - Yadav, Palla Parasuram, Amba Shetty, B. S. Raghavendra, and A. V. Narasimhadhan. "Gradient Based Spectral Similarity Measure for Hyperspectral Image Analysis." In 2021 IEEE International India Geoscience and Remote Sensing Symposium (InGARSS), pp. 242-245. IEEE, 2021. https://doi.org/10.1109/IGARSS46834.2022.9884485
   - Yadav, Palla Parasuram, Amba Shetty, B. S. Raghavendra, and A. V. Narasimhadhan. "Gradient Correlation Incorporated Similarity Measures in Matching Spectral Signatures." In IGARSS 2022-2022 IEEE International Geoscience and Remote Sensing Symposium, pp. 3199-3202. IEEE, 2022. https://doi.org/10.1109/IGARSS46834.2022.9884485

- Yadav, Palla Parasuram, Nikhil Bobate, Amba Shetty, B. S. Raghavendra, and A. V. Narasimhadhan. ”ATGP based Change Detection in Hyperspectral Images.” In IECON 2022–48th Annual Conference of the IEEE Industrial Electronics Society, pp. 1-6. IEEE, 2022. https://doi.org/10.1109/IECON49645.2022.9969049
- Yadav, Palla Parasuram, Amba Shetty, B. S. Raghavendra, and A. V. Narasimhadhan. ”Virtual Sample Generation Of Hyperspectral Mineral Data.” In 2023 International Conference on Machine Intelligence for GeoAnalytics and Remote Sensing (MIGARS), vol. 1, pp. 1-4. IEEE, 2023. https://doi.org/10.1109/MIGARS57353.2023.10064561

2. The publications that are not included in the thesis are listed at the end of the thesis under the section titled ‘publications’.

ABSTRACT

Hyperspectral image (HSI) analysis is a powerful technique in remote sensing that involves the acquisition and analysis of images captured across hundreds or even thousands of narrow and contiguous spectral bands. Unlike traditional remote sensing techniques that capture information in just a few broadbands, HSI provides detailed spectral information for each pixel in an image scene. This wealth of spectral data enables a more comprehensive understanding of the Earth's surface and the objects it contains. By analyzing the unique spectral signatures of different materials, HSI enables the identification and discrimination of various land cover types, vegetation species, soil properties, and even specific minerals. However, the analysis of hyperspectral data presents several challenges that require specialized approaches.

Endmember extraction (EE) is one such challenge, involving the identification of pure spectral signatures or reference spectra that represent specific target materials. Spectral matching is a vital component of HSI analysis that involves measuring the degree of closeness between the spectral signatures extracted from the image and those obtained through ground-based spectrometer measurements or known reference spectra. Spectral matching algorithms are useful not only for validating the accuracy of image-based signatures but also for feature extraction. This matching process helps in the identification, analysis, and interpretation of different materials or targets present in the HSI.

Through the combination of endmember extraction and spectral matching in HSI, diverse applications in geology and related fields are empowered, enabling tasks such as geological mapping, mineral exploration, environmental monitoring, and land cover analysis with increased accuracy and efficiency. Although hyperspectral imaging was originally developed for mining and geology, mineral identification using hyperspectral data has not been addressed adequately yet and remains a challenging task. HSIs due to advancements in spatial-spectral resolutions and the availability of multi-temporal information are in demand for many applications. Change detection (CD), in particular, is an important and challenging problem in monitoring changes such as deforestation, urban development, and landslides using time series HSI data.

Though several endmember extraction algorithms (EEAs) are developed, spectral matching algorithms (SMAs) have not been explored much in the extraction of spectrally distinct

signatures. Therefore, in this work, similarity measures based EEAs (SM-EEAs) are proposed to explore the fundamental characteristic, i.e. spectrally distinctive in nature, of endmembers. Experimental results on proposed EEAs i.e., a similarity measures-based subtractive clustering algorithm (SM-SCA) and a similarity measures-based endmember initialization algorithm (SM-EIA) showed the applicability of SMAs in extracting spectrally distinct signatures as the endmembers and also hinted the importance of endmember initialization. The darkest pixel identified as a target pixel of interest (TPOI) in the further investigation on endmember initialization strategies emerges not only as a potential TPOI but also contributes to improving the performance of EEAs when combined with the brightest pixel as TPOIs. Experiments carried out on an improved SM-EIA to test its applicability in extracting pure endmembers present maximin-distance algorithm (MDA) do not able to identify vertices of the simplex with simple metrics like Euclidean distance (ED) and other simple SMAS but with higher dimensionality metrics like volume. The proposed corner-driven iterative clustering algorithm (CDIC) appears to perform better in EE by identifying the corner pixels and thereby providing training samples for HSI classification.

Though few already developed spectral matching measures are available, the identification of diagnostic features of spectrally distinct signatures with the existing SMAs to discriminate them effectively is still a challenging task. Therefore, this work presents a gradient-based spectral similarity measure (GSSM) that captures the diagnostic (absorption) features to measure the degree of closeness between spectral signatures. The effectiveness of the proposed GSSM in distinguishing spectrally distinct signatures is studied with that of other spectral matching algorithms in (i) discriminating endmember signatures (ii) mixed pixel identification (iii) clustering spectral signatures of different classes and (iv) endmember extraction. The proposed GSSM was not only able to highlight diagnostic features of target signatures but also showed its effectiveness in discriminating spectrally distinct target signatures better than other SMAs. Further study on gradient correlation (GC) incorporated showed improved discrimination power with geometrical SMAs. Further, a meaningful way of measuring RSDPW is proposed. Reformulated RSDPW appears to be more meaningful in discriminating endmembers and obtaining the range of RSDPW values for different levels of discrimination than the former one.

The high dimensionality of HSI data and limited availability of hyperspectral CD data sets with ground-truth change map make CD not so easy but a difficult task. Though there

are many classical and deep learning (DL) based algorithms to detect changes, either their performance is not so better or the final performance depends on efficiency of pre-detection algorithms. In addition, there is not much comprehensive study on developing CD algorithms that not only simple to use but also as efficient as that of DL based algorithms is available. Therefore, an endmember related feature extraction is proposed for HSI-CD. Proposed ATGP based CD algorithms not only perform better than classical CD algorithms but also able to reach the performance of DL based CD algorithms. additionally, even a minimum number of features around three to five (3-5) also good enough to get high accuracy as that of DL models.

Mineral identification remains a challenging task due to the subtle differences among the spectral signatures of minerals and insufficient ground truth. The classical spectral angle measure (SAM) classifier is a simple model and does not yield high accuracy and an expert system for hyperspectral data classification (ExHype) is a binary classifier and therefore complex to train binary classifier modules equal to the number of minerals to be classified and obtain thresholds to gain accuracy. Due to lack of training samples and sufficient data with ground truth to be tested, DL models have not been explored much in mineral classification so far. To overcome this, a virtual sample generation to be able to generate more training samples that provide a chance to explore DL models that need variations in training samples in mineral classification is proposed. Further, a one-dimensional convolutional neural network (1-D CNN) model, trained on training samples generated by virtual sample generation, designed to classify minerals performed well in classifying the tested mineral classes with high accuracy.

Keywords: Endmember extraction, endmember initialization, target pixels of interest, spectral matching algorithms, relative spectral discrimination power, change detection, and mineral classification.

ACKNOWLEDGEMENT

I extend my heartfelt gratitude to my parents; my father Sri Palla Ramamurthy for his unwavering support and encouragement, especially in pursuing higher studies, and my mother Srimati Palla Rukminamma for her boundless care and affection. I express special gratitude to my brother Mr. Palla Arjunudu for his unwavering well-wishing, care, and continuous support. I am thankful to my maternal uncle Bathula Venkateswarlu and grandmother Bathula Kondamma for being a steady presence throughout this journey, offering care and support. Appreciation goes out to all my sisters and aunts for their affectionate care. I also acknowledge the support and encouragement from my brothers and uncles. Friends have played a crucial role, offering support and encouragement, making this academic journey possible. Finally, my deepest thanks to everyone who played a part in encouraging me to pursue this journey of higher education and attain a Ph.D.

I express my sincere gratitude to my institute NITK and Department E&C for granting me the opportunity to embark on my Ph.D. journey. I extend my deepest thanks to Dr. Sumam David S for the initial guidance, care, and support, especially for the insightful and invaluable suggestion on my Ph.D. topic. Her subtle yet impactful well wishes have been a constant source of encouragement, gently steering the course for a successful continuation of my academic journey.

I extend my sincere gratitude to my Research Supervisor and Teacher Dr. A V Narasimhadhan for his exceptional understanding and swift resolution of my difficulties in choosing a new PhD topic. Their assurance and immediate support paved the way for the continuation of my doctoral journey. I am thankful for the extensive care and unwavering encouragement provided during the finalization of my PhD topic, guiding me through challenging situations. I extend my heartfelt appreciation for the unwavering support and encouragement provided by him throughout my journey, which played a pivotal role in the successful completion of my PhD. Their patience and kindness in correcting my initial documents, despite their challenging nature, left an indelible experience. I am also thankful for his invaluable suggestions on document writing, English grammar, and academic paper structuring. Special gratitude for connecting and facilitating me with two other commendable research supervisors who have been invaluable mentors throughout this journey. I am grateful to my research supervisor for providing me with the opportunity to assist B.Tech and M.Tech students in their

mini and major project works, which was a valuable experience for my professional growth. I express my gratitude to Dr. A V Narasimhadhan for engaging discussions, a cherished memory with my Research Supervisor on various subject matters, and for the memorable and enjoyable moments, including funny incidents shared during our interactions. Finally, I appreciate the freedom granted to conduct research at my own pace and the flexibility in thesis submission, which greatly contributed to the successful completion of my PhD.

I extend my heartfelt gratitude to my Research Supervisor and Teacher Dr. B S Raghavendra for graciously taking on the role of a Research Supervisor and for the exceptional cooperation displayed alongside the other two supervisors. Special thanks for his meticulous attention given to the design, execution, and evaluation of the research methodology, as well as for the invaluable contributions in correcting documents and research articles. I acknowledge my Teacher Dr. B S Raghavendra for engaging discussions and insightful suggestions, particularly in matters pertaining to behavioral and formal aspects, including official research-related affairs. I express sincere gratitude to my Research Supervisor for engaging in valuable discussions conducted in a friendly manner, accompanied by moments of humor. Additionally, having meals together on several occasions has added a delightful touch to our interactions, creating a positive and enjoyable atmosphere. I offer a warm appreciation for the willingness to personally register two conference papers during a challenging financial period. Lastly, I express thanks for the balanced approach of being both gentle and strict in guiding me through critical aspects of the PhD journey, showcasing continuous support and encouragement throughout the research collaboration.

I extend my heartfelt appreciation to my Research Supervisor and Teacher Dr. Amba Shetty for her profound kindness and unwavering support, particularly during the crucial early stages of my research journey. I express gratitude for her generous gesture of providing a research topic during our initial meeting, demonstrating remarkable understanding of the challenges I faced in finding one — an act that surpassed expectations in organizational settings. I also emphasize the exceptional commitment shown in the early weeks, dedicating a significant amount of time to clarify doubts and ensure a smooth transition into the chosen research topic. This act, which went beyond conventional expectations, played a pivotal role in the initial stages of my PhD. Furthermore, I acknowledge my Teacher Dr. Amba Shetty for her consistent motivation and encouragement, offering support and care that exceeded the ordinary. I give special thanks for the nurturing role played, resembling motherly affec-

tion, encompassing both personal well-being and the progress of my PhD. I express gratitude for the unexpected but invaluable discussions and suggestions on various matters, including official research-related affairs and general behavioral aspects, notably the spiritual dimension. I extend my thanks for the meticulous attention given to publication matters, including the correction of documents and research articles. My Research Supervisor's dedication to ensuring the quality of my work has been invaluable in shaping the final outcome of my research. Overall, I convey my deep appreciation for the patience, forgiveness, and motherly nature that characterized the entire journey of care, support, and encouragement provided by Dr. Amba Shetty.

I extend my sincere appreciation to Dr. Ashvini Chaturvedi of Electronics and Communication Engineering (E&C) Department and Dr. Jidesh P from the Department of Mathematical and Computational Sciences (MACS) for their invaluable contributions as members of the Research Progress Assessment Committee (RPAC). Their thoughtful suggestions and encouragement played a crucial role at various stages of this work. Additionally, I express my gratitude to Dr. Arulalan Rajan and Dr. Sheron Figarado, former faculty members of the Institute, who served as members of the RPAC during the evaluation of my research proposal, providing valuable insights and suggestions.

I am deeply grateful to the former Heads of the Department, Dr. U Shripathi Acharya, Dr. T Laxminidhi, and Dr. Ashvini Chaturvedi, as well as the current Head, Dr. Neelawar Shekar Vittal Shet, for their unwavering support and provision of essential facilities during my tenure at NITK. My sincere thanks also extend to the dedicated faculty members of E&C Department for their valuable contributions to my academic journey.

I extend my special thanks to technicians Vagdevi Prabha Madam and Sowmya Madam, department office assistant Amitha Kotian Madam, and department assistant engineer Sanjeev Poojari Sir for their consistent and invaluable assistance throughout my journey. Gratitude to other technicians, Subrahmanya Karanth Sir, Guruthilak Sir, and Swathi Madam, as well as office assistants like Ratish Anna, for their continuous support. My sincere appreciation to all the staff including Pushpalatha Madam (Rtd.), Vasudev Shettigar Sir (Rtd.), Roshni Madam, V Pratap Singh Sir for their kind and patient help throughout. A separate thanks to Balkrishna Sir and Shubha L Kotian Madam for their assistance during the submission process and beyond.

I extend my heartfelt thanks to senior scholars, particularly Dr. Nagraj P Y, Dr. K

Shareef babu, Dr. Hanumantha Rao G, and others, for their invaluable help and valuable suggestions related to PhD matters. I express my sincere gratitude for the warm and friendly treatment extended by my senior colleagues, including Dr. Asha, Dr. Anu Shaju, Dr. Deepu S.P, Dr. Goutham Simha, Dr. K. Vasudeva Reddy, Dr. Jayaram Reddy M.K., Dr. Srinivasulu Polineni, Dr. G Rajesh, Dr. Prasad Naik, Dr. Gnane Swarnadh, Dr. Raghavendra M.A.N.S, Dr. Shilpa Suresh, Dr. Ragesh, Dr. Jnanesh Somayaji and others. Their guidance in navigating formalities, sharing materials and template documents, and warm and friendly treatment have been instrumental in my academic journey.

I extend my heartfelt acknowledgment to scholars like Dr. Sudhakar Reddy Pokala, Dr. Deepa C, and Ms. Priyanka Singh under the guidance of my supervisors. Their active involvement in technical discussions, conference matters, and friendly interactions has greatly enriched my academic journey and contributed to a positive and productive environment.

I express my heartfelt gratitude to my first year roommate Dr. Ritesh Parida and close friends like Dr. Vashista G A and Dr. G Saikrishna for creating a friendly and pleasant atmosphere during my first year. A big thanks to all my batch-mates and lab-mates, including Dr. Puneeth Kumar T R, Dr. Karthik R, Rajesh G, and Mr. Sravan Kumar Padala, for the enjoyable times we shared. I express my gratitude to my other fellow batchmates, especially Dr. Bethi Pardhasaradhi, Mr. Lad Kirankumar and others, for their friendly and supportive interactions. Special thanks to other research scholars namely Dr. Vijay Ratnam, Dr. Venkateswarlu P, Dr. B Anudeep, Dr. Srinath and others for their friendliness and contributing significantly to making my stay enjoyable. I extend my appreciation to junior scholars Mr. Mahesh T N, Mr. B N BalaRami Reddy, Mr. S Vinay Kumar and Mr. B Shubhaker for their help and the good times we had. I extend my gratitude to my senior research scholars, my junior research scholars, and all other research scholars across the department for making the overall experience delightful.

I extend my gratitude to scholars from other departments, including Dr. Govind Ekbote to Dr. Kiran Bathala, for the enjoyable moments, which significantly added to the overall positive experience. I also extend my gratitude to scholars from other departments, particularly Mr. M Chiranjeevi, Mr. Chiranjeevi Y, Mr. M Vinod, Mr. Manjunat, Mr. C Vinod, Dr. Kothuri Mahindra, Mr. Kaku Mahendra, Mr. Chiranjeevi, Mr. Rakesh Reddy, Dr. K Aditya, Mr. Sunil Mandal, Mr. Md Sartaj, Mr. Rasananda, Mr. Praveen, Mr. Sufiyan and others for their friendliness and collaborative spirit. I extend my heartfelt thanks to all my

hostel mates especially Mr. Ashish, Mr. Kunal, Mr. Pratik, Mr. Subodh, Mr. Ganesh, and others for contributing to the wonderful memories and friendships during our time together. I would like to express my appreciation to my hostel and mess friends, namely Mr. Sudeep, Mr. Ganesh, Mr. Mohansing and others, for making my stay enjoyable and memorable. My sincere thanks to my hostel mates and mess friends for making my stay memorable and enjoyable. I also extend my sincere thanks to all my colleagues for their continuous support, collaborative efforts, and friendly interactions throughout our academic journey. Their positive engagement has contributed to a harmonious academic environment.

I extend my gratitude to scholars like Mr. Vikas, Mr. Amal, Mr. Santosh A J and Mr. Shivanand for their valuable assistance and support during the placement process.

I extend special thanks to former B.Tech student Mr. Pardhu Madipalli and former M.Tech student Mr. Nikhil Bobate for their excellent execution of projects, showcasing commendable skills. Moreover, their willingness to contribute to my research work has been invaluable and greatly appreciated.

I extend my sincere gratitude to the esteemed officials at the institute, with a special acknowledgment for Dr. Jagannath Nayak, the Dean of Student Welfare, and Dr. Adka Nityananda Shetty, the Academic Dean. Their invaluable support and kindness have been instrumental in shaping my journey, and I am truly thankful for the unwavering understanding and trust extended to me during this significant period. Additionally, I want to express my appreciation to everyone, both within and outside the Institute, who, directly or indirectly, contributed to and supported me. Special thanks to those exceptional individuals for their kindness and support during this transformative journey. Your contributions have been truly invaluable.

I extend my heartfelt gratitude to all the officials, both official and non-official, at the institute who have played a crucial role in my journey. I express my heartfelt thanks to all the dedicated housekeeping personnel of the department and the hostel, whose efforts have contributed to making my stay pleasant and comfortable. Additionally, gratitude goes to the personnel of the security department for their kindness and helpfulness in ensuring a secure environment. Their diligence and support have been crucial, adding to the positive atmosphere during my time here.

I express my sincere gratitude to IEEE Geoscience and Remote Sensing Society (IEEE-GRSS), IEEE Industrial Electronics Society (IEEE-GRSS), and IEEE-GRSS (Bengaluru

Section) for their unwavering support in providing student travel grants for my conference participations. I am equally thankful to the Institute's Alumni Association (NITKSAA) for their kind and generous support in facilitating these opportunities. I extend special appreciation to my research supervisors and Nikhil Bobate for their support during financial challenges. Their responsible sharing of conference registration fees, later reimbursed, reflects their commitment to collaborative research.

I express my sincere gratitude to the thesis reviewers, Dr. Biplab Benerjee, IIT Bombay and Dr. Sirigina Rajendra Prasad, National University of Singapore (NUS), for their insightful feedback and constructive comments, which significantly contributed to the refinement of this work. I would also like to extend my thanks to the reviewers of all my publications for their time, expertise, and constructive comments that have significantly enriched the quality of my work.

I extend my deepest gratitude to HG Suvarna Gaurahari Das (HG SGHD) for generously allowing me to Shantipur - a VOICE center, where the special mercy of HDG Abhay Charanaravinda Bhaktivedanta Swami Prabhupada flows through HG Radheshyam Das (HG RSD), creating a spiritually nurturing environment. My heartfelt thanks to HG Vanamali Govinda Das (HG VGD), including HG SGHD, for their love, care, and unwavering support. I am immensely grateful for the unforgettable services provided, such as deity worship, tulsi care, garland making, and cleaning responsibilities. Special appreciation for the inspiring classes conducted by HH Radhanath Swami (HH RNS), HG RSD, HG Gauranga Das, HG SGHD, HG VGD, and other dedicated devotees. The wonderful atmosphere filled with celebrations, melodious kirtans, vibrant lectures on the Lord's pastimes, and the delicious prasadam made every moment special. I express my thanks for the delightful yatras to various places in South India and Dhams like Vrndavan in North India, as well as the weekly feasts and nourishing meals prepared by Bhakta Siddharth Prabhu and other cook devotees. Gratitude to all the inmates of Shantipur VOICE from 2016 to 2024 for their kindness, making my stay incredibly pleasant and blissful. A special acknowledgment to HG SGHD for understanding my challenges during my PhD and allowing me to proceed in my own way, especially during my stay at Shantipur VOICE. Thanks for graciously permitting my stay at Shantipur during the Covid lockdown. I also extend my thanks to all the devotees of Lord Krishna for their patience and forgiveness for any mistakes I may have made, seeking forgiveness from everyone. Lastly, a heartfelt thanks to the devotees at ISKCON Cultural

Center Bengaluru (ICC Bengaluru) for their warm reception during my visits and the Lord Jagannath's Rathayatras.

I express my profound gratitude to HDG A.C. Bhaktivedanta Swami Prabhupada for his divine books, which have served as a constant source of true knowledge, motivation, inspiration, and strength for me during my Ph.D. journey. Whenever I delved into these sacred texts, I found the solace and fortitude needed to navigate through challenges. I sincerely seek forgiveness for any unintentional mental offenses towards HDG A.C. Bhaktivedanta Swami Prabhupada, HH RNS, HG RSD, HG SGHD, HG VGD, and other devotees. I extend my heartfelt gratitude to all the members of Shreyas - ISKCON Youth Forum (IYF) Tirupati, under the wise guidance of HG Lakshmipathi Gaura Das. Special thanks to HG Kaliya Krsna Das and Bhaktha P Balaji Prabhu for their generous care and love. I humbly seek forgiveness from them as well.

I offer my heartfelt gratitude to my worshipable God, the Supreme Lord Sri Krishna, for orchestrating the events of my life, especially in the realm of my Ph.D. studies and the subsequent journey. Your benevolent influence has been truly heartwarming and transformative. I appreciate the divine arrangement that included both challenges and opportunities, placing me in difficult situations and yet silently standing behind, providing knowledge, wisdom, and strength to overcome adversities and learn invaluable life lessons. I extend my thanks to the Lord for the countless blessings, including good health, knowledge, wisdom, and unwavering strength that have accompanied me throughout. I am especially grateful for the numerous delightful experiences that have enriched my journey.

Lastly, I extend my heartfelt gratitude, especially to ChatGPT3.5, for the crucial role in designing CDIC, offering guidance in paraphrasing text, and providing valuable inputs in shaping the acknowledgment section of this thesis.

I humbly seek forgiveness from everyone, especially my parents and Ph.D. Supervisors. To my Supervisors, I express gratitude for their patience and understanding, acknowledging any lapses in consistently following instructions and any instances of playful behavior arising from a sense of familiarity. To my parents and the divine, including my Ph.D. Supervisors, I acknowledge and seek forgiveness for not giving them the credit they truly deserve. I recognize that my actions may not have reflected the love and expectations you hold for me.

Palla Parasuram Yadav
Research Scholar
ECE Dept., NITK, Surathkal

Dedication

To

The Lotus Feet of

Sri Sri Radha Govinda Ji Asta-Sakhi Vrnda

Hare Krsna Lotus Temple

ISKCON Tirupati

Contents

List of Figures

List of Tables

Chapter 1

Introduction

> The truth should be spoken in a straightforward way, so that others will understand actually what the facts are. Truthfulness demands that the facts be presented as they are for the benefit of others. That is the definition of truth.
>
> Bhagavad-gita As It Is 10.4-5, A.C. Bhaktivedanta Swami Prabhupāda

Introduction

This chapter lays the groundwork for hyperspectral data analysis, offering a fundamental introduction to the field. It navigates through the core challenges of endmember extraction and spectral matching, crucial facets addressed in this research. Furthermore, it provides insights into two pivotal applications in hyperspectral data analysis: change detection and mineral classification. The chapter concludes with an overview of the thesis structure, providing a roadmap for the reader to anticipate the organization of subsequent sections.

1.1 Background

Hyperspectral Image (HSI) is a powerful technique in remote sensing (RS) that involves the acquisition and analysis of images captured across hundreds or even thousands of narrow and contiguous spectral bands Martínez et al. (2006), Lin et al. (2023). Unlike traditional RS techniques that capture information in just a few broad bands, HSI provides detailed spectral information for each pixel in an image scene Shippert et al. (2004). This wealth of spectral data enables a more comprehensive understanding of the Earth's surface and the objects it contains Landgrebe (1999), Khan et al. (2018).

HSI plays a critical role in various applications, including environmental monitoring

Xingtang et al. (2004), agriculture Haboudane et al. (2004), geology Cloutis (1996), urban planning Cavalli et al. (2008), and mineral exploration Clark and Swayze (1995). Its importance lies in its ability to extract valuable information about the composition, characteristics, and changes occurring on the Earth's surface Huadong et al. (2001). By analyzing the unique spectral signatures of different materials, HSI enables the identification and discrimination of various land cover types Landgrebe (1999) Manolakis and Shaw (2002) and Ma et al. (2013), vegetation species Cochrane (2000), soil properties Asner and Lobell (2000) and even specific minerals Clark et al. (2003).

1.2 HSI

HSI is a powerful technique in RS that involves the acquisition and analysis of images captured across hundreds or even thousands of narrow and contiguous spectral bands available for detecting substances Manolakis and Shaw (2002) that are normally indistinguishable by multispectral and panchromatic imaging devices Gan et al. (2019). Unlike traditional RS techniques that capture information in just a few broad bands, HSI provides detailed spectral information for each pixel in an image scene Khan et al. (2018).

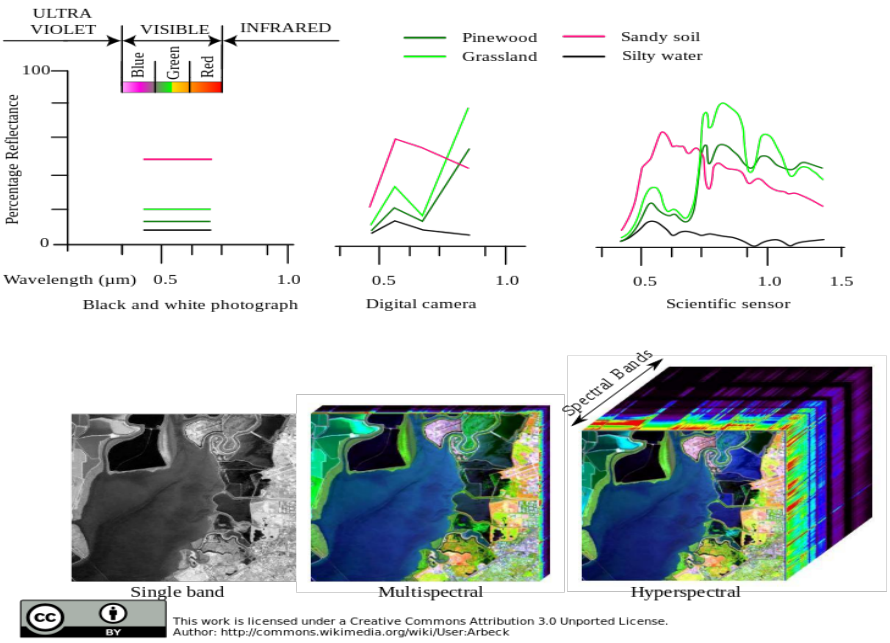

Figure 1.1: Unveiling the Spectrum: A Comprehensive Exploration of Bandwidth and Bands in Panchromatic, Multispectral, and Hyperspectral Imaging

Panchromatic, multispectral and hyperspectral are the three main imaging techniques in

the RS for collecting and processing the information of pixels of the imaging scene in the electromagnetic frequency range especially in visible to near infrared regions Shippert et al. (2004), Ortega et al. (2019). Figure 1.1 shows clearly the difference between three imaging techniques in terms of spectral information they provide in identifying and discriminating various Earth surface features.

Panchromatic images provide only one band of information with large bandwidth and multi spectral images provide few bands (few tens to less than hundred of bands) of information with moderate bandwidth, whereas HSIs provide larger number of bands (few hundreds to thousands of bands) Martínez et al. (2006) with less bandwidth and because of this HSIs are more useful in applications like study of earth surfaces and object recognition.

HSI is a group of images obtained by collecting image frames of the same site at contiguous wavelengths, hence its called hyperspectral image cube Shippert et al. (2004). HSI provide information of every pixel in the image scene in the form of reflectance(response on interaction with electromagnetic radiation) at the all wavelengths Bannon (2009). This reflectance response of a pixel depends on the type of earth surface feature and it is unique for each earth surface feature Plaza et al. (2004). Figure 1.2 shows the individual frames (spatial domain) forming HSI cube along wavelength axis (spectral domain) and how spectral profile of a particular pixel can be obtained from contiguous bands of HSI cube Dong et al. (2019).

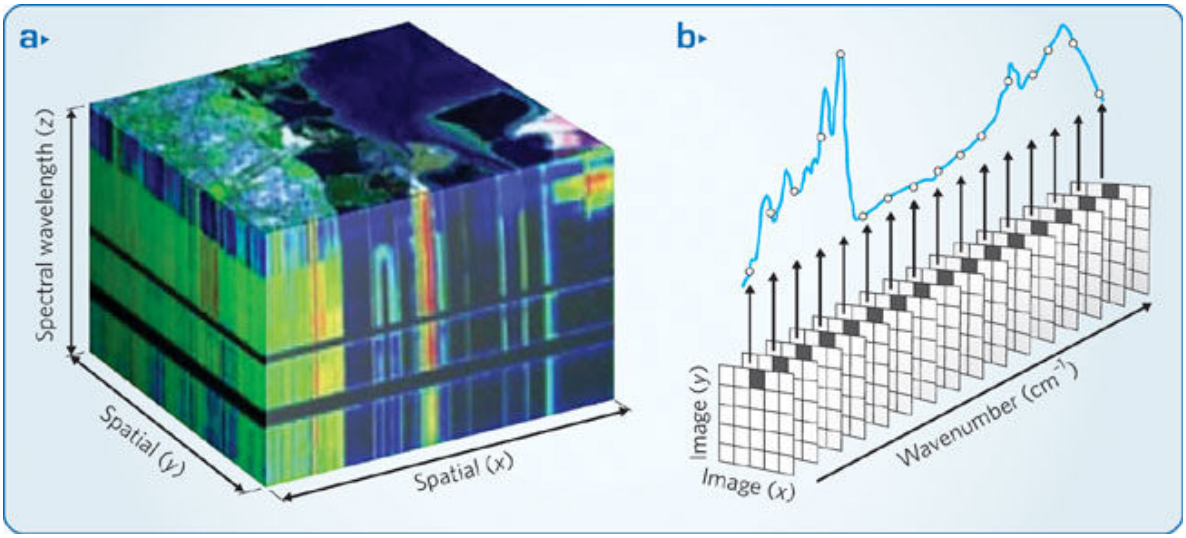

Figure 1.2: HSI Cube Composition: Unveiling Spectral Profiles Across Wavelengths in the Spatial Domain (Bannon (2009))

This spectral reflectance response is used as a finger print in detecting earth surface fea-

tures, hence it is called as spectral signature Shaw and hua K. Burke (2003). Because these signatures are unique for different materials present on the earth surface, HSI have many applications in various fields Manolakis and Shaw (2002), Keshava and Mustard (2002). Applications in Geoscience include study of earth surface features like soil type Gomez et al. (2008), vegetation, forestry, minerals and their abundance estimation. Figure 1.3 illustrates how spectral signatures of different Earth surfaces look like when observed using HSI.

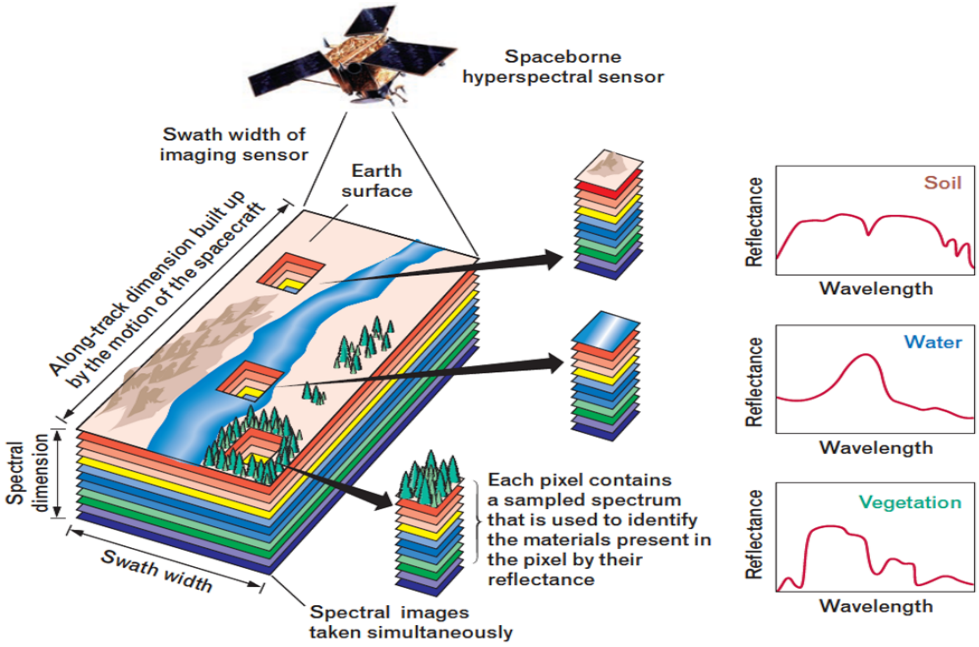

Figure 1.3: Visualizing Spectral Signatures: Earth Surfaces Captured through HSI Observation (Shaw and hua K. Burke (2003))

1.3 Challenges in HSI Analysis

The HSIs, despite the wealth of information, pose several challenges that require specialized approaches in analyzing them Ortega et al. (2019) Pandey et al. (2020). Endmember extraction (EE) is one such challenge, involving the identification of pure spectral signatures or reference spectra that represent specific target materials Deng et al. (2014). Accurate endmember extraction is crucial for subsequent analysis tasks, such as spectral unmixing and classification Singh et al. (2012). Spectral matching is a vital technique for comparing spectral signatures of unknown to known, measuring similarity or dissimilarity between them Robila and Gershman (2005). This matching process helps in the identification, analysis, and interpretation of different materials or targets present in the HSI Shanmugam and SrinivasaPerumal (2014).

Through the combination of endmember extraction and spectral matching in hyperspectral imaging, diverse applications in geology and related fields are empowered, enabling tasks such as geological mapping, mineral exploration, environmental monitoring, and land cover analysis with increased accuracy and efficiency.

In summary, HSI analysis is a valuable technique that enables detailed analysis of the Earth's surface by capturing and analyzing information across numerous narrow spectral bands Huadong et al. (2001), Transon et al. (2017). Endmember extraction, spectral matching, change detection, and mineral classification are essential components of HSI analysis, addressing specific challenges and applications within this field. These novel approaches in HSI analysis contribute to advancing our understanding of the Earth's surface, facilitating informed decision-making and resource management in various domains Huadong et al. (2001) and Paoletti et al. (2019).

1.3.1 Endmember Extraction

HSIs are highly mixed in nature Song and Wu (2019) due to reasons like low spatial resolution of the sensors and the presence of multiple substances at a single pixel Gu et al. (2021). Many application scenarios, such as target detection, require some degree of sub-pixel accuracy to improve HSI analysis Song and Wu (2019). (see Figure 1.4). It leads to finding set of macroscopically pure spectral components that can be used to unmix all other pixels in the HSI data (Deng et al. (2014) and Yin et al. (2020)). The spectrally pure signature is called as endmember Shippert et al. (2004), Jasmine and Pattabiraman (2015). The spectral signatures of pure materials i.e. endmembers used as reference for material identification through unmixing process are distinct or unique as well Plaza et al. (2004).

Endmembers are characteristic spectral profiles that encapsulate the unique features and properties of a material, enabling its discrimination from other materials . An endmember (also end-member or end member) in mineralogy is a mineral that is at the extreme end of a mineral series in terms of purity (refernce: Wikipedia). Endmembers are essential for subsequent tasks like spectral unmixing and classification. Spectral unmixing decomposes each pixel's spectral signature into a linear combination of endmembers Guerra et al. (2015), providing information about the relative abundance of different materials. Classification utilizes extracted endmembers as reference signatures for identifying land cover types or materials.

Selection of spectrally pure endmembers is the most crucial step in spectral mixture analysis (Singh et al. (2012) and Shi and Wang (2014)). Among the two methods for selecting endmembers Roberts et al. (1998), Rogge et al. (2006) – deriving them directly from the image (image endmembers) and using field or laboratory spectra of known target materials (library endmembers) – image endmembers hold the advantage of being collected at the same scale as the data, simplifying their association with features present in the scene Keshava and Mustard (2002). Endmember selection from HSI is the most crucial step in spectral mixture analysis (Singh et al. (2012) and Shi and Wang (2014)) and difficult because of composite nature of spectral information from the RS (Tompkins et al. (1997)). Additionally, the endmembers can't be identified with visual inspection from HSI because of the reasons like low spatial resolution, most image pixels being heavily mixed and etc Liu and Zhang (2011). Therefore, EE is an important challenge to be addressed in the HSI analysis related tasks and hence the need for developing algorithms to extract pure endmembers that are spectrally distinct and unique.

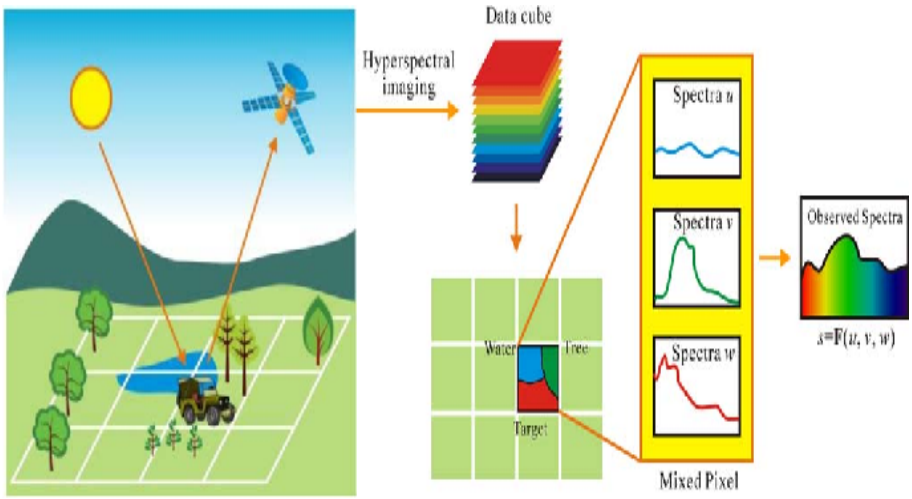

Figure 1.4: Challenges in Hyperspectral Image Analysis: Understanding Mixing and Resolving Complexity

1.3.2 Spectral Matching

Spectral matching is another key aspect of HSI analysis, focusing on comparing spectral signatures to measure similarity or dissimilarity between them Robila and Gershman (2005). Spectral matching algorithms (SMAs) play a vital role in identifying and analyzing different Earth surface features using hyperspectral data Shanmugam and SrinivasaPerumal (2014). SMAs are useful not only for validating the accuracy of image-based signatures but also for

feature extraction. These algorithms facilitate tasks such as target detection, classification, and anomaly detection Shanmugam and SrinivasaPerumal (2014).

Spectral characteristics provided by the HSIs have been used to identify the earth surface materials. Remotely sensed HSI spectral signature of materials may not completely match to the field-spectra (on-ground investigation or laboratory spectrometer measurements). Figure 1.5 illustrate the differences between spectral signatures of few minerals and their corresponding United States Geological Survey (USGS) library spectra (ground-truth spectra). Therefore spectral matching/comparing task may be very often laborious. However, the SMAs use similarity measures to match the spectral signatures of unknown materials present in the HSI with the available ground-truth (GT) signatures. Thus, SMAs play an important role in various applications of the HSI analysis.

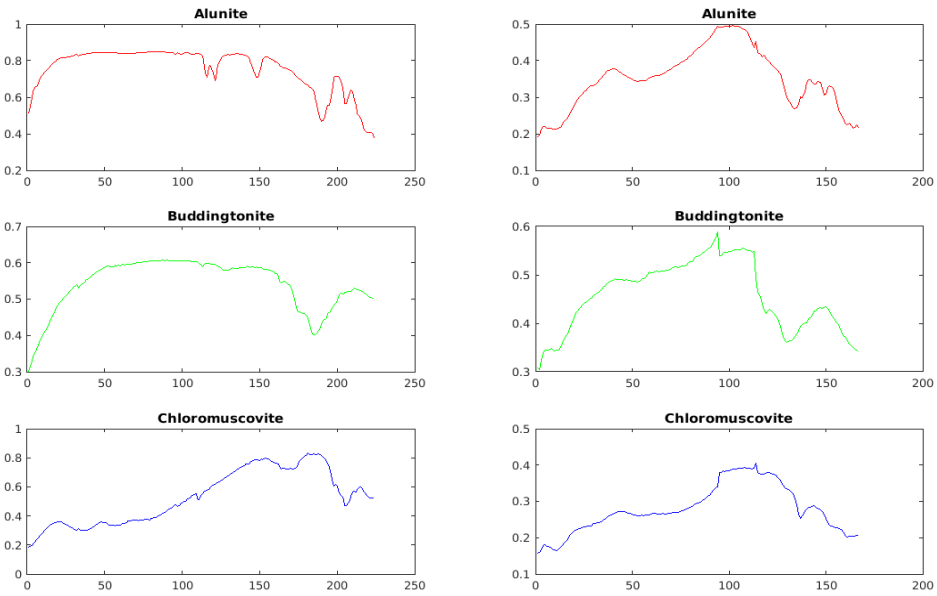

Figure 1.5: Comparing Hyperspectral Image Spectra with Ground-Truth: Understanding Discrepancies in Material Identification

1.4 HSI Applications

HSI data, with its high spectral resolution, is valuable for geological exploration and resource management Paoletti et al. (2019). Although originally developed for mining and geology (the ability of hyperspectral imaging to identify various minerals makes it ideal for the mining and oil industries, where it can be used to look for ore and oil), it has now widespread into

many fields. In RS, HSI data has numerous applications say classification Ortega et al. (2019) of earth features such as different types of soil, vegetation, urban, forestry, agriculture, terrestrial Brown et al. (2006) and also surface features of Mars Brown et al. (2010), and other human interested targets (Lohumi et al. (2016).

However, mineral identification remains a challenging task due to the subtle differences among the spectral signatures of minerals and insufficient ground truth Manolakis et al. (2019) . Mineral identification through field investigation is expensive. Added to this, many locations on the globe are not accessible. HSIs due to advancements in spatial-spectral resolutions and availability of multi-temporal information is in demand for many RS applications including change detection (CD). CD, in particular, is an important and challenging problem in monitoring changes such as deforestation, urban development, and landslides using time series HSI data.

1.4.1 HSI-CD

CD is an essential application of HSI analysis, allowing the identification and monitoring of temporal changes occurring on the Earth's surface. By comparing HSIs acquired at different time intervals, change detection methods enable the detection and analysis of changes such as deforestation, urban expansion, and natural disasters Malila (1980). The materials present in the HSIs are identified using their spectral signatures or characteristics. But, the high dimensionality of HSI data and lack of ground-truth information on changed and unchanged pixels make CD not so easy but a difficult task Zhan et al. (2020). In addition, non-homogeneity of the multi-temporal data in terms of sensors and atmosphere related factors made CD a challenging task Lei et al. (2020).

1.4.2 Mineral Identification

Mineral classification is a specific application within HSI analysis that aims to identify and map mineralogical compositions using spectral information De Kerf et al. (2022). Minerals often exhibit subtle differences in their spectral signatures, making their accurate identification and classification challenging Kodama (1979). These subtle differences in signatures makes classification of minerals very difficult without studying their response in the narrow bands. Hence HSI are in a demand for the classification of minerals. Figure 1.6 shows spec-

tral signatures of few minerals collected by field investigation of USGS spectography lab. In field investigation, spectral signatures of particular location are collected manually with the help of spectrometer.

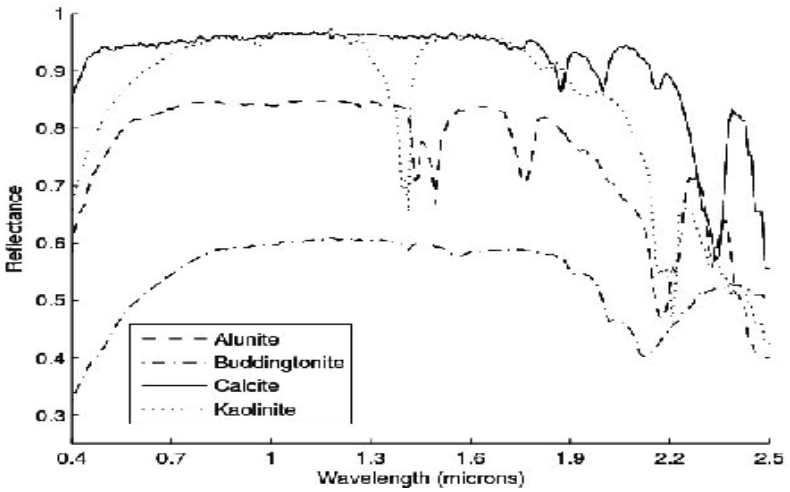

Figure 1.6: Challenges in Mineral Classification: Analyzing Subtle Differences in Hyperspectral Signatures (Ulhaq and Xu (2008))

The distinctiveness of spectral signatures for various materials lies in their ability to reflect, absorb, and emit electromagnetic energy at specific wavelengths Manolakis and Shaw (2002) and speciality of mineral signatures is that they exhibit subtle differences among them except the absorption features and it's depth of absorption at mineral specific wavelengths.

1.5 Motivation

The motivation behind exploring novel techniques in hyperspectral data analysis for endmember extraction, spectral matching, change detection, and mineral classification stems from the growing need for advanced tools to extract valuable information from hyperspectral imagery. These novel techniques aim to improve the identification of important materials in the images and enable precise comparisons of spectra to detect changes in the land and environment. By using these new approaches, we can achieve more accurate mineral classification, which is crucial for applications like mineral exploration and studying the Earth's surface. These techniques offer exciting possibilities to make better use of hyperspectral data for further analysis required for various scientific and practical purposes.

1.6 Thesis Contributions

This research makes significant strides in addressing the intricate challenges associated with HSI analysis, focusing on key aspects such as EE, SMAs, HSI-CD, and mineral classification. The primary contributions can be summarized as follows:

It introduces novel similarity measures-based endmember extraction algorithms, such as a similarity Measures based Subtractice Clustering Algorithm (SM-SCA) and a similarity Measures based Endmember Initialization Algorithm (SM-EIA), which exhibit superior performance. This research strategically incorporates the darkest pixel as a Target Pixel of Interest (TPOI) for endmember initialization, synergizing with the brightest pixel. This unique approach significantly enhances overall EE performance. Additionally, an improved SM-EIA variant is introduced, utilizing higher-dimensionality metrics like volume for extracting pure endmembers, deviating from traditional Euclidean Distance (ED) metrics. A new algorithm, Corner-Driven Iterative Clustering Algorithm (CDIC), is developed to improve endmember extraction by identifying corner pixels. This innovative approach aids in hyperspectral data classification.

The introduced Gradient-Based Spectral Similarity Measure (GSSM) effectively highlights diagnostic features and excels in discriminating spectrally distinct target signatures, surpassing other SMAs. The incorporation of gradient correlation (GC) enhances discrimination power, particularly when combined with geometrical SMAs. Moreover, a refined method for measuring Relative Spectral Discrimination Power (RSDPW) is proposed, providing a more meaningful assessment of endmembers and capturing the range of RSDPW values for different discrimination levels.

In change detection, an innovative endmember-related feature extraction method outperforms classical algorithms and matches deep learning models' performance. For mineral classification, the proposal of virtual sample generation and the application of a one-dimensional convolutional neural network (1-D CNN) model demonstrate high accuracy, addressing challenges of limited ground truth and training samples. These contributions collectively advance the field of HSI analysis.

In summary, this research makes substantial contributions to the field of HSI analysis by introducing innovative algorithms, strategies, and methodologies. These advancements aim to address limitations in data availability and complexity, ultimately enhancing the accuracy and efficiency of HSI analysis across various applications. The proposed methods have

been rigorously validated on multiple benchmark datasets, establishing their effectiveness and reliability.

1.7 Organisation of the Thesis

The thesis is presented in seven chapters. Organization of the thesis following the Chapter 1 is discussed here. Chapter 2 presents the summary on literature review and discussed the objective of this research research work using the research gaps identified. The details about the data sets used for conducting experiments to achieve objective of this research work is presented in Chapter 3. In chapter 4, the emphasis is on the research conducted concerning endmember extraction, where different approaches and outcomes are presented and examined. In chapter 5, the research focuses on the spectral matching. Chapter 6 is about research on change detection and mineral classification. It presents different studies and findings in these topics. Chapter 7 presents concluding remarks on experimental results obtained from the research carried out on the objectives identified. Additionally, the future directions to carry this research work also included.

Summary:

This chapter presents a basic introduction to hyperspectral data analysis along with the two important challenges and two important applications considered to address in this research work. Initially, fundamentals of HSI are discussed to detail the challenges like endmember extraction and spectral matching and applications of the hyperspectral data analysis like change detection and mineral classification. The organisation of the Thesis has been discussed at the end.

The next chapter presents reviews on relevent themes of literature identified for our work.

Chapter 2

Literature Review

> Good population in human society is the basic principle for peace, prosperity and spiritual progress in life. Such population depends on the chastity and faithfulness of its womanhood.
>
> Bhagavad-gita As It Is 1.40, A.C. Bhaktivedanta Swami Prabhupāda

Introduction

This chapter provides a concise summary of the literature review, outlining the identified research gaps that shape the objectives of this work. The review focused on endmember extraction, spectral matching, change detection, and mineral classification. Key research gaps include the under-explored spectrally distinctive nature of endmembers, the need for effective spectral matching, the absence of methods capturing diagnostic features, and the challenge of exploring sub-pixel features for change detection in hyperspectral imagery. Additionally, addressing mineral classification challenges and exploring deep learning algorithms are recognized as significant research gaps.

In HSI analysis, two primary types of spectral mixing analysis models (Veganzones and Grana (2008), Ma et al. (2013)) namely the linear mixing model (LMM) Adams et al. (1986), Boardman (1989) and the nonlinear mixing model (NLMM) are there. When it comes to endmember extraction, the LMM is a popular choice for endmember extraction compared to the NLMM due to its simplicity and effectiveness (Iordache et al. (2011) and Shi and Wang (2016)). The detailed discussion on SMA with LMMs and NLMMs can be found in Keshava and Mustard (2002). In the LMM, mixed pixels are treated as a linear combination of multiple endmember spectral signatures, as a linear combination of multiple endmember spectral signatures, where the combination is weighted by their corresponding abundance coefficients Shippert et al. (2004).

2.1 Endmember Extraction Algorithms

As per Li and Zhang (2011), EEAs mentioned so far that are designed based on various ideologies falls under two main criteria of interest, i.e. convex-geometry-based and least square error (LSE) based.

2.1.1 Convex-Geometry-based EEAs

It is a fact that some physical quantities, such as radiance and reflectance, are non-negative and because of this reason, HSI mixed pixels as a linear combination of endmembers lie within a convex region Ifarraguerri and Chang (1999). Endmembers constitute the vertices of a convex polytope covering (most of) the HSI data points in high dimensional space Veganzones and Grana (2008). Therefore, geometrical algorithms built on the basis of Linear SMA try to identify the endmembers to be the vertices of simplex formed by the HSI. Convex geometry based EEAs fall into two categories Song and Wu (2019). One category is based on the pure pixel assumption and the other is based on the non-pure pixel assumption. the pure pixel assumption methods assumes that there exists at least one pure pixel for every material present in the HSI scene.

EEAS Under Pure Pixel Assumption

In the context of pure pixel assumption, several EEAs have been proposed, and most of these algorithms either they try to search for pixels located at the corners of simplex formed data cube through maximum volume criteria or maximum projection criteria (projection based algorithms). Maximum simplex volume as a criterion to extract endmembers seems always a good measure for an EEA Wu and Chang (2007).

Projection based algorithms under pure pixel assumption including the orthogonal subspace projection (OSP) Harsanyi and Chang (1994), pixel purity index (PPI) Boardman et al. (1995), fast iterative PPI (FIPPI) Chang and Plaza (2006), APPI Chaudhry et al. (2006), vertex component analysis (VCA) Nascimento and Dias (2005), convex cone analysis (CCA) Ifarraguerri and Chang (1999). A Convex Polygon Maximization-Based Hyperspectral Endmember Extraction Algorithm Shah et al. (2021) aims to reduce Spectral Angle Error (SAE) and Spectral Information Divergence (SID) errors. Other convex-geometry-based endmember extraction under pure pixel assumption include Pearson's correlation coefficient-based

convex geometry for endmember extraction (PCGE) Shah and Zaveri (2021) and approach mentioned in Zhang and Mahmoud (2023). PPI, VCA and OSP are the popular projection based algorithms. The limitation of PPI method is that it is time consuming. PPI need human intervention in selecting final endmembers, hence it is laborious. OSP that tries to identify distinct signatures became useful tool for analysing HSI including EE, but it requires knowledge about endmember targets. This category EEAs, especially PPI and PPI related EEAs, are conceived not as a solution but as a guide. An automatic target generation process (ATGP)Ren and Chang (2003) is an another OSP based EEA. Ref. Tao et al. (2022) presents a method called "Fast Orthogonal Projection" for hyperspectral unmixing. Recently, a new algorithm, Dispersion Index based Endmember Extraction (DIEE) that utilizes convex geometry and the Dispersion Index for enhanced EE was introduced Shah and Zaveri (2023). Ref. Jiang et al. (2022b) introduces VD-MoEE, a method utilizing a novel vertex-directed local search operator and a memetic strategy to guide endmember estimation towards hyperspectral data manifold vertices, enhancing the identification of representative endmembers.

Maximum volume criteria based algorithms under pure pixel assumption include NFINDR Winter (1999), simplex growing algorithm (SGA) Chang et al. (2006), maximum simplex volume algorithm based on householder transformation (MVHT) Liu and Zhang (2011), AVMAX and SVMAX Chan et al. (2011) and an EEA based on QR factorisation using Givens rotations (EEGR) Gan et al. (2018). N-FINDR and SGA are popular maximum volume based algorithms. Endmembers extracted by N-FINDR and VCA are inconsistent unlike SGA. SGA is an improved version of N-FINDR. SGA needs separate procedure for endmember initialization. AVMAX and SVMAX Perform similar as N-FINDR and VCA. AVMAX have fast convergence under high SNRs.

EEAS Under Non-Pure Pixel Assumption

The other category algorithms falls under non-pure pixel assumption follow Craig's seminal belief and consider the endmembers to be the vertices of minimum simplex (minimum volume) formed by all the observed pixels of the HSI data Craig (1994). Such algorithms include a minimum volume transform (MVT) Craig (1994), minimum volume constrained non-negative matrix factorization (MVC-NMF) Miao and Qi (2007), a minimum-volume enclosing simplex (MVES) Chan et al. (2009), a minimum volume simplex analysis (MVSA)

Li and Bioucas-Dias (2008), simplex identification via split augmented Lagrangian (SISAL) Bioucas-Dias (2009) and iterated constrained endmembers (ICE) Berman et al. (2004). But this belief is capable of perfectly identifying the true endmembers when there exist pure pixels (Chan et al. (2011)). Ref. Rasti et al. (2022) is a recently introduced non-linear unmixing based approach under non-pure pixel assumption. In Plaza et al. (2012) it was observed that algorithms without the pure pixel assumption generally outperform those methods in the other considered category, although there is still an issue related with the quality of the generated endmembers from the viewpoint of spectral signature quality (particularly when the hyperspectral data is acquired under high noise conditions).

Spatial-Spectral Information-based EEAs

Most of the convex geometry based EEAs do not integrate the spatial and spectral information entirely. To overcome this limitation, automated morphological endmember extraction (AMEE) Plaza et al. (2002), spectral spatial endmember extraction (SSEE) Rogge et al. (2007), and hybrid endmember extraction algorithm (HEEA) Li and Zhang (2011) have been proposed, which integrate both spatial and spectral information for identifying endmembers. The usefulness of SSEE depends on the presence of high contrasted endmembers in the dataset. selection of optimal window size is a problem for HEEA. Other algorithms that come under this category of spatial-spectral information-based EEAs include Shen and Bao (2019) and Shen et al. (2020). Ref. Shah et al. (2020) proposes an innovative algorithm, utilizing entropy for spatial information and convex set optimization for spectral information in endmember extraction from HSIs. Ref. Cheng et al. (2021) introduces a spatial-spectral clustering algorithm for endmember extraction and hyperspectral unmixing, aiming to alleviate spectral variability. The method employs a spectral purity index calculation strategy to select pure pixels in different regions.

2.1.2 LSE based EEAS

Some of the EEAs like iterative error analysis (IEA) Neville (1999), unsupervised fully constrained least squares (UFCLS) Heinz et al. (2001) and and a fast algorithm for linearly unmixing hyperspectral data (FUN) Guerra et al. (2015) developed based on the theoretical idea that endmembers unmix the HSI data with minimum error and therefore try to extract pixels contribute to LSE as the endmembers. All LSE based algorithms work on minimum

error constraint (MEC) in unmixing. Wang *et al.* Wang and Chang (2006) used independent component analysis (ICA) to extract endmembers and their abundance. Ref. Chen et al. (2022) proposes a fast endmember extraction method based on LSE, showing performance similar to existing methods in spectral angle distance. A new EE based on LSE Chen et al. (2022) is relatively fast and perform comparable to and sometimes outperforms existing methods. Ref. Chetia and Devi (2022) is another recently introduced LSE based approach. Ref. Cui et al. (2023) introduces GSUU, a deep neural network for efficient blind hyperspectral unmixing, incorporating spatial group sparsity to enhance performance by recognizing similarities among adjacent mixed pixels. Recently, a Endmember Bundle Extraction (EBE) Liu et al. (2023) Improved Multiobjective Particle Swarm Optimization to identify endmembers that represent spectral variability within each class was introduced. A Global-to-Local Evolutionary Algorithm (GL-EA) employs a sequential global-to-local search strategy to effectively extract endmembers Cheng et al. (2023).

2.1.3 Other EEAs

Authors (Chiu (1994)) proposed a clustering based EEA called subtractive clustering algorithm (SCA) for endmember extraction. SCA is an improved version of the mountain method Yager and Filev (1994). subtractive clustering Bilgin et al. (2011) is proposed for endmember extraction. Some miscellaneous criterion in designing EEAs include higher statistics and dictionary learning framework. High-order statistics perform better than second lower order statics in automatic target identification Ren et al. (2006). End-net, an auto encoder based technique was proposed for EE Ozkan et al. (2018). End-net gives near optimal solution but implementation demands high Computational resources. Intelligent optimization based algorithms (Yang et al. (2015), Xu et al. (2017), Zhang et al. (2017) and Du et al. (2019b)) exploiting multiple constraints on EE to get better performance or promising results are also proposed but selection of parameters is a major problem for these techniques and they need high computational resources for implementation. Dictionary learning framework has been applied in hyper spectral endmember extraction Song and Wu (2019). Ref. Song et al. (2020) introduces a background endmember extraction algorithm based on robust non-negative dictionary learning for detecting sub-pixel targets in hyperspectral remote sensing imagery. However, dictionary learning based methods are not robust enough in noisy environments. A new probabilistic tensor moment strategy presents an efficient way

to extract endmembers Fernandez-Beltran et al. (2020). Merits and demerits of a few EEAs are presented in Table 2.1. Ref Zhang et al. (2022) proposes a Quadratic Clustering-Based Simplex Volume Maximization (CSVM) approach for hyperspectral endmember extraction, aiming to effectively mitigate spectral variability and extract endmembers. Ref Xu et al. (2023) proposes a method, Manifold Regularized Sparse Archetype Analysis, that considers endmember variability in unmixing hyperspectral data.

Table 2.1: Advantages and Limitations of Selected EEAs

Method	Author	Year	Merits	Demerits
PPI	Boardman et al.	1995	Pure signatures	Computaionally complex
CCA	Ifarraguerri et al	1999	No initialization	Eigenvector domain.
VCA	Nascimento et al.	2005	Better than PPI,N-FINDR	Initialization
N-FINDR	Winter et al.	1999	Fully automated	Inconsistency
SGA	Chang et al.	2006	Pure signatures	Initialization
SSEE	Rogge et al.	2007	Subclass endmembers	Only for high contrast endmembers
HEEA	Li et al.	2011	Integrates spectral and spatial	Optimal window size selection
SCA	Bilgin et al.	2011	Use of similarity measures	Selection of optimum parameter
EE-ABC	Zhang et al.	2015	Near optimal solution	High Computational resources
EE-DFA	Zhang et al.	2017	Robust to noise	Selection of parameters
EndNet	ozkan et al.	2018	Near optimal solutions	High Computational resources

2.1.4 Endmember Initialization

In general, all the EEAs depend on virtual dimensionality (VD) techniques (Chang and Du (2004), Bioucas-Dias and Nascimento (2008), Luo et al. (2013) and Tao et al. (2020)) to estimates the number of endmembers present in data. Few EEAs depend not only on VD techniques but also on appropriate set of initial targets. N-FINDR,VCA and HEEA faces initialization problem. ATGP (Ren and Chang (2003)), UFCLS (Heinz et al. (2001)), and maximin-distance algorithm MDA (Tou and Gonzalez (1974)) serves as endmember initialization algorithms (EIAs) that generates initial endmemeber targets. EEAs utilize the EIA generated initial endmemeber targets to begin the endmember search process. Plaza and Chang (2006) studied the impact of initialization in EE to address the initialization issues EEAs face.

2.1.5 Summary on EEAs

Though EE techniques were developed based on different criterion, the fundamental/basic concept that endmembers being mutually distinctive in nature has not been explored much. Li and Zhang (2011) mentions that so far most EEAs do not consider the correlation and similarity between endmembers. Therefore developing advanced algorithms to retain (i) coherency between spectral signatures of same classes and (ii) spectral variance between signatures of different classes in extracting endmembers (Elmore et al. (2000)) is need of the hour.

Research Gap: The fundamental characteristic of endmebers i.e. spectrally distinctive in nature has not been explored much in EE.

2.2 Spectral Matching Algorithms

Spectral angle mapper (SAM) Kruse et al. (1993) is one of the traditional similarity measures that extracts geometrical features and it measures the deviation of a signature from a reference signature. Spectral correlation mapper (SCM) De Carvalho and Meneses (2000) is similar to SAM but it measures negative correlation also. Spectral information divergence (SID), a stochastic measure, Chang (1999) measures information divergence between spectral signatures by considering them as random vectors. Phase correlation (PC), computes similarity using Fourier transform properties, Erturk and Erturk (2006) due to it's inherent whitening property, is able to detect spectrally similar signatures with ease. Different geometrical distance metrics like euclidean distance (ED) Gower (1985), mahalanobis distance (MD) Palacios-Orueta and Ustin (1996) and jeffries matusita distance (JMD) Richards and Richards (1999) were also considered ed as similarity measures for HSI analysis. Normalized euclidean distance (NED) proposed as a SMA Robila and Gershman (2005) offers computational simplicity while maintaining result accuracy. In Angelopoulou et al. (1999) spectral gradient is computed to identify the grey-scale image of a scene containing combinations of different colors and different materials and shapes under three different color filters with narrow band-pass filters (10nm wide) are tested. Cross correlogram spectral matching (CCSM) Van Der Meer and Bakker (1997) enables a statistically meaningful comparison between test and reference spectra of minerals. Recently proposed dice spectral similarity coefficient (DSSC) Kumar et al. (2021) is also a geometrical similarity measure like SAM

but showed better performance in discriminating different spectral signatures. Li et al. (2014) proposed Extended SAM (ESAM) to detect citrus greening disease in plants. Du et al. (2004) used hybrid similarity measure SAM-SID to measure both similarity and dissimilarity effectively. SAM-SID is obtained by multiplying their individual values and performance was evaluated using spectral discriminating measures proposed by Chang (1999). Researchers came up with other hybrid similarity measures like SCA-SID Kumar et al. (2011), JMD-SAM Padma and Sanjeevi (2014).

In literature different similarity measures were used and their effectiveness in classification of hyperspectral data is reported (Van der Meer (2006), Kong et al. (2010), Chauhan and Mohan (2014) and Adep et al. (2016)). In addition to that, impact of different similarity measures in clustering web documents (Strehl et al. (2000)) and text documents (Huang (2008)) were reported. A comparison study on different metrics to study the quality of spectral matching is carried out in Imai et al. (2002). Influence of scaling and offset in measuring correlation by a few SMAs is presented in Table 2.2.

Though similarity measures were developed to discriminate the spectral signature using different theoretical strategies, identification of diagnostic features and thereby capturing the overall patterns of spectrally distinct signatures, especially of mineral signatures which exhibit subtle differences among themselves, with the existing SMAs is still a difficult task.

Table 2.2: Impact of Scaling and Offset on Correlation Measurements by Various SMAs

SMAs	Author	Correlation	Offset	Scaling
SAM	Kruse et al. 1993	Positive	No effect	No effect
SID	Chang et al. 1999	Positive	Slightly affects	No effect
SCM	De Carvalho et al. 2000	Both positive and negative	No effect	No effect
PC	Erturk et al. 2006	Both positive and negative	No effect	No effect
SAM-SID	Du et al. 2004	Positive	Slightly affects	No effect
SCA-SID	kumar al. 2011	Both positive and negative	Slightly affects	No effect
JMD-SAM	Padma et al., Sanjeevi et al. 2014	Positive	affects	affects

Research Gap: Existing SMAs do not capture diagnostic features of spectra in discriminating them.

2.3 Hyperspectral Change Detection

2.3.1 Classical CD Algorithms

Classical CD algorithms include change vector analysis (CVA) Malila (1980) and slow feature analysis (SFA) Wu et al. (2013). CVA finds the magnitude of change, at pixel level, from time-1 to time-2 data to detect the changes by selecting an appropriate threshold. SFA algorithm tries to detect changes by discriminating the slowly varying features to fast varying features. A pixel pair algorithm (PPA) Ayhan and Kwan (2019) and a homogeneous pixel transformation (HPT) Liu et al. (2017) are proposed to detect changes using heterogeneous data. PPA aims to detect changes from the change map obtained from pixel pair differences of the bi-temporal data sets. HPT carries out converting both the data sets onto a common feature space to detect changes. However, these traditional algorithms are not so effective because of only spectral information is considered to detect changes in a pixel by pixel manner. Other classical techniques include some of the transformation based approaches like multivariate alternative detection (MAD) Schott et al. (1988) and principal component analysis (PCA) based CVA Baisantry et al. (2012) try to transform the shallow image features into a new feature space where changed to unchanged information is captured more efficiently. Recently, Principal Components Space Data Clustering Li et al. (2022) is investigated to address HSI-CD. These algorithms are not only computationally complex but also pose challenges in detecting changes.

2.3.2 Deep Learning based CD Techniques

Deep learning (DL) based models like a general end-to-end 2-D CNN (GETNET) Wang et al. (2018), Deep SFA architecture (DSFA-NET) Du et al. (2019a) and a three directions spectral–spatial convolution neural network (TDSSC) Zhan et al. (2020) were proposed for HSI CD tasks. GETNET uses affinity matrix calculated from original features and unmixing features of the data sets. DSFA-NET extract deep features of the CD data sets so that changes can be detected in a better manner with SFA algorithm. TDSSC extract spectral features as well as spectral-spatial features to detect changes effectively. Performance of TDSSC is superior to most existing CD algorithms Zhan et al. (2020). Though DL models are superior to other CD approaches because of their powerful learning ability to capture the high level deep features to detect changes, their dependency on pseudo-training samples gener-

ated by unsupervised CD approaches like classical CVA and non-homogeneity issues related to multi-temporal data make them not able to provide an universal or a straight-forward solution to general HSI-CD tasks.

Recently a CNN framework involving slow-fast band selection (SFBS) and feature fusion grouping (SFBS-FFGNET) Ou et al. (2022), a multiscale diff-changed feature fusion network (MSDFFN) Luo et al. (2023) and an end-to-end Siamese CNN (SiamNet) with a spectral–spatial-wise attention (SSA-SiamNet) mechanism Wang et al. (2021) are introduced to address HSI-CD. Ref. Guo et al. (2021) and Seydi and Hasanlou (2021) investigate DL and spectral unmixing based approaches to address HSI-CD. Other HSI-CD techniques include a a joint spectral, spatial, and temporal transformer (SST-Former) Wang et al. (2022) and a spectral–spatial feature extraction based on a simplified 3-D convolutional autoencoder (S3DCAECD) Zhao et al. (2021). A spatial–spectral attention mechanism for landcover CD using RS images has been presented in Lv et al. (2022b). A novel method investigating multiple morphological profiles (MMPs) Hou et al. (2021) that fuses the spatial and the spectral features effectively, achieves better detection performance.

2.3.3 Summary on CD Techniques

A review on DL based CD techniques for RS images Bai et al. (2023) including high-resolution (HR) Jiang et al. (2022a) and diverse data sets containing SAR, multispectral, and HSIs Shafique et al. (2022) has been reported in the literature. Other reviews include multi-class CD Zhu et al. (2022), and heterogeneous CD for landcover CD Lv et al. (2022a) using RS images.

Though there are many classical and DL based algorithms, either their performance is not so better or the final performance, especially of DL based CD algorithms, depends on efficiency of pre-change detection algorithms, that give prior knowledge on changed and unchanged samples from CD data sets, due to unavailability of ground-truth data. Recently, topological structure based approaches Lei et al. (2020) and Sun et al. (2021) that provide relationship between local regions of the image are developed to detect the changes in heterogeneous data sets. Forming pixel pair relations or construction of topological structure based graphs is certainly a complex task and this motivates us to make a proposition that choosing/designing topological structure based approaches to identify changes is not only a challenging but also an arduous task.

Though there are many classical and deep learning (DL) based algorithms to detect changes, either their performance is not so better or the final performance depends on efficiency of pre-detection algorithms. In addition, there is not much comprehensive study on developing CD algorithms that not only simple to use but also as efficient as that of DL based algorithms is available.

Research Gap: There are not many studies on developing CD algorithms that not only simple to use but also as efficient as that of DL based algorithms.

2.4 Mineral Identification

Mineral identification and its accuracy depends on extraction of optimum endmember which is used as reference spectrum for classification, similarity measures to distinguish similarity and dissimilarity between pixel spectrum and endmember, and dimensionality reduction techniques for extracting optimal features for classification. Applications of hyperspectral data classification include mineral identification and classification. The success of classification of hyperspectral data in any application especially mineral identification and mapping depends on algorithms used for classification. Few more details about algorithms used for classification of hyperspectral data are discussed in the following section.

- Clark and King (1987) used Segmented Upper Hull(SUH) algorithm to study the continuum of spectra. This study is useful in analysing the width and height of absorption bands which are are the most important discriminating features for classifying minerals.

- Spectral curve fitting analysis Brown (2006) of hyperspectral mineral data makes identification of distinct mineral endmembers easy by estimating their central wavelength of absorption band and also amplitude and width of absorption band.

- Few expert systems were developed such as SAM classifier (Kruse et al. (1993)), Tetra-coder (Clark et al. (2003)), X-Ray diffraction (Koerting et al. (2015)), EnGeoMAP2.0 (Mielke et al. (2016)) using their domain knowledge for different applications. These algorithms performs better than classical algorithms but accuracy is not very good and also accuracy assessment doe snot involve consideration of other class minerals for their true accuracy.

- Adep et al. (2017b) proposed EXhype to classify the minerals using SAM values of segmented spectrum with SUH and obtained very good accuracy(90.75 percent). This is a binary classification algorithm and needs binary classifiers equal to the number of mineral classes. Since it is binary classifier and number of features for each classifier depends on number of segments of that particular mineral class endmember. So ANN design is complex and also time consuming.

- K-means results applied to end member data considered for training SVM to classify new mineral data Gupta and Venkatesan (2020). An improved K-means algorithm Ren et al. (2020) is used with combined spectral matching to match the clustering results with a spectral library.

- An attenuation spectral absorption index vector (ASMLP)-based multi-layer perceptron (MLP) model Deng et al. (2021) was introduced to capture hierarchical features, enhancing the precision of mineral identification.

- Using reference spectra, a normalized cross-correlation algorithm is employed to identify four distinct corrosion minerals De Kerf et al. (2022).

- The study in Agrawal and Govil (2023) presents a deep residual convolutional neural network designed for mineral classification and introduce two innovative deep learning frameworks for mineral classification: mineral-CNN-LSTM and mineral-ResNet.

Few of the studies explored drill-core HSI data Contreras et al. (2020), Tuşa et al. (2020) De La Rosa et al. (2021) for mineral mapping . Few other studies like Yousefi et al. (2020) explored e longwave Infrared (LWIR) HSI and Ni et al. (2020) explored hyperspectral visible/near-infrared (VNIR) and shortwave infrared (SWIR) data with the hyperspectral thermal infrared (TIR) data and HSI data for mineral mapping. Remaining studies presented in Kumar et al. (2020) and Tsubomatsu and Tonooka (2023) use hydrothermal alteration data and multispectral data respectively for mineral mapping. A comparative analysis of mineral mapping for hyperspectral and multispectral imagery can be found in Vignesh and Kiran (2020).

The classical SAM classifier a simple model and do not yield high accuracy and ExHype is a binary classifier and therefore complex to train binary classifier modules equal to the number minerals to be classified and obtain thresholds to gain accuracy.

Research Gap: Though there are many advanced algorithms like machine learning techniques were designed for HSI classification, there is no DL based expert system specifically for mineral classification is available.

2.5 Research Gaps

Based on the research gaps identified in the literature review carried out on the different themes of the research work presented in Chapter 2.1 - Chapter 2.4, overall research gaps are presented here.

- The fundamental characteristic of endmebers i.e. spectrally distinctive in nature has not been explored much in EE.
- Existing SMAs do not capture diagnostic features of spectra in discriminating them.
- There are not many studies on developing CD algorithms that not only simple to use but also as efficient as that of DL based algorithms.
- Though there are many advanced algorithms like machine learning techniques were designed for HSI classification, there is no DL based expert system specifically for mineral classification is available.

2.6 Objectives of The Thesis

Based on the literature gaps identified, development of endmember extraction algorithm, investigating on targets of interest for endmember initialization, designing new spectral matching algorithms and study their influence on target discrimination and exploring deep learning techniques for mineral identification and change detection applications have been identified as the research objectives.

- To devise EEAs, that explore spectrally distinctive nature of endmembers with the help of SMAs, for the generation of distinct endmembers.
- To develop a novel spectral matching algorithm that captures the diagnostic features of endmembers for effective discrimination.

- To design a simple yet effective algorithm to detect changes in HSI and explore deep learning techniques in mineral classification.

Summary:

This chapter detailed the summary on the literature review and discusses the objective of this research work identified from the research gaps. The literature review was focused on Endmember extraction, spectral matching, change detection and mineral classification topics that are considered for this research. ”Spectrally distinctive nature of endmembers being not explored much in identifying or extracting them” has been identified as a research gap. An effective spectral matching capturing/highlighting diagnostic features of the spectral signatures is missing. Exploring sub-pixel level features instead of simple pixel level features to detect changes in HSI data is considered as a research gap for this research work on HSI-CD. Addressing challenges in mineral classification to explore DL algorithms has been identified as an another research gap.

The next chapter presents experimental data sets used for this research work.

Chapter 3

Experimental Data

> In the *Manu-saṁhitā* it is clearly stated that a woman should not be given freedom. That does not mean that women are to be kept as slaves, but they are like children. Actually, a woman should be given protection at every stage of life.
>
> Bhagavad-gita As It Is 16.7, A.C. Bhaktivedanta Swami Prabhupāda

Introduction

This chapter provides an overview of the experimental data used to address the research objectives. It includes hyperspectral unmixing datasets, comprising four real datasets and one synthetically generated dataset, employed for endmember extraction and spectral matching tasks. Additionally, details on three widely-used hyperspectral datasets for change detection applications and a benchmark hyperspectral dataset for mineral identification are presented.

Based on the objectives identified, different kinds of HSI data sets that are available exclusively for unmixing, change detection and classification are chosen for the experimentation purposes. The complete details regarding above mentioned categories of HSI data sets are described below.

3.1 HSI Data for Unmixing

The hyperspectral data sets used in the experiments include four real data sets: Samson, Jasper Ridge, Urban, and Cuprite, as well as a synthetic mineral data set. These data sets were selected based on the presence of targets with both spectrally distinct and subtle differences in their signatures. The four real hyperspectral data sets are shown in Figure 3.1. Subsets of

these data sets, along with the reference endmember signatures manually picked from them, are available online[1] for research purposes.

(a) Samson (b) JR data (c) Urban (d) Cuprite

Figure 3.1: Real Hyperspectral Data Sets for Unmixing Experiments

3.1.1 Samson Data

The Samson data set (SD) is a subset of the larger Samson data, and has three endmembers: Soil (Sl), Trees (Tr), and Water (Wt). The first eight bands were removed from this subset, as some pixels in those bands contained no information. The size of the Samson subset is $95 \times 95 \times 148$.

3.1.2 Japser Ridge Data

The Jasper Ridge data set (JR) is a popular hyperspectral data set used in unmixing applications. The size of the sub-image used in this study is $100 \times 100 \times 198$, and it contains four endmembers: Road (Rd), Soil (Sl), Water (Wt), and Trees (Tr).

3.1.3 Urban Data

The Urban data set (UR) is widely used in hyperspectral unmixing studies. The size of the image is $307 \times 307 \times 162$, and it contains six endmembers: Asphalt (As), Grass (Gr), Tree (Tr), Roof (Rf), Metal (Mt), and Dirt (Dr).

3.1.4 Cuprite Data

The Cuprite Scene (CS) is a subset of the Airborne Visible/Infrared Imaging Spectrometer (AVIRIS) data captured with an ER-2 aircraft. The Cuprite subset used in this study has a size

[1] http://lesun.weebly.com/hyperspectral-data-set.html

of 250×190 and 187 spectral bands, and contains minerals such as Alunite (Al), Andradite (An), Buddingtonite (Bu), Dumortierite (Du), Kaolinite1 (K1), Kaolinite2 (K2), Muscovite (Mu), Montmorillonite (Mo), Nontronite (No), Pyrope (Py), Sphene (Sp) and Chalcedony (Ch).

3.1.5 Synthetic Data

Finally, a synthetic data set (SY) consisting of 15 minerals was generated for the study. This data set has a size of 90000×224 ($N \times L$, where N is number of pixels and L is number of bands), and the minerals included are Alunite (Al), Andradite (An), Buddingtonite (Bu), Calcite (Ca), Chalcedony (Ch), Chlorite (Cl), Desert Varnish (Dv), Dickite (Di), Dumortierite (Du), Kaolinite (Ka), Montmorillonite (Mo), Muscovite (Mu), Nontronite (No), Pyrope (Py), and Sphene (Sp). The data was generated without adding any noise using a method described in Bioucas-Dias and Nascimento (2008). Although there are numerous mineral classes available, the research focuses on identifying only fifteen mineral classes, most of which are abundant in the Cuprite area.

3.2 HSI Data for CD

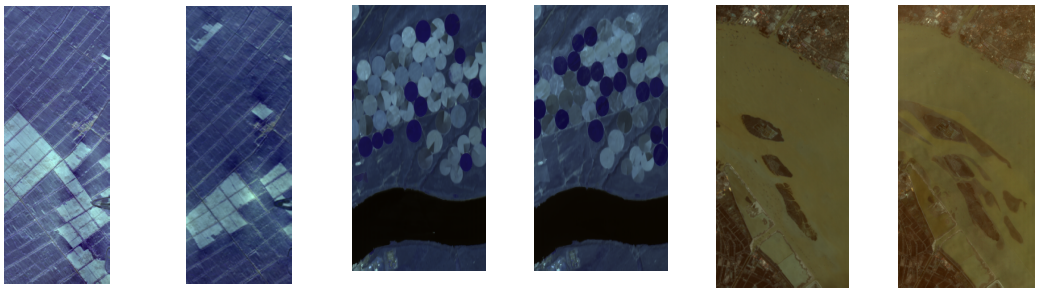

(a) China T-1 (b) China T-2 (c) USA T-1 (d) USA T-2 (e) River T-1 (f) River T-2

Figure 3.2: Benchmark HSI Data Sets for Change Detection Experiments

To evaluate the proposed algorithm's change detection capabilities, three benchmark HSI datasets are selected. The first two, namely the China and USA datasets, are standard datasets with accompanying ground truth, accessible online[2]. The third dataset, known as the "River"

[2]https://rslab.ut.ac.ir/data

dataset, is also utilized for change detection analysis and is accessible online[3]. Figure 3.2 visually represents all the change detection datasets.

3.2.1 The China Data Set

The China data set time-1 and time-2 were acquired near the city of Yuncheng Jiangsu province in China on May 3, 2006, and April 23, 2007 respectively. The China data set belongs to a farmland near the city of Yuncheng Jiangsu province. Size of the China (Farmland) is $307 \times 241 \times 154$.

3.2.2 The USA Data Set

The USA data set time-1 and time-2 were acquired over Hermiston city in Umatilla County, Oregon, OR, the USA, on on May 1, 2004, and May 8, 2007, respectively. The USA data set belongs to an irrigated agricultural field. Size of the USA data sets is $420 \times 140 \times 154$.

3.2.3 The River Data Set

Time-1 and time-2 data sets were captured on a riverbank taken on May 3 and December 31,2013 respectively. The river data set contains 436×241 pixels and 198 bands.

3.3 HSI Data for Mineral Classification

In this investigation, a real hyperspectral data obtained over the Cuprite region is employed to examine the abundance of diverse minerals. Collected via the Airborne Visible/Infrared Imaging Spectrometer (AVIRIS) during an ER-2 aircraft mission in the USA, particularly in Nevada, the dataset provides valuable insights. Figure 3.3 displays the RGB image of the Cuprite scene.

This image contains 224 contiguous bands of data from wavelength 0.38-2.5 micro meters with 10 nanometers interval. The size of image is 522×601 pixels and pixel resolution 15.5m $\times$ 15.5m on the site. Bands with poor information because of low signal to noise ratio (SNR) and water absorption are treated as bad bands (1-3, 104-113, 148-167 and 221-224) and removed.

[3] http://crabwq.github.io

Reasons for selecting hyperspectral data over this region are: (i) it have good exposure of several minerals and their abundance (ii) it is freely available at website[4] for research purpose and (iii) availability of ground truth. United States Geological Survey (USGS) spectral library provides the ground truth signatures for various minerals.

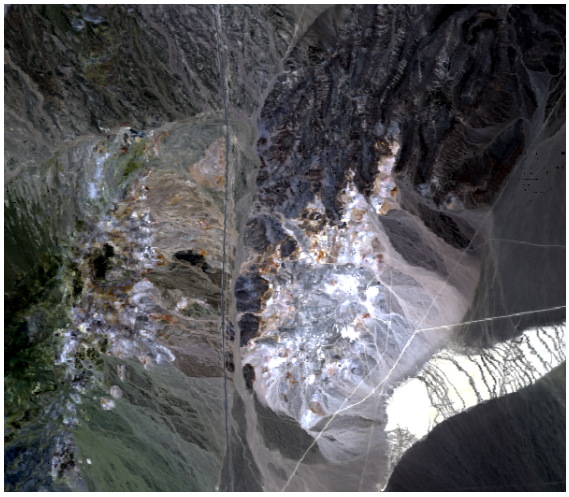

Figure 3.3: AVIRIS Cuprite Scene (Nevada): Real HSI for Mineral Exploration

3.4 HSI Data for Landcover Classification

To explore and assess the effectiveness of the proposed algorithm for landcover classification using hyperspectral imaging data, three benchmark datasets are employed. These datasets include the Pavia University (PU) dataset, the Washington DC Mall (W DC mall) dataset, and the Indian Pines (IP) dataset. While PU and W DC mall datasets offer distinct landcover classes, the IP dataset, although lacking exclusive classes, provides valuable information for landcover analysis and classification tasks. These data sets are available at online at website[5] and website[6] for research purposes. Figure 3.4 shows all the three data sets.

3.4.1 University of Pavia

This scene was captured by the ROSIS sensor during a flight campaign over Pavia, a city in northern Italy. Pavia University used 103 spectral bands for their data. The Pavia University image is 610×610 pixels, but some samples in the image don't have useful information and need to be removed before analysis. The image has a resolution of 1.3 meters. There are

[4] www.harrisgeospatial.com
[5] https://rslab.ut.ac.ir/data
[6] http://lesun.weebly.com/hyperspectral-data-set.html

9 different classes, ie. the asphalt, meadows, gravel, trees, metal sheet, bare soil, bitumen, brick, and shadow, in the image's ground truth.

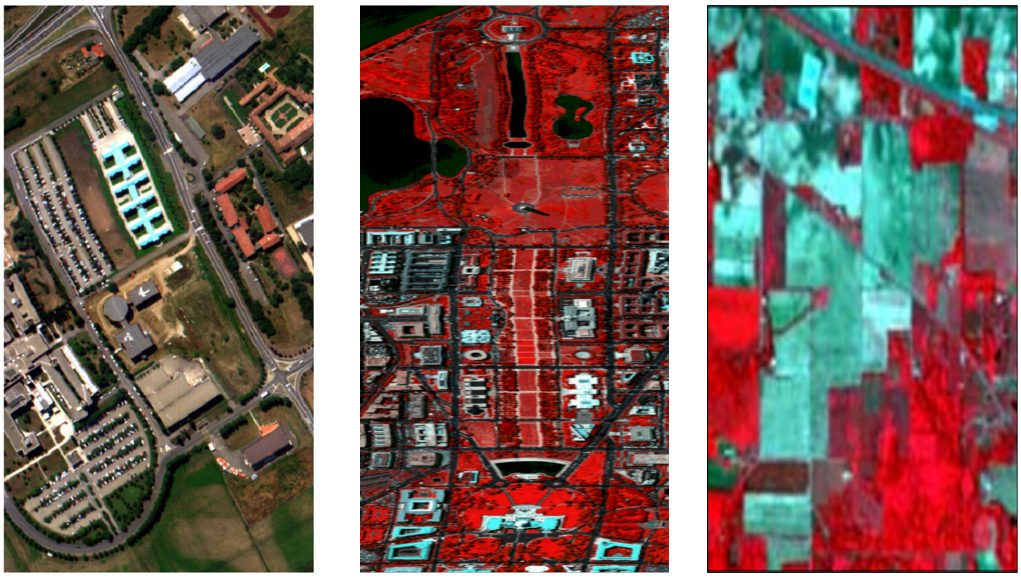

(a) Pavia (b) DC Mall (c) Indian Pines

Figure 3.4: Benchmark Datasets for Land Cover Classification using HSI Data

3.4.2 Washington DC Mall

The figure shows a simulated color IR view of an airborne hyperspectral data flight line over the Washington DC Mall. The sensor system measured pixel response in 210 bands from 0.4 to 2.4 µm, but excluded bands in the 0.9 and 1.4 µm range due to atmospheric opacity. This resulted in a dataset of 191 bands. The data set contains 1208 scan lines with 307 pixels per scan line. In the Washington DC Mall dataset, there six classes that include Water, Trees, Grass, Roads, Roof, and Shadows are present. Additionally, there are unlabeled samples present in the dataset, which do not belong to any specific class.

3.4.3 Indian Pines

AVIRIS captured this scene over Indian Pines test site in Indiana. It's a 145×145 pixel image with 224 spectral bands from 0.4–2.5 µm. It's a subset of a larger image. The scene contains two-thirds agriculture, one-third forest, roads, highways, housing, and a rail line. Crops like corn and soybeans are in early growth stages, covering less than 5%. Ground truth has sixteen classes, not all mutually exclusive. The Indian Pines dataset is primarily a crop classification dataset, featuring subclasses like alfalfa, corn (notill, mintill, clean), grass/pasture,

oats, soybeans (notill, mintill, clean), and wheat. It also includes classes for wooded areas, buildings with grass, trees, driveways, and bare soil. We reduced bands to 200, excluding water absorption regions: [104-108], [150-163], and 220.

Summary:

This chapter presents details on experimental data considered to explore and address the objectives formed in this research. Hyperspectral unmixing data sets that include four real and synthetically generated hyperspectral data considered for endmember extraction and spectral matching related tasks are presented. Details on three popular hyperspectral data sets available for HSI-CD applications and a bench mark hyperspectral data for mineral identification are also presented.

The next chapter presents research work on endmember extraction.

Chapter 4

Endmember Extraction

> *Brāhmanas* are the symbol of spiritual education, and *cows* are the symbol of the most valuable food; these two living creatures, the *brāhmanas* and the *cows*, must be given all protection — that is real advancement of civilization.
>
> Bhagavad-gita As It Is 14.16, A.C. Bhaktivedanta Swami Prabhupāda

Introduction

This chapter investigates the critical task of EE, specifically exploring the unique nature of endmembers. We propose and analyze Similarity Measures-Based Endmember Extraction Algorithms (SMEEAs), particularly SM-SCA and SM-EIA, emphasizing the importance of endmember initialization. The introduction sheds light on our exploration of the darkest pixel as a Target Pixel of Interest (TPOI) and its synergies with the brightest pixel, showcasing significant improvements in EE performance. Additionally, the Corner-Driven Iterative Clustering Algorithm (CDIC) takes the spotlight, not only identifying endmembers but also providing valuable samples for subsequent HSI analyses. These investigations lay the groundwork for a comprehensive understanding of EE methodologies.

Though several EEAs are developed, SMAs have not been explored much in the extraction of spectrally distinct signatures. Therefore, in this work, a similarity measures based endmember extraction algorithms (EEAs) are proposed to explore the fundamental characteristic of endmembers, i.e. spectrally distinctive in nature, in identifying and extracting them. Present study on EE considers pure pixel assumption and follows linear unmixing.

4.1 Similarity Measures based Endmember Extraction Algorithms (SMEEAs)

Present study considers exploring similarity measures in designing EEAs to identify spectrally distinct endmembers and therefore the proposed EEAs are termed as similarity measures based EEAs (SMEEAs). A similarity measures based subtractive clustering algorithm (SM-SCA) proposed to identify spectrally distinct and abundant endmembers is presented below. SCA tries to identify abundant materials by clustering HSI data samples and similarity measures tries to identify spectrally distinct signatures. Therefore, SM-SCA makes sure identified endmembers are spectrally distinct as well as abundant.

4.1.1 SM-SCA

Classical SCA (Chiu (1994)) is an improved version of the mountain method Yager and Filev (1994) that effectively identify clusters present in the HSI data. The cluster centers of the identified clusters are considered as the endmembers that represent the different targets/earth-surfaces present in the data. SM-SCA is a modified version of classical SCA. SCA uses distance metric (square of ED) in finding mountain function value whereas SM-SCA utilizes similarity measures. In the beginning, SM-SCA considers every sample as an individual cluster center and finds the mountain function value using equation

$$M(x_i) = \sum_{j=1}^{n} SMA(x_i, x_j) \tag{4.1}$$

where SMA is a spectral matching algorithm and n is total number of samples to be clustered. The sample having maximum mountain value is considered as the first clustering center and it is identified using Eq. 4.2.

$$M_1^{max} = \max_i(M(x_i)) \tag{4.2}$$

The mountain function values of samples belongs to first cluster are as high as that of their cluster center. Therefore, in order to to avoid samples from the first cluster to be identified as the next cluster center, the mountain function needs to be updated. In the updated mountain function a quash distance/similarity factor that controls the closeness/similarity is used in order to suppress samples from first cluster and identify the second cluster center

from distinct/dissimilar/new cluster. The updated mountain function is given by Eq. 4.3.

$$M^k(x_j) = M^{k-1}(x_j) - M_{k-1}^{Max}.(\alpha.SMA(x_j, x_{k-1}^{max})) \tag{4.3}$$

where α is a positive constant used as a quash distance factor Bilgin et al. (2011) and k=2,3,...,N. N is the estimated VD. Typically, exponential, linear or triangular function can be used for calculating the mountain function value Yager and Filev (1994), in this work a linear function for SM-SCA and an exponential function for classical SCA are considered.

The sample having maximum mountain value obtained from the updated mountain function (Eq. 4.3) is identified as the second cluster center. Similarly, remaining cluster centers are identified by avoiding samples from previously identified clusters using the the updated mountain function. This procedure is repeated until desired number of cluster centers are identified.

Selection of α

In classical SCA algorithm, there is no specific criterion is proposed to fix the value of α, rather it is fixed experimentally. Selection of α is not only difficult but also a laborious task when applied on new data set. The fundamental concept in hyperspectral data that endmembers contribute to maximum volume of simplex formed by the HSI data cube is explored to fix α. N-FINDR and SGA work based on this principle only. Hence, the value of α for which SM-SCA extracted endmembers contribute to maximum volume is selected as the optimum value of α.

Performance Evaluation

The accuracy/closeness of extracted endmember signatures (EEMs) from real and synthetic hyperspectral data is mentioned in terms of spectral angle distance (SAD) values (in degrees) and abundance fractions with respect to the ground truth (GT) endmembers. Lesser the SAD value, more the correlation with corresponding GT endmember and vice versa. To check the overall performance, average SAD values of extracted endmembers is also reported. Bold values represent SAD values of the best endmember set extracted from the experimental data sets.

Experimental Results

Table 4.1: Performance of SM-SCA in EE from Samson, Synthetic and Cuprite Data Sets

(a) EE from Samson Data

EEMs	NFINDR	SGA	OSP	VCA	SCA (ED)	SM-SCA			
						SAM	SID	SCM	PC
Soil	**2.25**	**2.25**	**2.25**	**2.25**	7.74	8.79	6.55	9.41	5.26
Tree	2.81	**1.25**	**1.25**	4.31	2.43	18.90	4.07	4.31	2.85
Water	68.07	62.66	62.66	7.50	13.59	42.03	7.50	**5.75**	6.31
Avg SAD	24.38	22.05	22.05	**4.69**	7.92	23.24	6.04	6.49	4.81

(b) EE from Synthetic Data

EEMs	NFINDR	SGA	OSP	VCA	SCA (ED)	SM-SCA			
						SAM	SID	SCM	PC
A	1	1	1	1	0.38	0.36	0.43	0.47	0.20
B	1	1	1	1	0.68	0.31	0.31	0.58	0.96
C	1	1	1	1	0.87	0.37	0.32	0.27	1
Ch	1	1	1	1	0.85	0.38	0.27	0.34	1
K	1	1	1	1	0.88	0.22	0.09	0.27	0.73
Avg	**1**	**1**	**1**	**1**	0.73	0.33	0.28	0.39	0.65

(c) EE from Cuprite Data (Overall performance in Avg SAD)

EEMs	NFINDR	SGA	OSP	VCA	SCA (ED)	SM-SCA			
						SAM	SID	SCM	PC
Avg SAD	**5.18**	5.43	5.41	5.41	5.63	6.55	7.10	6.49	6.16

(d) Alpha (α) Values Obtained for Better Performance by SM-SCA with Various SMAs

Similarity Measure	Synthetic Data	Samson Data	cuprite Data
ED	0.45	0.30	1.45
SAM	0.70	0.85	0.50
SID	0.50	4.80	0.35
SCM	0.90	1.35	0.50
PC	2.25 38	2.35	0.40

The applicability of SM-SCA in endmember extraction is studied using simple similarity measures like SAM, SID, SCM and PC. The performance in endmembers extraction by classical EEAs like N-FINDR, SGA, OSP, VCA and proposed SCA and SM-SCA with different similarity measures, on three experimental data sets is presented below.

Samson Data

From Table 4.1a illustrates that the performance of proposed SM-SCA is better than classical SCA and classical EEAs except VCA which is inconsistent in endmember extraction. Classical EEAs other than VCA, failed to extract Water spectral signature though it is different from Soil and Trees signatures. Whereas, SCA and SM-SCA with all the similarity measures except SAM are identified all the three endmember signatures (including Water) present in the data. Spectrally distinct pixels which may not contribute to maximum volume are avoided from being extracted as the endmembers might be the reason for poor performance of classical EEAs. Among similarity measures used with SM-SCA, PC showed better performance compared to other similarity measures.

Synthetic Data

Classical EEAs performed well in EE from synthetic data and the same is shown in Table 4.1b. N-FINDR is initialized with ATGP, that utilizes the concept of OSP as that of VCA, generated targets. In case of high signal to noise ratio (SNR), OSP perform better. This might be the reason why classical EEAs are performing well with synthetic data.

Performance of SM-SCA in EE from synthetic data is good with PC only. SM-SCA with PC able to identify pure endmembers for Calcium and Chloromuscovite but with other similarity measures not able to perform well in discriminating and identifying pure endmembers. The poor performance of SM-SCA in terms of endmembers purity reveals that mixed pixels become more in population and forming better classes than pure endmembers with their corresponding classes with respect to spectral similarity. Because of this reason, spectrally distinct mixed pixels instead of pure pixels are identified as endmembers. From this it can be inferred that if a mixed pixel is identified as a endmember then there is a high chance for mixed pixels to be identified as the subsequent endmembers. Therefore results suggest that SCA and SM-SCA require endmember initialization in order to avoid spectrally distinct mixed pixel identification but identify pure endmembers and thereby perform better in

endmember extraction.

Cuprite Data

The Table 4.1c illustrates that performance of the classical EEAs are better than SCA and SM-SCA. Since NFINDR is initialized with ATGP (an OSP based EEA) and SGA is an improved version of NFINDR, performance of NFINDR, SGA and OSP is almost similar. Overall, the performance of SCA and SM-SCA are comparable to that of Classical EEAs.

Among SCA and SM-SCA, performance of SCA is somewhat better than SM-SCA. The term, square of ED in calculating mountain value using Eq. 4.1 might be increasing similarity between same endmember class minerals and dissimilarity between different endmember class minerals. Hence, this might be the reason for this difference in performance of SCA and SM-SCA.

Performance of SCA and SM-SCA

The reasons for SCA and SM-SCA not to perform up-to the level of classical EEAs in case of synthetic dataset and the factors that may improve the performance of SM-SCA in endmember extraction are discussed in this section.

SAM and SCM are similar in nature. SAM measures positive correlation only whereas SCM measures negative correlation as well. SID measures information divergence. However, PC measures the similarity between spectral signatures by transforming them into frequency domain to extract curvature information. Hence, this may be the reason that SM-SCA with PC is able to identify better endmembers than with other similarity measures and perform comparably good to that of classical EEAs.

Though the performance of SM-SCA depends on similarity measures, PC identified all endmembers from the three data sets used in this experiment in a better manner than other similarity measures. Using square of similarity metric and nonlinear function to measure mountain value may improve the performance of the proposed algorithms. And, hybrid combination of similarity measures may improve the performance of SM-SCA further.

Influence of Initialization on Endmembers Extraction

Overall performance of SM-SCA is good with PC only, where as with other similarity measures not able to perform well in identifying pure endmembers. The possible reason for the

poor performance of SM-SCA might be initialization of endmembers. The first endmember has maximum mountain value, that means first endmember is similar to the almost many pixels in the image, causing it to become less pure. If first endmember is less pure, then there are more chances for subsequently identified endmembers also to become less pure.

Influence of α

The performance of SM-SCA with similarity measures in extracting endmembers from all data sets is observed by varying the α value from 0 to 5 in step size of 0.05. Since SM-SCA depends on similarity measures in extracting endmembers and effectiveness of different similarity measures is not same in discriminating mineral endmembers, it is observed that α values to get better performance are different for different similarity measures. The reasons for this is that the inter and intra class variations among spectral signatures and effectiveness of similarity measures in distinguishing spectrally distinct endmembers. The values of the quash distance factor (α) for ED (with SCA), SAM, SID, SCM and PC for better performance in extracting endmembers from the data are shown in the Table 4.1d.

Though the selection of (α) is not a difficult task of this algorithm, the performance of the algorithm depends on it and this may not be helpful to improve the performance of the algorithm in extracting optimal endmembers. Not only initialization of first endmember but also spectral variance among endmembers becomes a reason for reduction of purity of endmembers to be identified subsequently (especially in case of synthetic data) with SM-SCA. Selection criteria proposed to fix α may handle spectral variance among endmembers to some extent but not fully because of unequal spectral variances among endmembers. Optimizing α, that controls distance/similarity between clusters, every time a new endmember need to be identified and along with an appropriate endmember initialization can be a solution to avoid spectrally distinct mixed pixels to be identified as endmembers. Otherwise, this problem can be solved by avoiding the parameter (α) in the extraction of endmembers using similarity measures will be investigated in the further experimentation.

Inferences

- Experiments carried in this work reveal that similarity measures have potential not only in discrimination but also in identification of spectrally distinct signatures.
- Experimental results show the power of proposed SM-SCA in identifying spectrally

distinct endmembers of different land covers (Samson data) in a better manner over the classical EEAs.

4.1.2 SM-EIA

Based on the improvement factors suggested for SM-SCA, a new SMEEA that can generate spectrally distinct signatures as the initial endmember target signatures which provide a good idea on actual endmembers is developed. EEA that generates initial endmember target signatures is termed as EIA. Therefore, the proposed EIA is called as SM-EIA.

Inspired by farthest first traversal, SM-EIA is developed to identify spectrally distinct signatures as initial endmember targets. In farthest first traversal, first sample is selected in a random manner. Whereas, SM-EIA selects a pixel with maximum length, also called as the brightest pixel, to avoid a mixed pixel as a first endmember. The length of a spectral signature is calculated as norm using

$$norm(i,j) = \sqrt{\sum_{k=1}^{L} HSI(i,j,k)^2} \tag{4.4}$$

where (i,j) represents pixel location, k the band number of input HSI data and L is the number of bands. Location of the brightest pixel e_1 is identified using

$$(a_1, b_1) = \max_{i,j}(norm). \tag{4.5}$$

The initial endmember e_1 is extracted from the HSI data as

$$e_1 = HSI(a_1, b_1, k)_{k=1}^{L} \tag{4.6}$$

Then the similarity of spectral signatures of all the pixels of HSI data with initially generated endmember target signature is measured using spectral similarity value (SSV)

$$SSV(i,j) = SMA(HSI(i,j), e_1) \tag{4.7}$$

Then, a pixel which is distinct from (more dissimilar to) the first endmember is extracted as next endmember. Higher similarity value represents more similarity and lower similarity value represents less similarity. A pixel with the lower similarity value is considered to be

more dissimilar and generated as next target endmember e_2 using

$$(a_2, b_2) = \min_{i,j}(SSV). \tag{4.8}$$

A pixel which is distinct (less correlation, i.e lower similarity value) simultaneously from both the endmember signatures is considered as third endmember e_3. Similarly, remaining endmembers $(e_n)_{n=3}^{VD}$ are extracted as the pixels whose signatures are more dissimilar to the already extracted endmember subset E_n. Where $E_n = (e_1, e_2, ..., e_n)$. Therefore, in a generalized form, the locations of next target endmember to be generated is identified as

$$(a_n, b_n) = \max_{i,j}(SSV(HSI, E_{n-1})) \tag{4.9}$$

where

$$SSV(HSI, E_{n-1}) = \min(SSV(HSI, e_1), SSV(HSI, e_2), ..., SSV(HSI, e_{n-1})) \tag{4.10}$$

This procedure is repeated till the required number of endmembers (i.e VD) are generated. Proposed SM-EIA is actually a detailed implementation of MDA Plaza and Chang (2006) using various similarity measures.

Experimental Results

ATGP Ren and Chang (2003), a popular EIA, is adapted to compare the performance of SM-EIA proposed in this study to generate spectrally distinct signatures. Closeness of EIA generated targets in referring to the GT endmembers is measured in terms of SAD in degrees.

Samson Data

Table 4.2a presents SAD values between the targets generated by ATGP and SM-EIA with different similarity measured used and ground truth endmembers. It is can be seen that, ATGP is not able to identify water signature though distinct from rock's and tree's. This implies that water signature is neither the brightest pixel nor contributes to the maximum projection length in orthogonal subspace spanned by the already generated targets and if it is true, selection of the very first target signature must also be playing an important role in generating initial set of endmembers. In such case, selecting the brightest pixel, that has

maximum length, as an initial or very first target/endmember is not sufficient for generating a reasonable/better set of initial endmember signatures. Since popular EIAs and EEAs rely on pixel with maximum length to be chosen as the very first target to begin their search process, this issue will be investigated in the future work.

Table 4.2: Effectiveness of SM-EIA in Generating Endmember Target Signatures

(a) Samson Data

EEMs	**ATGP**	**SM-EIA**								
		SAM	**SID**	**SCM**	**PC**	**SAMSID**	**SCMSID**	**PCSID**	**SAMPC**	**SCMPC**
Sl	2.25	15.73	10.55	23.42	51.46	10.25	12.50	9.86	51.46	37.35
Tr	1.25	1.25	1.25	1.25	1.25	1.25	1.25	1.25	1.25	1.25
Wt	62.66	7.50	7.50	6.18	5.82	8.49	8.49	4.47	1.87	6.31
Avg	22.05	8.16	6.43	10.28	19.51	6.66	7.41	**5.19**	18.19	14.97

(b) Overall Performance of SM-EIA on Cuprite Data (Avg SAD)

EEMs	**ATGP**	**SM-EIA**								
		SAM	**SID**	**SCM**	**PC**	**SAMSID**	**SCMSID**	**PCSID**	**SAMPC**	**SCMPC**
Avg	5.41	5.81	5.78	**4.58**	5.25	5.80	5.10	5.21	5.24	5.63

SM-EIA with all the similarity measures is able to identify trees and water signatures properly but not soil's. SAD values of soil are higher for SM-EIA with few similarity measures and same can be found in Table 4.2a. Presence of variation in orientations with no subtle differences in the curvatures of soil and trees signatures made similarity measures to extract deviated/mixed signature, which is distinct from soil signature, as soil target. This might be the reason for hybrid similarity measures, which can improve the similarity between similar targets as well as dissimilarity between different targets, to have little higher SAD values than remaining. Overall performance of SM-EIA with all the similarity measures in generating spectrally distinct targets is better than that of ATGP.

Cuprite Data

SAD values of targets generated by EIAs from Cuprite data to the ground truth endmembers is presented in Table 4.2b and it is understood that SM-EIA with few simple as well as hybrid similarity measures perform better than ATGP while it's performance with remaining

similarity measures are comparable with that of ATGP's. Table 4.2b clearly reveals that the performance of SM-EIA with different similarity measures in capturing different mineral signatures is different. Spectral variations among these mineral signatures and the fashion in which similarity measures capture the diagnostic features of mineral signatures are the possible reasons for SM-EIA to perform differently with different similarity measures. Overall performance of SM-EIA with SCM is better than SM-EIA with remaining similarity measures and ATGP.

4.2 Endmember Initialization

The EIAs provide necessary initialization in terms of initial targets to the EEAs as they rely on appropriate targets. Such initial target signatures so generated, significantly improve the performance of EEAs Plaza and Chang (2006). These EIAs also rely on target pixel of interest (TPOI) to start the search process. The use of TPOI can help reduce the number of false endmembers and improve the accuracy of the endmember identification process. Moreover, TPOI can provide a useful starting point for the initialization to the EIAs

The selection of TPOI is crucial, and many EIAs use the brightest pixel as the TPOI. This is because the brightest pixel eventually becomes one of the final endmembers, though the search process do not begin with it. The assumption in linear mixing models is that the endmembers lie at the corners of the linear simplex, which is defined by the convex hull of the observed spectra in the hyperspectral dataset. The corners of this convex hull correspond to the purest spectra or endmembers that are present in the data. The endmember extraction algorithms aim to estimate these endmembers by searching for the pixels that contribute to the maximum volume of the linear simplex. Thus, the brightest pixel is often selected as one of the final endmembers because it contributes to the largest volume of the simplex. The brightest pixel is a commonly used TPOI in endmember extraction, which has proven to be more effective than random or average pixel initialization. Increasing the knowledge of the endmember targets can potentially enhance the performance of both EIAs and EEAs.

Experimental results in generating endmember target signatures by SM-EIA revealed the importance of endmember initialization in identifying the spectrally distinct signatures. Therefore, present study focuses on identifying a new TPOI that begin the endmember search process.

4.2.1 Influence of The Darkest Pixel in EE

In the present study, the concept of extreme pixels or boundary pixels is explored to identify TPOIs for endmember initialization. The reason behind this is that the fundamental concept in HSI that endmembers lie at extreme locations of the simplex formed HSI data. The darkest pixel is identified to be an another extreme pixel as that of the brightest pixel and therefore the darkest pixel is proposed to use as a new TPOI for this study to test it's utility in generating endmember target signatures by EIAs. It is accepted from the abundance maps that if the brightest pixel represents the presence of a pure pixel of a particular material then the darkest pixel automatically represents the absence of that particular material or presence of another material. This is also an another reason for selecting the darkest pixel as a new TPOI for endmember initialization.

As the brightest pixel is considered to have maximum length, similarly the darkest pixel is considered to have minimum length. Therefore, the darkest pixels as the TPOI in generating the required number of initial endmember targets by an EIA. Vector norm as presented in Eq 4.4 is measured to identify the location of the darkest pixel as

$$(d_i, d_j) = \min_{i,j}(norm). \tag{4.11}$$

The spectral signatures of the TPOI identified is extracted using Eq 4.6.

In this paragraph, the rationale for selecting the proposed TPOI is further explained. In reference to the statement made in Liu and Zhang (2011), which states that the norm of any mixed pixel is smaller than the largest norm of endmembers under the pure pixels assumption. This implies that all the mixed pixels lie within the simplex formed by the endmembers as the vertices, and the norm of any mixed pixel must be smaller than the largest norm and larger than the smallest norm of the endmembers. Based on this assumption, it is proposed that the darkest pixel with the smallest norm or minimum length is a valid additional TPOI to the brightest pixel as present study considers the pure pixel assumption. This approach is expected to improve the performance of EIAs.

Experimental Results

ATGP Ren and Chang (2003), and recently developed SM-EIA Yadav et al. (2020b) are adapted to generate initial targets with the proposed initialization strategy. Performance of

the EIAs in generating target signatures for the materials present in the Samson dataset with the proposed targets of interest is given in Table 4.3a.

Table 4.3: Influence of The Darkest Pixel as a TPOI in EE by SM-EIA

(a) Samson Data

EEMs	**ATGP**	**SM-EIA**								
		SAM	**SID**	**SCM**	**PC**	**SAMSID**	**SCMSID**	**PCSID**	**SAMPC**	**SCMPC**
Sl	2.25	10.00	2.09	21.98	38.09	**1.30**	8.82	38.09	38.09	38.09
Tr	**1.25**	4.31	4.07	3.00	68.94	4.07	5.95	4.07	4.31	3.00
Wt	8.80	8.80	8.80	8.80	**6.31**	8.80	8.80	**6.31**	**6.31**	**6.31**
Ag	**4.10**	7.70	4.99	11.26	37.78	4.73	7.86	16.16	16.24	15.80

(b) Cuprite Data (Avg SAD)

EEMs	**ATGP**	**SM-EIA**								
		SAM	**SID**	**SCM**	**PC**	**SAMSID**	**SCMSID**	**PCSID**	**SAMPC**	**SCMPC**
Avg	6.34	5.06	5.03	**4.74**	6.15	5.58	**4.74**	5.62	6.77	5.45

Samson Data

ATGP do not able to generate water signature, though it is distinct from soil and trees signature, when the brightest pixel is used as TPOI (See Table 4.3a.). The reason for this is that water signature may be either not having maximum length or not contributing to maximum length when projected orthogonal to the previously generated targets. Performance of ATGP has improved when the darkest pixel is used as a target of interest. Though Samson dataset have spectrally distinct materials, say soil (S), trees (T) and water (W), two of them i.e. soil and trees do not have significant curvature differences to be discriminated appropriately. Due to this, SM-EIA, especially with PC and it's hybrid similarity measures, is able to generate reasonable signatures for only one of them and a diverse signature (deviated one) for the other one. PC, that computes Fourier transform to correlate spectral signatures, try to generate spectrally distinct signatures might be the reason for this. The same is the reason for hybrid combinations of PC to replace the target of interest with another signature (see Table 4.3a) when target of interest is the darkest pixel. SM-EIA generated comparatively good or better target signatures in the case of the darkest pixel used as a target of interest.

Targets generated by EIAs for the endmembers present in Samson data with the proposed targets of interest reveals the importance of using the darkest pixel as a target of interest. Performance of ATGP and SM-EIA with various similarity measures is improved in the case of the darkest pixel used as a target of interest. In addition, the experimental results clearly show the ability of SID in discriminating soil and trees signatures and therefore significance of SID in change detection applications especially deforestation of earth surfaces.

Experiments on Cuprite Data

Performance of EIAs with the proposed targets of interest in generating targets for minerals whose spectral signatures have subtle differences present in a benchmark dataset over the Cuprite scene is given in Table 4.3b. Overall performance of SM-EIA with SCM is consistent in identifying near optimal targets of mineral signatures in both the cases of targets of interest. SM-EIA, not only with SCM but also with other similarity measures including few of their hybrid combinations, performs better than ATGP. Both the ATGP and the SM-EIA with many similarity measures have shown better performance in the case of the darkest pixel as a target of interest. The results suggests the usefulness/utility of the darkest pixel as an another target of interest in searching for endmembers.

4.2.2 Comprehensive Study on EE with The Darkest and Brightest Pixels as TPOIs

The use of only one signature as a TPOI has been found to be limiting, as noted in Heinz et al. (2001). In this work, we propose using a combination of the brightest and darkest pixels as TPOIs, and it is aimed to study their effectiveness in generating endmember targets by EIAs and extracting endmembers by EEAs, in comparison to using only the brightest or darkest pixel as a proposed TPOIs.

Proposed Methodology

Figure 4.1 shows flowchart of the proposed algorithm. For initialization of the EIAs, we select (i) a pixel with maximum length (B) (ii) a pixel with minimum length (D) and (iii) pixels with maximum and minimum length (BD) as the TPOIs in extracting the required number of initial targets. We propose to use ATGP and variants of a similarity measures

based EIA called SM-EIA Yadav et al. (2020b) to generate initial targets. The output targets generated are used as initial endmembers to EEAs. The final endmembers extracted are compared with the ground truth endmembers of corresponding materials. As it is mentioned, performance of both ATGP and SM-EIA with different similarity measures is verified and assessed.

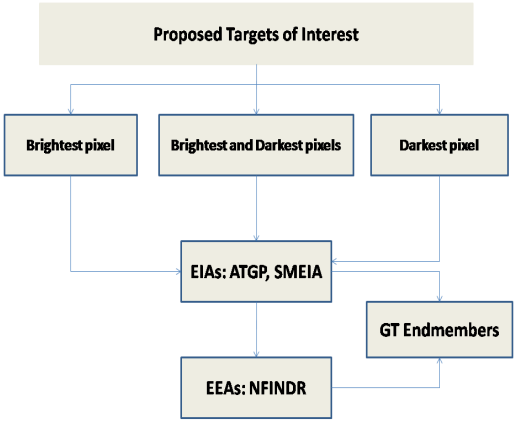

Figure 4.1: Endmember Initialization Strategies and EE in HSI Analysis: A Flowchart

Results and Discussion

The type of materials present in the GT of the experimental data sets are considered to generate the targets. Spectral angle distance (SAD) between EIA/EEA generated endmembers and ground truth endmembers is computed to study the influence of proposed targets of interest in guiding EIAs/EEAs searching for endmembers. Lesser the SAD value, more the closeness of the extracted endmember is with the ground truth endmember and vice versa. To compare the overall performance, mean of all individual endmembers is computed. Bold values are corresponding to SAD values of the best endmembers extracted by EIAs/EEAs. The number in the bracket represents the number of target/endmember signatures extracted by an EIA/EEA in the best possible way.

Table 4.4 show the average SAD values calculated for the EEMs by proposed EIAs from the experimental data sets. From Table 4.4, it is understood that popular ATGP showed better performance in the case of four out of five experimented data sets when proposed TPOIs either the darkest pixel or combination of both the brightest and darkest pixels are considered. The significant improvement in overall performance in the cases of better performance and on par performance in other cases of ATGP initialized with proposed TPOI suggests the

benefits of using combination of the brightest and darkest pixels as TPOIs in EE tasks.

Table 4.4: EE by SM-EIA with Different TPOI Strategies on Various Data Sets

EIAs	TPOIs	Samson	Jasper Ridge	Urban	Cuprite	Syntheic
ATGP	**B**	22.05	18.50	22.63	**5.41**	**1.00**
	D	**4.10**	**9.07**	**21.51**	6.34	**1.00**
	BD	**4.10**	**9.07**	**21.51**	6.40	**1.00**
SM-EIA(SAM)	**B**	8.16	19.41	27.35	5.81	**0.51**
	D	7.70	20.90	**23.94**	**5.06**	**0.51**
	BD	**7.01**	**19.24**	24.31	5.57	**0.51**
SM-EIA(SID)	**B**	6.43	**33.30**	28.96	5.78	**0.56**
	D	4.99	35.14	29.37	**5.03**	**0.56**
	BD	**3.63**	**33.30**	**28.67**	5.60	**0.56**
SM-EIA(SCM)	**B**	**10.28**	18.92	**14.44**	**4.58**	**0.49**
	D	11.26	**16.78**	19.68	4.74	**0.49**
	BD	10.68	18.51	25.35	4.73	**0.49**
SM-EIA(PC)	**B**	19.51	**17.93**	**17.05**	**5.25**	**0.59**
	D	37.78	24.70	21.10	6.15	0.46
	BD	**15.22**	19.73	25.00	6.75	0.50

Experimental results on SM-EIA with all the data sets show that proposed TPOIs either either the darkest pixel or combination of both the brightest and darkest pixels lead SM-EIA to perform better many a times than when the brightest pixel used as TPOI. In addition, the variation in the performance of EIAs when proposed TPOI considered for initialization is very less in most of the times and comparable in other few times. Therefore it is suggested that proposed TPOI can be considered in EE tasks for initialization and to test comprehensively in other HSI analysis related tasks.

Among the SMAs tested with SM-EIA, SAM and SID take advantage of proposed TPOI combination to get their performance improved to compete with ATGP. Whereas, SCM and PC performed better when SM-EIA is initialized with the brightest pixel. Though SM-EIA could generate endmember better endmember signatures, selection of SMAs in endmember extraction with SM-EIA depends on the nature of endmember signatures present in the data. Experimental results on Samson data bringing into the notice that PC needs significant frequency components i.e. curvature features among spectral signatures for endmembers to be discriminated and extracted appropriately.

Spectral Distinctiveness/Variance of GT Endmembers vs SM-EIA Endmembers

Table 4.5: Average SAD for Endmember Pairs Extracted by EIAs with Different Target Pixel of Interest (TPOI) Strategies on Various Data Sets

EIAs	TPOI	Samson	Jasper Ridge	Urban	Cuprite	Syntheic
ATGP	**B**	17.62	26.32	43.67	8.73	14.72
	D	18.90	26.07	44.91	8.63	14.72
	BD	18.90	26.07	44.91	8.63	14.72
SM-EIA(SAM)	**B**	49.80	55.43	51.65	10.49	14.50
	D	40.96	53.30	45.34	9.99	14.13
	BD	40.22	55.24	44.94	10.34	14.50
SM-EIA(SID)	**B**	49.60	42.81	51.31	10.42	14.22
	D	41.86	48.27	45.86	9.96	14.73
	BD	40.94	42.81	47.11	10.43	14.22
SM-EIA(SCM)	**B**	49.19	48.57	27.51	9.40	10.30
	D	39.32	51.90	33.75	9.06	11.20
	BD	40.40	47.89	24.83	9.34	10.30
SM-EIA(PC)	**B**	49.33	51.13	25.37	7.98	7.61
	D	12.30	49.64	24.21	6.11	8.53
	BD	48.87	51.32	26.98	6.71	8.35

To get an idea about the quality of endmembers, average SAD for endmember to endmember pairs from the endmember set extracted by the EIAs on various data sets has been reported in Table 4.5. The average SAD for endmember to endmember pairs presented in Table 4.5 show that SM-EIA especially with SAM and SID generated most distinctive signatures. From these results, it can be concluded that SMAs try to extract most distinctive signatures and at the same time from Table 4.4 (especially results on Synthetic data), it is clear that quality of endmembers are not good. SM-EIA with SMAs trying to identify distinct signatures without considering their locations is the the reason for SM-EIA not to perform as it is expected to. Though endmembers are mutually distinctive in nature, SMAs due to comparing the overall spectral signatures without considering their diagnostic features is the main reason for SM-EIA to generate spectrally distinct mixed pixels as endmember set (see Table 4.4, especially results on Synthetic data). The another reason that amount of mixing happens in synthetic data may not be possible in the cases of real HSIs though they are highly mixed in nature due to several factors like spatial resolution, multiple reflections and etc. This is the main

reason for existence of many varied spectral signatures in the case of synthetic data because of all the combinations of mixing proportions (large number of abundant combinations by the endmember set). The same might be the reason for SM-EIA not performing well especially on synthetic data. But, ATGP is able to outperform on Synthetic data also due to it's ability to identify spectrally distinct signatures by projecting data onto a subspace formed by already generated endmembers. Overall, performance of ATGP is outperforming other EIAs when intialized with proposed TPOI combination.

Inferences

- Experimental results once again proved the darkest pixel as a potential TPOI.
- Experimental results on Synthetic data clearly show the darkest pixel is not only a potential TPOI but also better TPOI to be combined with the brightest pixel.
- Experimental results on ATGP with all the data sets and Synthetic data with all the EIAs show that the darkest pixel influences the performance when proposed TPOI combination is used. Overall, the darkest pixel dominates the brightest pixel.
- Experimental results on Synthetic data clearly show that SMAs with SM-EIA are not able to capture distinct signatures present at extreme locations.
- Experimental results proved that SM-EIA try to extract spectrally distinct signatures as endmembers.

Though the performance of SM-EIA perform reasonably good in the case real HSIs, poor performance on synthetic data suggests the need for improving SM-EIA to perform better in extracting quality endmembers.

4.3 Improved/Modified SMEEAs

The experimental study on TPOIs suggests the need for improving the SM-EIA algorithm to extract quality endmembers. SM-EIA not being able to capture extreme pixels that are spectrally distinct signatures as well is to be achieved with the improved SM-EIA. For this reason, the basic concepts on endmembers that they lie at extreme locations and mutually distinctive in nature are fully exploited in designing improved/modified SMEEAs to improve their performance in extracting quality endmembers. Therefore, distance metric ED

is explored as an additional metric to the SMAs to capture extreme pixels that are spectrally distinct signatures as endmembers.

4.3.1 Improved SM-EIA (ISMEIA)

A slight modification in calculating SSV is adapted by exploring ED as an additional metric to the SMAs in the ISMEIA. The modified SSV is calculated as

$$SSV(i,j) = ED(HSI(i,j), e_n) \times SMA(HSI(i,j), e_n). \tag{4.12}$$

The term *ED* give weight-age to the pixels located at extreme locations. Therefore, it is expected that ISMEIA perform better than SM-EIA in capturing spectrally distinct signatures from extreme locations which are the more probable endmembers. The working principle of ISMEIA is similar as that's of SM-EIA but differ only in how they calculate *SSV*. SM-EIA and ISMEIA are similar except this one modification proposed to calculate *SSV*. The rest of the experimental set-up to test the performance of ISMEIA is similar in-terms of the HSI data sets used and TPOI considered for experimentation. Since, simple SMA are compare overall spectral signatures without considering diagnostic features, gradient correlation (GC) incorporated SMAs are considered to test their performance in endmember extraction with the proposed ISMEIA. GC incorporated geometrical SMAs showed better performance in discriminating different endmember signatures and hence GC incorporated SAM (GSAM), GC incorporated SCM (GSCM) and GC incorporated DSSC (GDSSC) are explored in this study.

Experimental Results

Table 4.6 presents average SAD values calculated from the endmembers extracted by ISMEIA with the proposed TPOI on different HSIs tested with SM-EIA. The experimental results show that ISMEIA with the modified *SSV* could extract better endmembers than that's of SM-EIA. To test the utility of *ED*, ISMEIA with *ED* alone is implemented to extract endmembers. Unfortunately *ED* also failed to identify extreme pixels and same can be observed from the results on Synthetic data. Interestingly, performance of ISMEIA with SMAs is better than that's of their counterparts i.e. similar combinations of SMAs with SM-EIA and same can be observed by comparing Table 4.4 and Table 4.6.

Table 4.6: Performance Evaluation of ISMEIA in EE Utilizing The Brightest and Darkest Pixels (BD) as TPOIs

	SD	JR	UR	CS	SY
ED	4.19	8.68	**20.64**	5.72	**0.53**
ED_SAM	4.08	12.17	**20.16**	5.18	**0.62**
ED_SID	**3.84**	**15.28**	**25.15**	**4.91**	**0.60**
ED_SCM	6.68	12.12	20.56	4.79	**0.58**
ED_PC	7.38	**10.38**	21.26	6.31	**0.49**
ED_DSSC	11.63	13.36	**26.65**	**5.78**	**0.49**
ED_GSAM	3.53	8.95	27.17	**5.18**	**0.69**
ED_GSCM	4.13	9.30	**19.05**	**5.47**	**0.58**
ED_GDSSC	4.34	9.30	**18.56**	6.04	**0.66**

Inferences

- The performance of ISMEIA is improved and it is better compared to that's of SM-EIA.
- Experimental results proved once again that GC incorporated SMAs have better discrimination power than simple SMAs.

Though ISMEIA showed better performance than SM-EIA, overall performance on all the data sets especially Synthetic data set is not satisfactory. Therefore, it is understood that the MDA criterion proposed in reference and farthest first traversal criterion proposed for SM-EIA are not suitable to identify either extreme pixels with *ED* or spectrally distinct signatures with SMAs.

4.3.2 Does Maximin-Distance Criterion Identify Vertices

Since MDA criterion and farthest first traversal criterion proposed for SM-EIA are not suitable to identify endmembers, it is considered that there is a need for testing the applicability of MDA and farthest first traversal criterion in identifying the vertices of a geometrical polygon. Hence, an experiment to identify vertices of geometrical shapes from triangle to decagon in a 2-D plane is considered to test the performance of proposed criterion as shown in Figure 4.2.

Maximin distance criterion in identifying vertices geometrical shapes

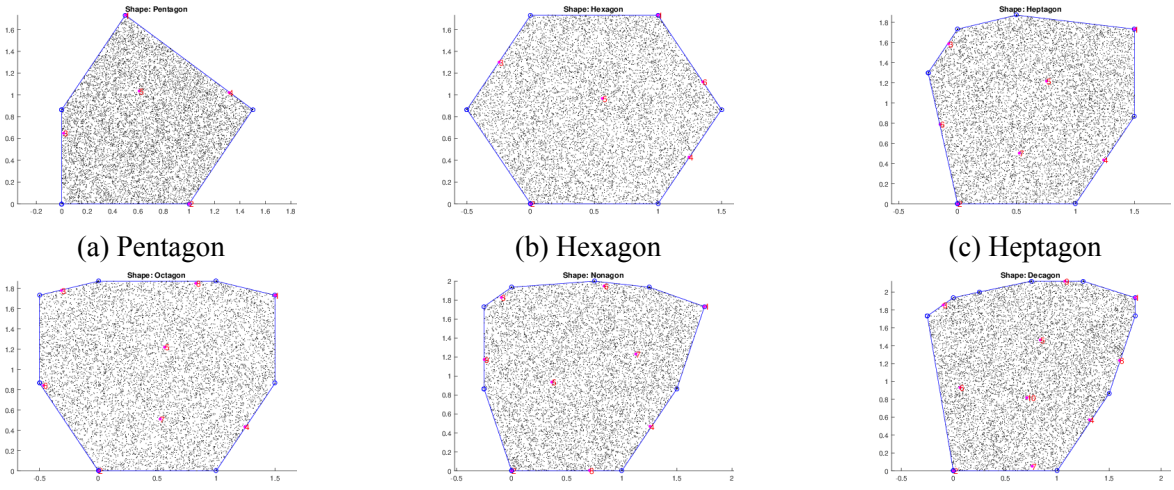

(a) Pentagon (b) Hexagon (c) Heptagon

(d) Octagon (e) Nonagon (f) Decagon

Figure 4.2: Performance Evaluation of MDA in Identifying Vertices of Geometric Shapes: An Experimental Study

Initially, a point located at the top most position (similar as that of the brightest pixel selection) is consider to begin the vertex identification process as illustrated in Figure 4.2. Therefore, a point F is selected and considered as the first vertex of hexagon to start the search process. Then, distance of all the points on the hexagon from the first vertex F is measured. An another extreme point C is selected as next/second vertex due to its being very far (largest distance) from the first vertex. Then distances from first two vertices F and C are measured. As shown in Figure 4.2, the middle points G and H of the line segment joining AB and DE respectively have the minimum distance at maximum than the remaining vertices. This is the reason either G or H are identified as vertices, by vomiting actual vertices, by MDA and farthest first traversal criterion. Since both G or H are mutually distant as well as distant from F and C and at the same time, both of them being selected as a vertices have higher scope. Eventually, F, C, G and H in the way looking for a point whose minimum distance is maximum, end up finding centroid (in the case of irregular polygon a point near to centroid) of the hexagon i.e one of the interior points. This is the reason SM-EIA and ISMEIA do not able to perform better in generating pure endmembers especially in the case of Synthetic data.

Interestingly, the experimental analogy clearly show that the proposed criterion may not be helpful in identifying vertices of a hexagon present in a 2-D plane. Then what to speak of identifying the vertices of a n-dimensional simplex formed by HSI data. Therefore, it is

concluded that either the maximin distance or farthest first traversal are either not suitable or need to be improved for SM-EIA/ISMEIA with the simple SMAs to extract quality endmember in all the cases especially Synthetic data. Hence, it is suggested that either the criterion considered to identify extreme or spectrally distinct pixels can be improved else higher dimensional metrics like volume or solid spectral angle distance (SSAD) kind of metrics can be the better alternatives either for SM-EIA or for ISMEIA.

Table 4.7: Performance Evaluation of MDA in Identifying Vertices of Various 2-D Geometrical Shapes and n-Dimensional Simplexes

2-D Geometical Shapes			**N-D Simplex**		
N (Geometry)	**Equal Sides (Rgular)**	**Unequal Sides (Irregular)**	**N-Simplex**	**Non-Ortho Sides**	**Ortho Sides**
3 (triangle)	3	3	**3-simplex**	2	1
4 (square)	4	4	**4-simplex**	1	2
5 (pentagon)	3	2	**5-simplex**	2	2
6 (hexagon)	2	2	**6-simplex**	2	1
7 (heptagon)	5	2	**7-simplex**	2	2
8 (octagon)	7	2	**8-simplex**	2	2
9 (nonagon)	5	2	**9-simplex**	2	2
10 (decagon)	2	2	**10-simplex**	2	2

An experiment to identify vertices of different regular and irregular 2-D geometrical shapes and n-Dimensional simplex-es are carried out to test the performance of proposed MDA criterion as shown in Figure 4.2. The number of vertices identified by MDA are presented in Table 4.7. In the Table 4.7, 'N' stands for the number vertices in a 2-D geometry and the dimension of a simplex designed for the experiment. A N-D simplex have N+1 vertices. Interestingly, the experimental results clearly show that the MDA criterion doe snot helpful in identifying vertices of a 2-D geometrical shapes and the vertices of a N-dimensional simplex-es. Therefore, it is concluded that either the MDA or farthest first traversal are either not suitable or need to be improved for SM-EIA/ISMEIA.

Inferences: The experimental results and the subsequent analysis of the Minimum Determinant Algorithm (MDA) criterion's performance in vertex identification for 2-D geometrical shapes and N-dimensional simplexes yield several important inferences. Few of the inferences are mentioned below.

- MDA consistently demonstrates robust performance in accurately identifying vertices for regular 2-D geometrical shapes such as triangles, squares, and hexagons.

- MDA faces challenges in accurately identifying vertices for irregular 2-D geometrical shapes. Notably, irregular polygons, such as pentagons and octagons, present difficulties for the algorithm.

- The performance of MDA varies across N-dimensional simplexes. While the algorithm shows consistency in identifying vertices for certain configurations, it struggles in other cases, especially when dealing with non-orthogonal sides.

- MDA's ability to identify vertices appears to be sensitive to the complexity and irregularity of the shapes. Regular geometries with clear patterns yield more reliable results compared to irregular and complex configurations.

- The experimental results cast doubt on the suitability of MDA for spectral mixture endmember identification algorithms (SM-EIA/ISMEIA). The algorithm may require further refinement or alternative traversal methods to address the specific challenges posed by spectral mixture analysis.

- The study highlights the need for further investigation and potential enhancements to MDA or alternative approaches to improve its efficacy in identifying vertices, particularly in irregular geometrical shapes and certain N-dimensional simplex scenarios.

- Given the observed limitations of MDA, researchers and practitioners in spectral mixture analysis may need to explore alternative methods or criteria for vertex identification in the context of endmember analysis.

- The findings provide valuable insights for future research directions, urging a deeper exploration of algorithms that can effectively handle the intricacies of irregular geometries and complex N-dimensional simplexes in the realm of spectral mixture analysis.

In summary, the inferences drawn from the experimental results emphasize the nuanced performance of MDA and underscore the importance of addressing challenges associated with irregular shapes and certain simplex configurations in the context of spectral mixture endmember identification.

4.3.3 Higher Dimensional Metrics for Endmember Identification by SM-EIA

As the experimental results on ISMEIA suggested, the volume metric is considered to test it's applicability with modified ISMEIA. In modified ISMEIA, volume coefficient (VC) is considered instead of *ED* metric. The volume coefficient is defined as the ratio of new volume formed by a pixel with the already generated endmember set E_n to the volume formed by the already generated endmember itself. VC is calculated as

$$VC(i,j) = \frac{volume(E_n, HSI(i,j))}{volume(E_n)} \tag{4.13}$$

and the volume formed by an endmember set E_n is measured as

$$VC(i,j) = \frac{volume(E_n, HSI(i,j))}{volume(E_n)} \tag{4.14}$$

VC gives an idea about how an pixel contribute to increase the volume at every step. SGA works based on the principle of growing the volume of the simplex formed by data set. The same criterion is considered to test the applicability of modified ISMEIA as suggested by experimental results on ISMEIA.

The poor performance of ISMEIA suggests higher dimensional metrics like volume or n-Dimensional solid spectral angle (NSSA) Tian et al. (2016) metrics can be the better alternatives for SM-EIA. Use of volume metric helps in better endmember extraction and NSSA due to it's limitation on the number of bands to be used in the n-dimensional space, not able to perform well but it can be explored in band selection to reduce dimensionality (see Table 4.8).

Table 4.8: Enhanced Performance of SM-EIA with Higher Dimensional Metrics in EE (Abundances for SY and Avg SAD for Other Data Sets)

Metric	**SD**	**JR**	**UR**	**CS**	**SY**
Volume	4.10	9.07	21.09	6.40	1.0
NSSA	13.84	24.44	27.65	6.39	0.41
ATGP	4.10	9.07	21.51	6.40	1.00

4.4 Corner-Driven Iterative Clustering (CDIC) Algorithm

Though SM-EIA able to perform better in EE when higher dimensional metric like volume is explored, the endmembers give good idea on distinct signatures present in the data. But, identification of endmembers by exploring the fundamental concept of endmembers that they lie at corners or vertices formed by data cube using simple ED metric is what required for practical applications to get a feasible solution. Therefore, identification of abundant endmember signatures from extreme locations is proposed with the Corner-Driven Iterative Clustering (CDIC) algorithm. Proposed CDIC is designed for EE from the experimental unmixing HSI data sets. The algorithm incorporates a corner-driven approach to refine the initial endmember estimates obtained through k-means clustering. CDIC aims to enhance the accuracy of endmember extraction by leveraging the distinctive properties of corner pixels in HSIs.

4.4.1 CDIC Algorithm

The algorithm begins by computing the number of endmembers required based on the application's needs. It then performs an initial k-means clustering step to extract preliminary endmembers. Next, the algorithm computes the median of the hyperspectral data, which serves as a reference point for distance computations. CDIC evaluates the distance of each pixel from the median, capturing its deviation from the central tendency. Additionally, it calculates the distance of each cluster center from the median to establish a reference distance for each cluster. Points within a cluster that are closer to the median than their respective cluster center are considered outliers and removed from the dataset.

The iterative process continues until the desired number of iterations is reached. In each iteration, CDIC updates the dataset by removing the identified outlier points and performs k-means clustering on the refined data. The median and distances are recomputed for the new clusters, and the removal of outlier points is repeated. This iterative refinement progressively enhances the endmember extraction by focusing on the corner pixels.

Finally, CDIC identifies the final set of endmember points using the cluster assignments. These endmembers represent the distinct spectral signatures present in the hyperspectral data. Abundance maps can be computed to quantify the spatial distribution of each endmember, providing valuable insights into the underlying materials within the scene. The CDIC algo-

rithm ultimately yields a clustered image, where each pixel is assigned to the closest endmember based on spectral similarity.

By incorporating a corner-driven approach and iterative refinement, the CDIC algorithm offers an effective solution for accurate endmember extraction in HSI analysis.

4.4.2 Experimental Results

The Table 4.9 displays the performance of CDIC and ATGP in terms of endmember identification, specifically measuring the average Spectral Angle Distance (SAD) for all data sets, including SY. Each column represents a different data set, labeled as SD, JR, UR, CS, and SY. The values in the table represent the average SAD for each algorithm in each respective data set.

Table 4.9: Performance Assessment of CDIC in EE (in Avg SAD for All The Data Sets including SY)

Data Set	**SD**	**JR**	**UR**	**CS**	**SY**
CDIC	2.75	7.00	5.37	6.51	4.19
ATGP	4.10	9.07	21.51	6.40	0.00

The main observation from the Table 4.9 is that CDIC consistently outperforms ATGP in three out of five cases (SD, JR, and UR). The average SAD values for CDIC are notably lower than those for ATGP in these cases. This indicates that CDIC is more effective in identifying endmembers compared to ATGP in the context of land cover mapping-related data sets, specifically for the Samson (SD), Jasper Ridge (JR), and Urban (UR) data sets. ATGP try to identify distinct signatures present in the data to give a good idea on possible endmebers and CDIC tries to identify endmembers of abundant materials is the reason why CDIC outperformed ATGP in the case of three land cover mapping related data sets (Samson, Jasper ridge and Urban data sets).

In summary, Table 4.9 provides quantitative evidence supporting the claim that CDIC yields better performance in endmember identification compared to ATGP, particularly in the context of three land cover mapping-related data sets.

Spectral Matching

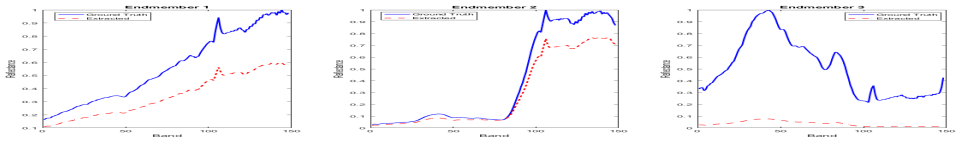

(a) SD

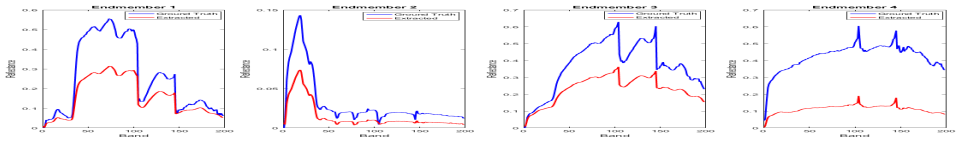

(b) JR

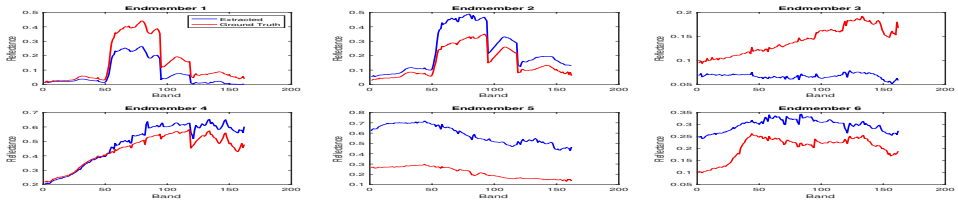

(c) UR

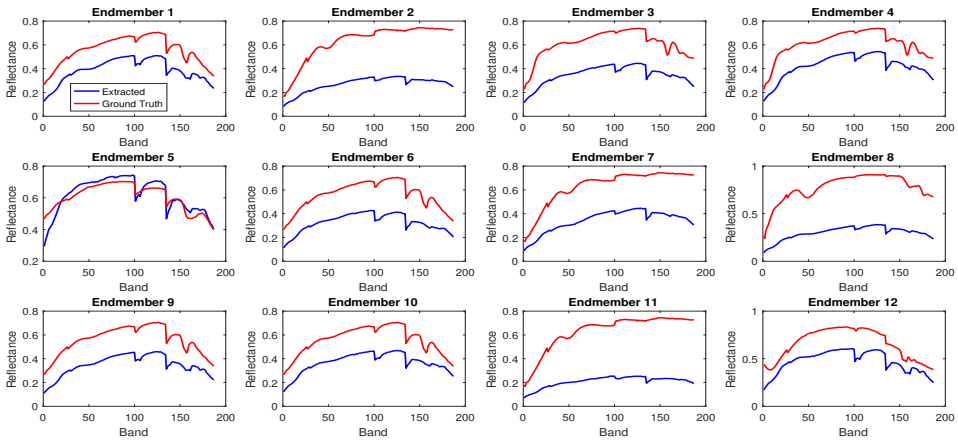

(d) CS

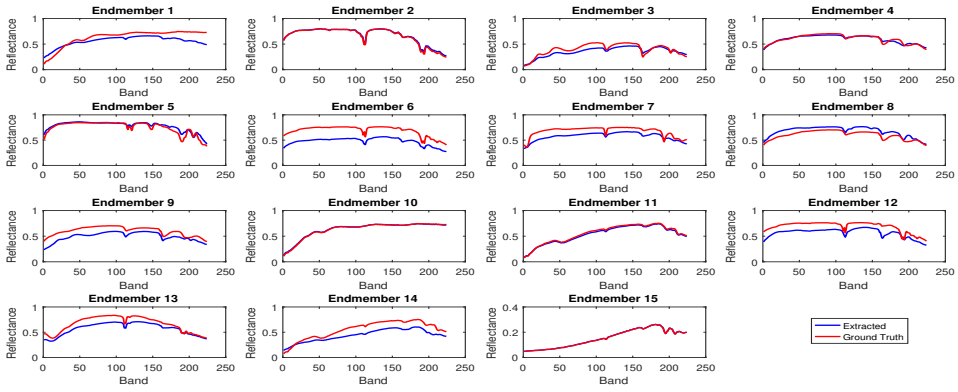

(e) SY

Figure 4.3: Mapping of CDIC-Extracted Endmembers to Ground Truth: Comparative Analysis Across Multiple Data Sets

CDIC extracted endmembers are mapped to the GT endmembers and showed them in Figure 4.3 for all the data sets. From Figure 4.3 illustrates that most of the CDIC endmembers are matching with the GT endmembers with highest accuracy and in other cases their diagnostic features are matching. Unlike manual mapping, an automatic EE mapping technique has been used in this work. Proposed EE mapping measures the closeness every extracted endmember to all the GT endmembers. An extracted endmmeber that have more closeness to any GT signature is considered to be mapped together first. Then, remaining endmembers are mapped to remaining GT endmembers considering a next more closeness of extracted endmember with any of the GT endmembers. Removing the mapped extracted and Gt endmembers, the process continue untill all the extracted endmembers are mapped to any one of the GT endmembers. This mapping allows one extracted endmember to be mapped with one GT endmember only. This mapping of endmembers makes sure of identifying mismatched or excluded or deviated endmembers from the GT signatures.

From Figure 4.3, it can be observed that Cuprite endmembers do not have great matching with their ground-truth (reference) endmembers. Subtle differences in mineral signatures and presence of non-mineral pixels in the data are the possible reasons for not so quality endmember extraction of mineral endmembers. But, the endmembers profiles from the data sets with land cover mapping are greatly matching with the diagnostic features (locations of absorption features at material specific wavelengths). Therefore, it is inferred that CDIC is reasonably good choice in identifying the endmebers present in the land cover mapping related data sets.

Unmixing Performance by CDIC Endmembers

Unmixing results by CDIC on SD, JR and UR comparing to their reference abundance maps (see Figure 4.4) illustrates that CDIC extracts high quality endmembers. From Figure 4.4, it is clear that CDIC obtained abundance maps are resembling to their corresponding ground-truth (reference) abundance maps. From this, it is inferred that CDIC is better in identifying quality endmembers from the unmixing data sets related to land-cover mapping. Therefore, it is concluded that CDIC can be a better choice to choose in land cover related applications.

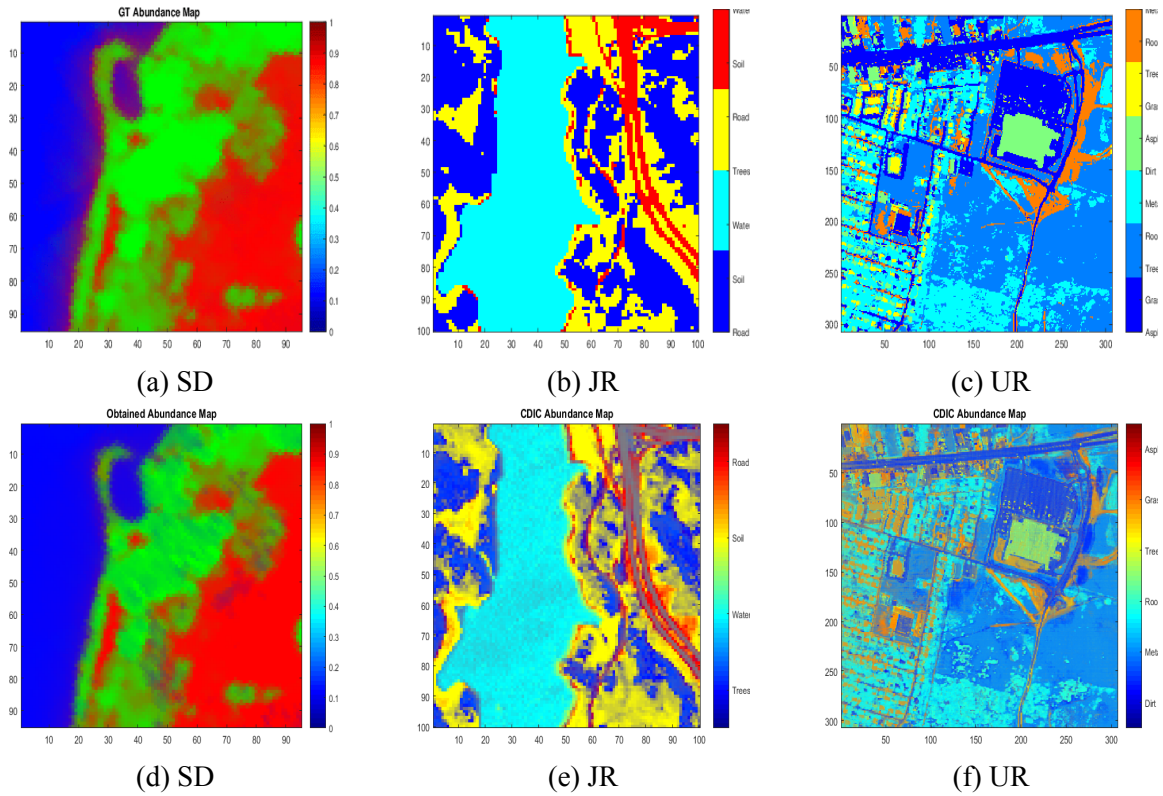

(a) SD (b) JR (c) UR

(d) SD (e) JR (f) UR

Figure 4.4: Comparison of Ground Truth (First Row) and CDIC Unmixing Abundances (Second Row) Across Multiple Data Sets: SD, JR, and UR (First Column, Second Column and Third Column)

Classification Performance by CDIC Endmembers

CDIC endmembers used for classifying different land cover classes present in HSI classification data sets like Indian pines (first row), Pavia University (second row) and Washington DC mall (third row). The classification maps obtained from classification by CDIC endmembers are presented in Figure 4.5. From Figure 4.5, it is clear that classification by CDIC extracted endmembers greatly matches to the ground-truth maps of Pavia University and Washington DC mall. Insignificant classes like grass present in Pavia University RGB image are not labeled in the ground-truth classification map and this is the reason for random mismatches with the CDIC generated classification map. But, due to subtle differences present in the subclasses crop pixels of Indian pines makes CDIC not able to generate matched classification maps properly. Results once hint that CDIC can be a reasonably good choice for land cover mapping related applications and may not be a good choice for crop identification. Figure 4.5, first column presents the RGB images, second column presents ground-truth classification map and third column presents CDIC generated classification maps respectively.

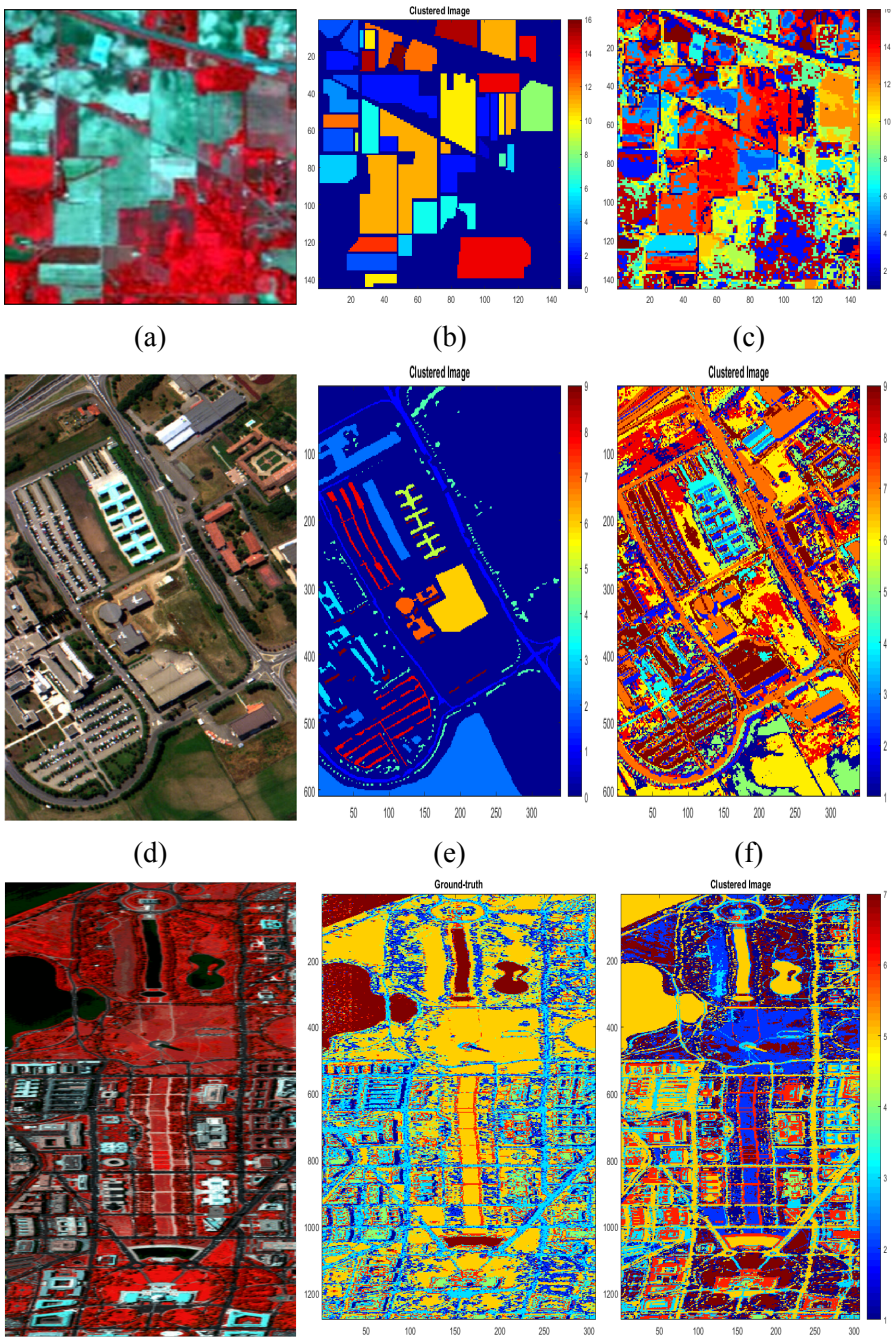

(a) (b) (c)

(d) (e) (f)

(g) (h) (i)

Figure 4.5: Comparison of Classification Maps using CDIC Endmembers for Indian pines (First Row), Pavia University (Second Row) and Washington DC mall (Third Row) Data Sets: Original Image (RGB) (First Column), Ground Truth (Second Column), and CDIC Obtained (Third Column)

Summary:

Spectrally distinct nature of endmembers is explored in EE task to form SMEEAs, using/incorporating similarity measures, to identify endmembers. Experimental results illustrates that proposed

SMEEAs i.e, SM-SCA and SM-EIA are able to identify distinct endmembers and also highlights the importance of endmember initialization. Experimental results show that the darkest pixel identified as a TPOI, in the further investigation on TPOIs to begin endmember search process by EIAs, not only a potential TPOI but also improved the EE performance when combined with the brightest pixel (influenced the brightest pixel). Experiments carried on an improved SM-EIA to test it's applicability in extracting pure endmembers presents MDA do not able to identify vertices of simplex with simple the metrics like ED and other simple SMAs but with higher dimensionality metrics like volume. Finally, the proposed CDIC not only able to identify endmembers but also provide samples for each endmember class that can be utilized for further analysis of HSI data.

The next chapter presents research work on spectral matching.

Chapter 5

Spectral Matching

> A good leader is hard like a thunderbolt and soft like a rose. One without the other does not work. If a leader is just soft like a rose, he cannot train anyone. If he is just hard like a thunderbolt, he will burn everyone out.
>
> Radhanath Swami

Introduction

In this section, we embark on a comprehensive exploration of the effectiveness of various Spectral Matching Algorithms (SMAs) in the intricate task of distinguishing spectral signatures of minerals. To assess their capabilities, we propose four distinct criteria, ranging from discerning different endmember signatures to the crucial task of endmember extraction. The classical SMAs are rigorously examined in light of these criteria. Our focus then shifts to the innovative Gradient-based Spectral Similarity Measure (GSSM), a novel approach that accentuates diagnostic features at mineral-specific wavelengths. We extend our inquiry to the Spectral Gradient, derived from GSSM, to evaluate the efficacy of gradient correlation in contrast to simple correlation methods. Lastly, we introduce a refined variant of the Relative Spectral Discrimination (RSDPW) to discern spectral signatures in a more meaningful manner. This chapter aims to provide a nuanced understanding of the capabilities and limitations of various SMAs in the context of mineral spectral signature analysis.

Spectral matching involves quantifying the similarity between spectra. Spectra are considered similar when their spectral distance is small, indicating a close match, while dissimilarity suggests a significant difference. This technique finds applications in various fields, including target detection and spectra classification. By assessing spectral similarities, researchers can effectively identify and classify different materials and objects based on their spectral characteristics.

Indeed, various SMAs have been developed based on distinct theoretical strategies. These algorithms leverage different mathematical approaches and principles to measure the similarity between spectra, tailoring their applications in spectral analysis tasks. These diverse SMAs techniques contribute to a comprehensive toolbox for researchers and practitioners to choose the most suitable method for their specific spectral analysis needs. Below are several Classical SMAs commonly used in spectral analysis.

Classical SMAs

Classical SMAs encompass a range of techniques, including the Spectral Angle Mapper (SAM), Spectral Correlation Mapper (SCM), Spectral Information Divergence (SID), and Phase Correlation (PC). These algorithms have been widely used in various fields, such as remote sensing, image processing, and hyperspectral data analysis. Spectral matching using these Classical SMAs is illustrated below.

(i) SAM

SAM Kruse et al. (1993) is one of the traditional similarity measures. SAM considers the spectra of two pixels as vectors and calculate the angle between them. A small value of angle represents more correlation and high values represent less correlation. A cosine version of SAM is used for this purpose.

$$\Theta = \cos^{-1}\left(\frac{\sum_{i=1}^{L} x_i \times y_i}{\left(\sum_{i=1}^{L} x_i^2\right)^{1/2} \times \left(\sum_{i=1}^{L} y_i^2\right)^{1/2}}\right) \tag{5.1}$$

(ii) SID

SID measures divergence in information between two spectral signatures. SID was proposed by Chang (1999) and it varies from 0 to 1. In extracting endmembers with proposed algorithm, it is negated from 1 for measuring similarity. SID Chang (1999) considers two spectral signatures as random vectors to measure the information divergence between them and it is formulated as

$$SID = (x, y) = 1 - (D(x \parallel y) + D(y \parallel x)) \tag{5.2}$$

where $D(x \parallel y) = \sum_{l=1}^{L} p_l \times \log\left(\frac{p_l}{q_l}\right)$ and $D(y \parallel x) = \sum_{l=1}^{L} q_l \times \log\left(\frac{q_l}{p_l}\right)$ are relative entropies with respect to each other and called as Kullack-Leibler information function, where p_l and q_l are probabilities of distributions of two signatures (say x and y) and can be obtained by considering pixel signature as vector ($x = (x_1 x_2 \ldots . x_L), y = (y_1 y_2 \ldots . y_L)$), where $p_l = \frac{x_l}{\sum_{l=1}^{L} x_l}$ and $q_l = \frac{y_l}{\sum_{l=1}^{L} y_l}$.

(iii) Pearson Correlation (SCM)

This measures linear correlation between two variables. Pearson correlation coefficient varies from -1 to 1. Pearson correlation is used as SCM (De Carvalho and Meneses (2000)) similarity measure. It is defined as

$$SCM = \frac{\sum_{i=1}^{L} (x_i - \bar{x}) \times (y_i - \bar{y})}{\left(\sum_{i=1}^{L} (x_i - \bar{x})^2\right)^{1/2} \times \left(\sum_{i=1}^{L} (y_i - \bar{y})^2\right)^{1/2}} \tag{5.3}$$

where $\bar{x}$ and $\bar{y}$ are the means of vectors x and y.

(iv) Phase Correlation (PC)

The phase correlation (PC) between two signatures is calculated as; Erturk and Erturk (2006)

$$PhaseCorelation(x, y) = F^{-1}\left(\frac{X.Y^*}{|X.Y^*|}\right) \tag{5.4}$$

where X and Y are discrete Fourier transform (DFT) of pixels x and y respectively and F^{-1} represents inverse DFT.

5.1 Effectiveness of SMAs in Distinguishing Spectral Signatures

There are good number of studies on effectiveness of similarity measures and most of them concentrated on discriminating different endmember signatures and a few concentrated on mixed pixel identification. Though similarity measures are used as classification algorithms, a comprehensive study on identification/segmentation of endmember class targets by different similarity measures is lacking. The objective of this work is to explore the applicability

and check the effectiveness and robustness of different similarity measures in (i) distinguishing different endmember signatures (ii) identifying a mixed pixel signature (iii) endmember class targets identification/segmentation/clustering and (iv) endmember extraction. A spectral library of five minerals is formed to study the effectiveness of various similarity measures using four different criterion.

5.1.1 Spectral Library

A real hyperspectral data that is acquired over the Cuprite region to capture the abundance of different minerals is used in this experimentation. Though the number of minerals available in this area is larger, this research is focused on identification of minerals which are in abundance in that area and earlier research Plaza et al. (2002), Wang and Chang (2006), Adep et al. (2017a) also used for spectral matching analysis.

Environment for Visualizing Images (ENVI) is used to form a spectral library. Minimum noise fraction rotation (MNF) and pure pixels Index (PPI) are performed to visualize extreme pixels on n-Dimensional visualizer to form spectral library of minerals under study. USGS spectral library is used as reference for checking the signatures of samples in creating spectral library of minerals under study. The remaining details of the spectral library formation is clearly described in our previous work Yadav et al. (2020a). In Adep et al. (2017a), a similar kind of spectral library, of five mineral classes to be used for training and assessing the performance of a neural network based mineral classifier, was formed.

This spectral library contains five mineral signatures namely Alunite (Al) (124), Calcite (Ca) (64), Kaolinite (Ka) (147), Desert varnish (Dv) (129) and Chlorite + Muscovite (Cm) (193). The number in the brackets represents number spectral signatures of corresponding minerals. Figure 5.1 shows the locations of minerals, identified for spectral library, using n-Dimensional visualizer in ENVI. Alunite, Calcite, Kaolinite, Desert varnish and Chlorite + Muscovite samples are shown in green, cyan, blue, yellow and red colors respectively.

5.1.2 Proposed Methodology

The proposed methodology for studying the effectiveness of similarity measures in distinguishing spectral signatures is presented here.

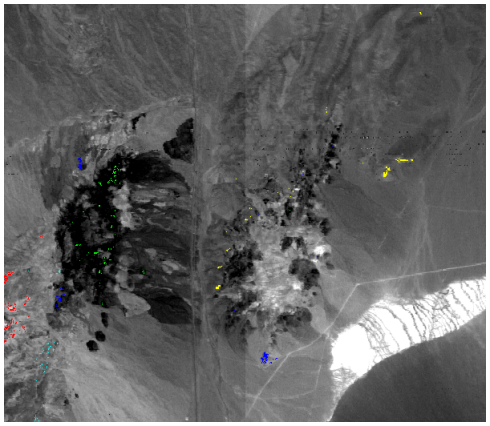

Figure 5.1: Identifying Extreme Pixels for Formation of Spectral Library: Utilizing ENVI for Visualization and Identification of Minerals

Discriminating Endmember Signatures

To study the effectiveness of similarity measures in discriminating endmember signatures, endmembers are extracted using PPI technique. Endmember signatures of minerals under study are extracted by averaging the spectral library signatures of respective mineral classes and shown in Figure 5.2. In Figure 5.2, x-axis and y-axis represent wavelength and reflectance respectively.

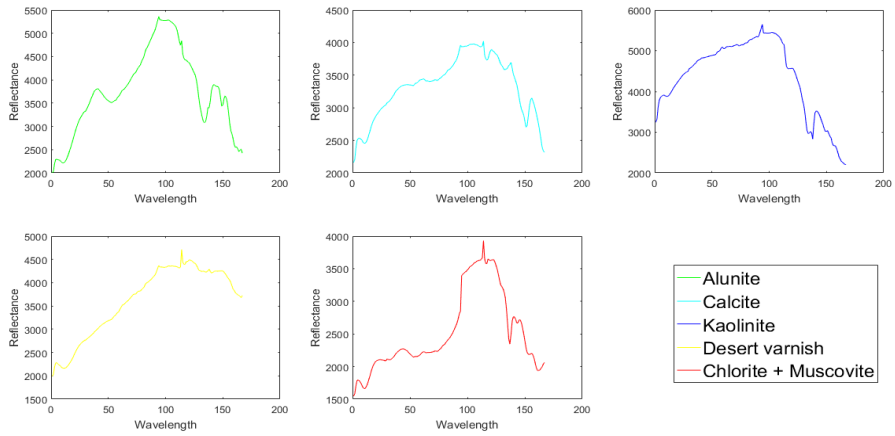

Figure 5.2: EE from Mineral Spectral Library Signatures: Leveraging PPI Method

Mixed Pixel Identification

To study the effectiveness of similarity measures in identifying a mixed pixel, targets generated from the mixture of endmembers extracted by PPI, Target-1 and Target-2 are considered. Target-1 (T-1) consists of 0.1, 0.6, 0.1, 0.1 and 0.1 fractions of Alunite (A), Calcite (C), Kaolinite (K), Desert varnish (D) and Chlorite + Muscovite (CM) endmembers respectively.

Similarly, mixture/abundance of target-2 (T-2) are 0.1, 0.1, 0.6, 0.1 and 0.1. T-1 and T-2 are considered as Calcite and Kaolinite endmember class target signatures respectively, by looking at their abundance values of mineral endmembers.

Endmember Class Target Signatures Identification

Segmentation/clustering of the data samples is carried out to identify endmember class targets. PPI endmembers are used for clustering the samples in spectral library. In order to study the effectiveness of similarity measures in identifying endmember class target signatures and distinguishing with other endmember class target signatures, two statistic measures called sensitivity and specificity are reported to validate the clustering performance.

Sensitivity: Sensitivity is also called as true positive rate or probability of detection. Sensitivity of single class is measured as

$$sensitivity = TP/(TP + FN) \tag{5.5}$$

where TP is true positive and FN is false negative values with respect to that particular class for which sensitivity is measured. Sensitivity of overall classification/clustering can be obtained by taking mean of sensitivity of all classes.

Specificity: Specificity is also called as true negative rate and for a particular class, it is given by

$$specificity = TN/(FP + TN) \tag{5.6}$$

where TN is true negative and FP is false positive values of the class. Specificity of overall classification/clustering is measured as mean of specificity of all classes.

Endmember Extraction

The ability of similarity measures in distinguishing spectrally distinct signatures is studied with task of identifying endmember for each mineral class from the spectral library samples.

5.1.3 Experimental Results

Spectral similarity between different endmember class signatures is measured to evaluate the discrimination power of similarity measures. Lesser the correlation between different endmembers higher the discrimination power is. Similarly, higher the correlation between

different endmembers lesser the discrimination power is. To evaluate the performance of similarity measures in identifying a mixed pixel, experiments are conducted with two synthetically generated target signatures T-1 and T-2. Spectral similarity matching between the targets T-1 and T-2 with the endmembers is carried out to evaluate the performance. Target class endmember must be matched with higher similarity while non-target class endmembers match with lower similarity values. The data samples which are more similar to particular endmember is clustered into that endmember class. Higher the sensitivity and specificity values, better the classification/clustering accuracy is. To evaluate performance of similarity measures in endmember extraction, SM-SCA is adapted.

Table 5.1: Comparative Analysis of SMAs in Distinguishing Spectral Signatures

(a) Endmember Discrimination

E-E pair	**SAM**	**SCM**	**SID**	**PC**
Al-Ca	0.99	0.89	0.98	**0.42**
Al-Ka	0.99	0.70	0.97	**-0.21**
Al-Du	0.99	0.71	0.97	**0.58**
Al-Cm	0.99	0.75	0.97	**0.35**
Ca-Ka	0.99	0.61	0.97	**-0.18**
Ca-Du	0.99	0.74	0.98	**0.44**
Ca-Cm	0.99	0.83	0.98	**0.39**
Ka-Du	0.96	0.05	0.91	**-0.75**
Ka-Cm	0.97	0.31	0.93	**-0.40**
Du-Cm	0.99	0.78	0.98	**0.54**

(b) Target Identification

E-T pair	**SAM**	**SCM**	**SID**	**PC**
Al-T1	0.99	0.92	0.99	0.57
Ca-T1	**1.00**	**0.99**	**1.00**	**0.86**
Ka-T1	0.99	0.61	0.97	-0.29
Du-T1	0.99	0.77	0.98	0.64
Cm-T1	0.99	0.89	0.99	0.64
Al-T2	0.99	0.87	0.98	0.10
Ca-T2	1.00	0.81	0.99	0.08
Ka-T2	**1.00**	**0.95**	**0.99**	**0.79**
Du-T2	0.98	0.35	0.95	-0.38
Cm-T2	0.98	0.59	0.96	-0.04

(c) Clustering Endmember Targets

	SMAs	**Al**	**Ca**	**Ka**	**Du**	**Cm**	**OA**
Sn	SAM	1	1	1	1	1	1
	SCM	1	1	0.99	1	1	1
	SID	1	1	0.99	1	1	1
	PC	0.81	0.89	0.99	1	1	0.94
Sp	SAM	1	1	1	1	1	1
	SCM	1	1	1	1	1	1
	SID	1	1	1	1	1	1
	PC	1	1	1	0.95	1	0.99

(d) Endmember Extraction (SM-SCA)

SMAs	**Al**	**Ca**	**K**	**D**	**CM**
SAM	✓	✓	-	✓	✓
SCM	✓	✓	✓	-	✓
SID	✓	✓	-	✓	✓
PC	✓	✓	✓	✓	✓

Similarity Measures in Discriminating Endmember Signatures

Table 5.1a shows correlation measurements between endmembers extracted by PPI method. It is observed that PC has high discrimination power than remaining similarity measures in distinguishing different endmember signatures. Performance of SCM is better than SAM and SID.

Similarity Measures in Mixed Pixel Identification

Performance of similarity measures in mixed pixel identification is shown in Table 5.1b. All similarity measures are correlating T-1 and T-2 with endmembers C and K respectively, but except PC remaining are failed to discriminate non-target endmembers with less correlation. In the case of T-2, PC is able to discriminate non-target endmembers with less correlation. Overall performance of PC is better than SAM, SCM and SID in discriminating target and non-target endmembers.

Similarity Measures in Endmember Class Target Signatures Identification

Performance of similarity measures in identifying target class signatures and discrimination with non-target class signatures is tabulated in Table 5.1c with the help of sensitivity and specificity respectively. SAM has high sensitivity and specificity values and hence it's performance is better than other similarity measures. Performance of SCM and SID are almost similar and better than that of PC. Though the clustering performance of PC is low, it is reasonable but not worse.

Similarity Measures in Endmember Extraction

Similarity measures are explored in endmember extraction and their ability in extracting endmember signatures of different classes from the experimental data is presented in Table 5.1d. The ✓ mark represents the endmembers that are extracted by the proposed endmember extraction algorithms. PC is the only similarity measure that extracted endmembers of all classes. SAM measures only positive correlation whereas SCM measures negative correlation also and hence their performance is little different in endmember extraction. Performance of SID is similar that of SAM and SCM.

Since SAM, SCM and SID considers spectral signatures as vectors in measuring simi-

larity between spectral signatures, their performance is similar almost in all the experiments. PC has advantage of considering frequency domain information in measuring correlation between signatures, and therefore overall performance of PC is better than remaining similarity measures almost in all experiments conducted in this study. Hence PC is recommended for hyperspectral data analysis.

Inferences

- It is inferred that PC is not only an effective but also a robust similarity measure among the similarity measured used to identify different target signatures.
- Experimental results show the ability of similarity measures, especially PC, in endmember extraction also.

5.2 GSSM

The diagnostic features considered in identifying and discriminating spectral signatures, especially of minerals, contain absorption features in terms of shape, depth and wavelength position of the absorption Clark et al. (2003). Though various SMAs were developed to discriminate the spectral signature using different theoretical strategies, identification of diagnostic features and thereby matching the overall patterns of spectral signatures with the existing ones is still a difficult/challenging task. Therefore, in this work, a gradient based spectral similarity measure (GSSM) to identify (highlight) the diagnostic features of spectral signatures in a better manner is presented. Effectiveness of proposed GSSM in distinguishing spectral signatures is studied with the four criterion by using spectral signatures of minerals present in the spectral library formed earlier.

5.2.1 Proposed GSSM

GSSM is designed by deploying gradient correlation (GC) proposed in Penney et al. (1998) to measure similarity between two images in the medical field. GC captures the edge information and therefore it is explored to capture diagnostic features of spectral signatures for better analysis of HSI data. To the best of our knowledge, the gradient correlation has not been employed in HSI data analysis so far.

Spectral Gradient

gradient correlation is incorporated by measuring spectral gradient or gradient of spectral signature (GS). GS is measured as the first derivative of the spectral signature. In the discrete case, differences in reflectance values between the adjacent bands is calculated as GS. Thus, dimensionality of the GS is usually one less than that of the original spectral signature (OS). Considering two spectral signatures X and Y, their GS is calculated using

$$\Delta X_i = X_{i+1} - X_i \;\; and \;\; \Delta Y_i = Y_{i+1} - Y_i \tag{5.7}$$

where ΔX_i and ΔY_i represent ith values of difference vectors for X and Y.

GSSM

The GSSM similarity between the spectral signatures is calculated as the normalized correlation or Pearson's correlation, as that of SCM, of the GS vectors. Spectral matching between X and Y using GSSM is measured as

$$GSSM = \left(\frac{\sum_{i=1}^{L}\left(\Delta X_i - \bar{\Delta X}\right) \times \left(\Delta Y_i - \bar{\Delta Y}\right)}{\left(\sum_{i=1}^{L}\left(\Delta X_i - \bar{\Delta X}\right)^2\right)^{1/2} \times \left(\sum_{i=1}^{L}\left(\Delta Y_i - \bar{\Delta Y}\right)^2\right)^{1/2}}\right) \tag{5.8}$$

where $\bar{\Delta X}$ and $\bar{\Delta Y}$ are the means of vectors ΔX and ΔY.

5.2.2 Spectral Gradient in Identifying Absorption Features

The PPI endmembers and their spectral gradients are shown in Figure 5.3 Yadav et al. (2021). In the Figure 5.3, x-axis is the band number and y-axis is the reflectance value. From the Figure 5.3, it is evident that spectral gradients highlight absorption features of different mineral signatures with the peaks representing the depth of absorption at mineral specific wavelengths. In addition, it is also observed that spectral gradients may appear noisy as they represent high-frequency components of the signatures.

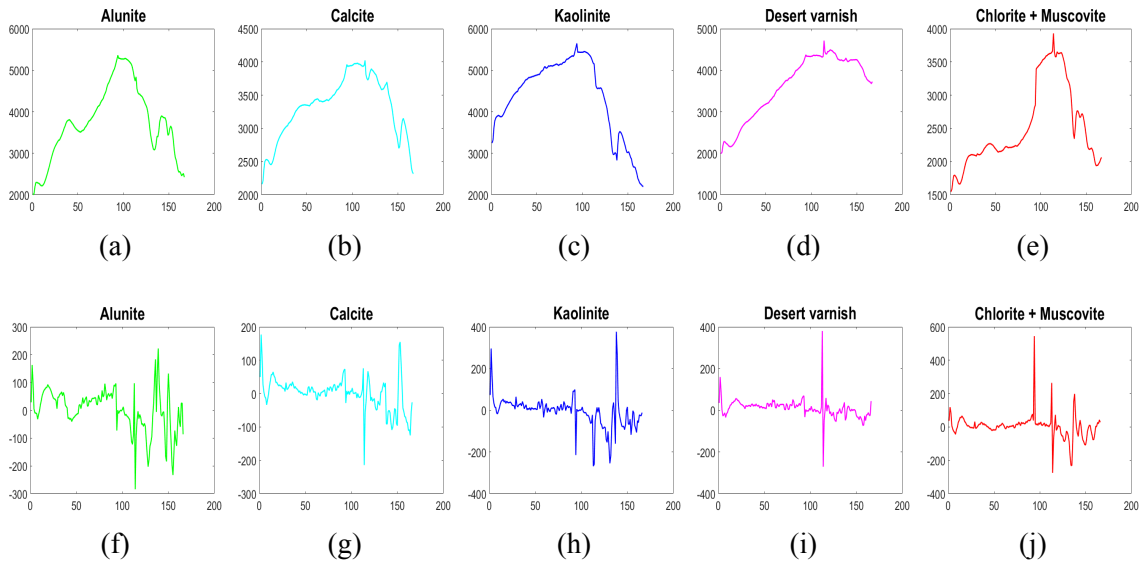

Figure 5.3: Mineral Endmember Signatures (First Row) and Their Spectral Gradients (Second Row): A Comparative Visualization

5.2.3 Experimental Results

To compare the effectiveness of proposed GSSM in distinguishing spectral signatures, different spectral similarity measures like SAM Kruse et al. (1993), SCM De Carvalho and Meneses (2000), SID Chang (1999), PC Erturk and Erturk (2006) and DSSC Kumar et al. (2021) are implemented. All the similarity values are normalized from 0 to 1 for making comparison easy.

Similarity Measures in Discriminating Endmember Signatures

From the Table 5.2a, it is clear that proposed GSSM is able to discriminate PPI endmembers with less similarity values as that of PC. Proposed GSSM performed not only better than PC almost in half of the times and but also reasonably good as that of PC and better than remaining similarity measures in discriminating PPI endmembers.

Similarity Measures in Mixed Pixel Identification

Target-1 (T-1) and Target-2 (T-2) are synthetically generated by considering mixture of all the endmembers. Targets T-1 and T-2 belongs to Calcite and Kaolinite endmembers as their abundances values are 0.6 and remaining endmembers have 0.1 abundances values. The proposed GSSM is able to match the target endmembers with high similarity as well as discriminate non-target endmembers with less similarity values in case of both the targets

T-1 and T-2 and same can be observed from the Table 5.2b. DSSC failed to identify target T-2. Overall performance of PC and proposed GSSM are better than remaining similarity measures in discriminating target and non-target endmembers.

Table 5.2: Performance Assessment of GSSM in Distinguishing Spectral Signatures

(a) Endmember Discrimination

E-E pair	SCM	PC	DSSC	GSSM
Al-Ca	0.95	0.71	0.98	**0.67**
Al-Ka	0.85	**0.40**	0.98	0.84
Al-Du	0.85	0.79	0.99	**0.77**
Al-Cm	0.87	0.67	0.91	**0.65**
Ca-Ka	0.80	**0.41**	0.95	0.66
Ca-Du	0.87	**0.72**	0.99	0.78
Ca-Cm	0.91	0.70	0.96	**0.65**
Ka-Du	0.53	**0.13**	0.94	0.62
Ka-Cm	0.66	**0.30**	0.84	0.60
Du-Cm	0.89	0.77	0.93	**0.73**

(b) Target Identification

E-E pair	SCM	PC	DSSC	GSSM
Al-T1	0.96	0.78	0.98	0.76
Ca-T1	**0.99**	**0.93**	**1.00**	**0.95**
Ka-T1	0.81	0.35	0.95	0.75
Du-T1	0.88	0.82	0.99	0.85
Cm-T1	0.94	0.82	0.96	0.81
Al-T2	0.94	0.55	**0.99**	0.86
Ca-T2	0.91	0.54	0.98	0.74
Ka-T2	**0.97**	**0.89**	**0.99**	**0.97**
Du-T2	0.68	0.31	0.98	0.73
Cm-T2	0.80	0.48	0.91	0.75

(c) Clustering Endmember Targets

	SMAs	Al	Ca	Ka	Du	Cm	OA
Sn	SCM	1	1	0.99	1	1	**1**
	PC	0.81	0.89	0.99	1	1	0.94
	DSSC	0.89	0.98	0.99	0.92	0.86	0.93
	GSSM	0.99	1	1	0.99	1	**1**
Sp	SCM	1	1	1	1	1	**1**
	PC	1	1	1	0.95	1	0.99
	DSSC	0.99	0.93	0.99	0.99	1	0.98
	GSSM	1	1	1	1	1	**1**

(d) Endmember Extraction

SM-SCA

SMAs	Al	Ca	K	D	CM
SCM	✓	✓	✓	✓	✓
PC	✓	✓	✓	✓	✓
DSSC	✓	✓	✓	✓	✓
GSSM	✓	-	✓	✓	✓

SM-EIA

SMAs	Al	Ca	K	D	CM
SCM	✓	✓	✓	✓	✓
PC	✓	✓	✓	✓	✓
DSSC	✓	✓	✓	✓	✓
GSSM	✓	-	✓	✓	✓

Similarity Measures in Endmember Class Target Signatures Identification

The spectral library samples are clustered into PPI class endmembers with which they have highest similarity. Sensitivity and specificity values are reported to measure the clustering performance. The sensitivity and specificity parameters obtained on performing clustering operations are presented in Table 5.2c and it is inferred that proposed GSSM is performed well as that of SAM which outperformed among all similarity measures used.

Similarity Measures in Endmember Extraction

SM-SCA Palla et al. (2020) and it's improved version a SM-EIA Yadav et al. (2020b) are adapted to explore proposed similarity measures in endmember extraction. From the Table 5.2d, it is observed that proposed GSSM is the only similarity measures that extracted endmembers for all the minerals when SM-EIA is tested. The designing criterion of SM-SCA is the reason for GSSM not able to extract less abundant Calcite (64 samples out of 657) mineral, though GSSM is as good as PC in discriminating endmember signatures (see Table 5.2a). This experiment clearly shows the need for improving the design process of both SM-SCA and SM-EIA, to improve performance of all the similarity measures, and to come up with better version which can incorporate the benefits of both the algorithms.

Considering all the criterion used to experiment with the different similarity measures in identifying spectrally distinct target signatures, it is concluded that proposed GSSM is a reasonably better choice to explore in the HSI analysis. Though noise present in the data is exposed with the first derivatives of the spectral signatures, GSSM is not much affected with that noise when discriminating spectral signatures. The reason for this may be that all the spectral signatures are influenced by same amount of noise, which might be suppressed in measuring similarity by GSSM (see Eq. (5.8)). Another reason is that the diagnostic features were highlighted in a better manner.

5.3 GC Incorporated SMAs

The diagnostic features considered in identifying and discriminating spectral signatures, especially of minerals, contain absorption features in terms of shape, depth and wavelength position of the absorption Clark et al. (2003). Recently developed geometrical similarity measure called GSSM Yadav et al. (2021) is not only useful in identifying the diagnostic

features but also out-performed in discriminating the spectral signatures. By assessing the rate of change in reflected intensity with respect to wavelength, spectral gradient eliminates variations in geometry and incident illumination Angelopoulou et al. (1999).

Many of the classical SMAs except GSSM try to match overall pattern of the spectral signatures without considering diagnostic features. Though SMAs were developed to distinguish the spectral signatures using different theoretical strategies, discrimination of the overall patterns by capturing the diagnostic features is of great importance. Hence, this study explores to compare the effectiveness of the gradient correlation (GC) in comparison with simple correlation (SC) measures of the commonly used SMAs in discriminating spectrally distinct signatures.

5.3.1 Spectral Matching using Gradient Correlation

GC is incorporated by measuring GS as mentioned in 5.7. Consider X and Y and ΔX_i and ΔY_i are two spectral signatures and their spectral gradients measured respectively, then SC between them is measured as

$$simplecorrelation = SMAs(X, Y) \tag{5.9}$$

The GS is explored in measuring correlation with the classical SMAs to incorporate GC. The GC is measured as

$$Gradientcorrelation = SMAs(\Delta X, \Delta Y) \tag{5.10}$$

5.3.2 Experimental Results

The effectiveness of proposed GC comparing to SC use of the proposed GS in discriminating spectrally distinct signatures is assessed with different SMAs like SAM, SCM, PC and DSSC. All the similarity measures are normalized to have value between 0 and 1 which makes the comparison easy. Performance of the SMAs in distinguishing spectral signatures using the proposed GC is explored in (i) discriminating endmember signatures and (ii) mixed pixel identification.

Discriminating Endmember Signatures

The similarity values computed between PPI endmember pairs, presented in Table 5.3a, show that the GC measured with all the geometrical SMAs have higher discriminating power than the SC. The mismatch in locations of the peaks in GS of different mineral signatures might be the reason for them to be discriminated better by GC. Fourier transform of a difference signal enhances high-pass filtering and because of this reason low frequency components, which may accountable to represent absorption features, are suppressed and high frequency components that represent noise are enhanced. GC using PC is not able to produce expected results in discriminating distinct signatures.

Table 5.3: Impact of GC on SMAs in Distinguishing Spectral Signatures

(a) Endmember Discrimination

SMAs	**SAM**		**SCM**		**PC**		**DSSC**	
E-E pair	**SC**	**GC**	**SC**	**GC**	**SC**	**GC**	**SC**	**GC**
Al-Ca	0.99	**0.35**	0.95	**0.67**	0.71	**0.68**	0.98	**0.32**
Al-Ka	0.99	**0.68**	0.85	**0.84**	**0.40**	0.67	0.98	**0.68**
Al-Du	0.99	**0.54**	0.85	**0.77**	0.79	**0.75**	0.99	**0.49**
Al-Cm	0.99	**0.30**	0.87	**0.65**	0.67	**0.60**	0.91	**0.30**
Ca-Ka	0.99	**0.32**	0.80	**0.66**	**0.41**	0.52	0.95	**0.29**
Ca-Du	0.99	**0.56**	0.87	**0.78**	**0.72**	0.85	0.99	**0.56**
Ca-Cm	0.99	**0.29**	0.91	**0.65**	0.70	**0.62**	0.96	**0.27**
Ka-Du	0.96	**0.21**	**0.53**	0.62	**0.13**	0.53	0.94	**0.19**
Ka-Cm	0.97	**0.19**	0.66	**0.60**	**0.30**	0.46	0.84	**0.19**
Du-Cm	0.99	**0.47**	0.89	**0.73**	0.77	**0.69**	0.93	**0.43**

(b) Target Identification

SMAs	**SAM**		**SCM**		**PC**		**DSSC**	
E-T pair	**SC**	**GC**	**SC**	**GC**	**SC**	**GC**	**SC**	**GC**
Al-T1	0.99	**0.52**	0.96	**0.76**	0.78	**0.72**	0.98	**0.45**
Ca-T1	**1.00**	0.91	**0.99**	0.95	**0.93**	**0.93**	**1.00**	0.90
Ka-T1	0.99	**0.49**	0.81	**0.75**	**0.35**	0.57	0.95	**0.41**
Du-T1	0.99	**0.69**	0.88	**0.85**	**0.82**	0.89	0.99	**0.69**
Cm-T1	0.99	**0.63**	0.94	**0.81**	0.82	**0.77**	0.96	**0.55**
Al-T2	0.99	**0.73**	0.94	**0.86**	**0.55**	0.77	0.99	**0.69**
Ca-T2	0.99	**0.49**	0.91	**0.74**	**0.54**	0.66	0.98	**0.48**
Ka-T2	**1.00**	0.94	**0.97**	**0.97**	**0.89**	**0.89**	**0.99**	0.89
Du-T2	0.98	**0.44**	0.68	**0.73**	**0.31**	0.70	0.98	**0.43**
Cm-T2	0.98	**0.49**	0.80	**0.74**	**0.48**	0.64	0.91	**0.47**

Mixed Pixel Identification

Target-1 (T-1) and Target-2 (T-2) are synthetically generated considering mixture of all the endmembers. Targets T-1 and T-2 belongs to Calcite and Kaolinite endmembers as their abundance values are 0.6 and remaining endmembers have abundance values of 0.1.

Performance of the GC in mixed pixel identification is similar to that of discrimination of endmember signatures as observed in Table 5.3b. The GC with all the geometrical SMAs is able to match and identify the target endmembers with high similarity as well as distinguish non-target endmembers with less similarity values in case of both the targets T-1 and T-2. As it is expected, GC using PC have mixed results in the case of T-1 and average performance in the case of T-2.

Overall Performance of GC Incorporated SMAs

Considering all the criterion used to experiment with the different SMAs in discriminating spectrally distinct target signatures, it is clear that measuring gradient correlation using spectral gradients discriminate all the spectral signatures with the geometrical SMAs especially SAM and DSSC in a better manner. From this it is ascertained that the absorption features identified by spectral gradient dominate the enhanced noise in HSI analysis to identify target spectral signatures as well as discriminate non-target spectral signatures.

Considering both the experiments for discriminating spectrally distinct target signatures with the various SMAs explored here in this work, it is clear that incorporating the GC significantly discriminates the spectral signatures with the geometrical SMAs, especially SAM and DSSC. From this, it is ascertained that the absorption features identified using GS dominate the high frequency components in the HSI analysis in identifying target spectral signatures as well as in discriminating non-target spectral signatures.

5.4 Relative Spectral Discrimination Power (RSDPW)

Though different SMAs developed based on different theoretical strategies, choosing an effective SMA is still a challenging task. To evaluate the performance of different SMAs in distinguishing different spectral signatures, in Chang (1999) three statistics spectral discriminatory probability (SDP), spectral discriminatory entropy (SDE) and relative spectral discriminatory power (RSDPW) were introduced. RSDPW is one such a performance measure

to know the spectral discrimination power of SMAs in distinguishing two target signatures with a reference signature.

RSDPW discriminates how one spectral signature is distinct from another relative to a reference spectral signature. Classical way of measuring RSDPW do not takes into account of spectral matching between the two spectral signatures to be discriminated. This is what makes classical way of measuring RSDPW not so robust in measuring discrimination power of SMAs. Though, there are studies that reported RSDPW in Chang (1999), Adep et al. (2016) and Kumar et al. (2021), a meaningful way of discussion on discrimination by RSDPW is further needed with a comprehensive study. Therefore, in this paper, a reformulation for RSDPW by incorporating the spectral matching between the two spectral signatures to be discriminated is presented to measure it in a more meaningful manner and study spectral discrimination for further.

5.4.1 RSDPW

RSDPW assesses the SMA's spectral discrimination power. When two SMAs are given, it aids in the discovery of an effective SMA. Considering two spectral signatures s_i and s_j and d be a reference spectral signature, then, RSDPW of an SMA m in discriminating s_i and s_j with respect to d is measured as

$$PW^{m}_{s_i,s_j:d} = max\left(\frac{m(d,s_i)}{m(d,s_j)}, \frac{m(d,s_j)}{m(d,s_i)}\right) \tag{5.11}$$

where $PW^{m}_{s_i,s_j:d}$ is RSDPW value of SMA called m and $m(d,s_j)$ is spectral matching or similarity measurement between d and s_j) by SMA m. The more the RSDPW value, higher the discrimination power of SMA is.

In general, RSDPW value is higher than 1. Higher RSDPW value represents the number of times a SMA could discriminate s_i and s_j with respect to d. But often, the intra and inter class variations present especially amongst mineral signatures, due to their subtle differences, questions the meaningfulness of measured RSDPW value. This is what makes RSDPW appears not robust. The reason for this is that classical way of measuring RSDPW do not takes into account the spectral matching between the two spectral signatures to be discriminated. Therefore, RSDPW value serves just as a number which do not have much meaning in actually measuring power of discriminating spectral signatures.

5.4.2 Reformulated RSDPW

Reformulated RSDPW of an SMA m in discriminating s_i and s_j with respect to d is given as

$$PW^{m}_{s_i,s_j:d} = \frac{|m(s_i, s_j)|}{|m(d, s_i)| + |m(d, s_j)|}. \tag{5.12}$$

The numerator term in the reformulated RSDPW is to incorporate how a SMA discriminates s_i and s_j and the denominator term is to get an idea about how distinct the s_i and s_j with respect to that SMA are. In short, the reformulated RSDPW looks at the two spectral signatures that are to be discriminated and the reference spectral signature simultaneously (at the same time) and try to find how far they are from each other and from the reference spectrum as well in-order to be perspicacious to get a good idea about the spectral diversity of spectral signatures.

If the distance or discrimination value between two spectral signatures match with their cumulative distances from the reference signature, then the two spectral signatures are considered to be oppositely correlated or spectrally distinct and can be completely discriminated with respect to the reference signature without any ambiguity. In that case RSDPW value would be 1. In other cases, in general, RSDPW value would be less than 1 and varies from 0 (in case of similar signatures). That is, power to discriminate similar spectral signatures is less and zero (see numerator term in Eq. 2) if same/similar signatures are to be discriminated. If the RSDPW value is around 0.5, then two spectral signatures are said to be marginally discriminable. If the RSDPW is more than 0.5, then it is considered that discrimination power is good, and higher for values more than 0.7.

5.4.3 RSDPW vs Reformulated RSDPW Measurements

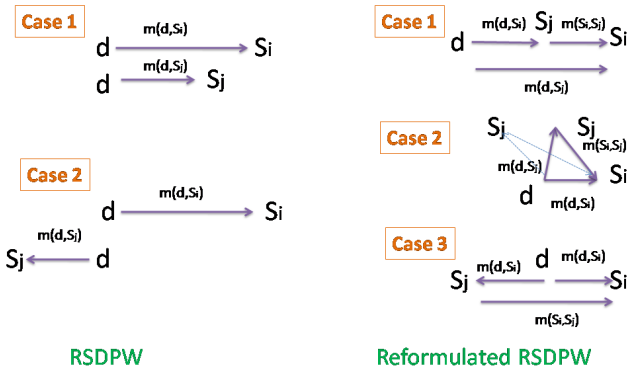

Figure 5.4: Measuring RSDPW: Classical vs. Reformulated Approaches

Figure 5.4 depicts the possibilities/cases of measuring RSDPW in a classical way and reformulated way. From the Figure 5.4, it is clearly understand that reformulated RSDPW have much more meaningful measurements than the former RSDPW's.

5.4.4 Experimental Results

The PPI endmembers extracted from the spectral library of 5 minerals are considered to form different combinations of reference signature (d) and the two spectral signatures (s_i and s_j) to be discriminated to evaluate the performance of proposed RSDPW with the former RSDPW. This study considers Alunite endmember (A) and Desert Varnish endmember (D) as d as two different cases.

Table 5.4: Comparative Analysis of RSDPW Values: Former vs. Proposed Metrics in SMAs

(a) Former RSDPW

d	s_i	s_j	**ED**	**SAM**	**SID**
Al	Ca	Ka	1.38	2.66	1.50
		Du	1.03	4.81	1.50
		Cm	2.03	77.00	1.50
	Ka	Du	1.43	1.81	1.00
		Cm	1.47	29.00	1.00
	Du	Cm	2.10	16.00	1.00
Du	Al	Ca	1.11	6.25	1.50
		Ka	2.12	3.00	3.00
		Cm	1.84	5.13	1.50
	Ca	Ka	2.34	2.08	4.50
		Cm	2.04	1.22	1.00
	Ka	CM	1.15	1.71	4.50

(b) Proposed RSDPW

d	s_i	s_j	**ED**	**SAM**	**SID**
Al	Ca	Ka	0.80	0.13	0.60
		Du	0.44	1.08	0.40
		Cm	0.43	1.18	0.40
	Ka	Du	0.87	1.07	1.50
		CM	0.90	2.20	1.50
	Du	Cm	0.59	4.82	0.33
Du	Al	Ca	0.54	0.66	0.40
		Ka	0.46	0.45	0.25
		Cm	0.74	0.01	0.60
	Ca	Ka	0.65	0.09	0.27
		Cm	0.49	0.51	0.50
	Ka	Cm	0.80	0.51	0.64

Former RSDPW

Table 5.4a presents the RSDPW values measured in a classical way. From the Table 5.4a, it is clear that ED has lower discrimination power as it have lower to marginal RSDPW values, and, SID also have lower discrimination power as that of ED. Table 5.4b illustrates that ED has shown better discrimination power (good to higher RSDPW values) through proposed

measurements than the former. SAM is reasonably better SMA to be able discriminate most of the endmember pairs, and, it is able to discriminate Chloromuscovite (CM) from Calcite (C), Kaolinite (K) and Desert varnish (D) with high RSDPW (because of CM being distinct from C, K and D and same can be observed from the endmember patterns shown in Figure 5.3) with reference to Alunite (A). SAM also able to discriminate all the endmember pairs with marginal to good discrimination power in reference to D.

Reformulated RSDPW

The RSDPW values for SMAs in discriminating PPI endmembers obtained through proposed reformulation are presented in the Table 5.4a. Table 5.4b illustrates that ED has shown better discrimination power (good to higher RSDPW values) through proposed measurements than the former. Additionally, Alunite (A) has complete discrimination power in distinguishing all the endmember pairs except Calcite (C) to Kaolinte (K). A scrutinizing observation on visual inspection of PPI endmembers from the Figure 5.3 depicts the same and supports the proposed RSDPW values of SAM. SID also showed reasonably good discrimination power as that of ED when compared with former measurements.

Former RSDPW vs Proposed RSDPW

Table 5.5: Degree of Discrimination: Comparative Analysis of Former vs Proposed RSDPW Values

Degree of discrimination	**RSDPW range**	
	Former	**Proposed**
No discrimination	Do not exists	0.00
Poor discrimination	<1.50	<0.20
Marginal discrimination	1.50-2.50	0.20-0.35
Good discrimination	2.50-5.00	0.35-0.65
High discrimination	5.00-10.00	0.65-1.00
Complete discrimination	>10.00	>=1.00

Among all the SMAs tested to discriminate PPI endmembers, SAM showed better discrimination power both with the former and proposed RSDPW. But, proposed reformulation appears to be more reasonable in measuring RSDPW of all the SMAs tested. Surprisingly,

proposed RSDPW said to be reported higher values (more than 1, as it is out of expectation). Endmember pairs being more distinct to each other than they are with the reference spectral signature is the reason for yielding unexpected higher values of RSDPW. Overall, the experimental results show that proposed reformulated RSDPW not only a meaningful way to measure it but also robust/standard enough to compare various SMAs by measuring it.

As per the results obtained from the Table 5.4a and Table 5.4b and comparing them with the visual inspection, an in-situ method, of the endmemeber spectral signatures, the range of RSDPW values for different levels of discrimination is demonstrated for the present study (for the PPI endmembers tested) in the Table 5.5. Table 5.5 is valid for this study only and sufficient experimental validation is required to affirm/confirm/verify it further. Visual inspection considers the orientation of overall spectral pattern, shape, size and position (at mineral specific wavelengths) of diagnostic features and other noticeable differences in the patterns of the endmember pairs to obtain the range of RSDPW values for different levels of discrimination.

Overall, the experimental results show that the proposed reformulated RSDPW not only a meaningful way to measure it but also robust/standard enough to compare various SMAs by measuring it. In future, sufficient experimentation would be carried out to check the robustness of proposed RSDPW and also to validate the range of RSDPW values for different levels of discrimination.

Summary:

This chapter presents study on effectiveness of various SMAs in distinguishing spectral signatures of minerals. Initially, four different criterion: (i) distinguishing different endmember signatures (ii) identifying a mixed pixel signature (iii) endmember class targets identification/segmentation/clustering and (iv) endmember extraction are proposed to study the effectiveness of classical SMAs. Further, effectiveness of proposed GSSM that highlights diagnostic features at mineral specific wavelengths is studied. Additionally, spectral gradient adapted from GSSM is explored to study the effectiveness of gradient correlation in comparison to simple correlation. At the end, a reformulated RSDPW that distinguish spectral signatures in a meaningful way is presented.

The next chapter presents research work on change detection and mineral classification.

Chapter 6

Change Detection and Mineral Classification

Enduring difficulty for a meaningful purpose is a sublime pleasure.

Radhanath Swami

Introduction

This chapter delves into the intricacies of change detection and mineral classification. Commencing with the application of endmembers derived from the ATGP algorithm, which serve as comprehensive representatives of the HSI, our focus is on discerning sub-pixel features beyond simplistic characteristics. The introduction of endmember-related features is pivotal, undergoing scrutiny against original and deep features in change detection through our proposed ATGP-CD methodology. Additionally, we present a virtual sample generation technique, augmenting training samples. Culminating the chapter is the unveiling of a meticulously designed 1-D CNN model crafted for the classification of hyperspectral mineral data. This chapter is a nuanced exploration aimed at enhancing the precision of change detection and mineral classification in hyperspectral imaging.

6.1 HSI-CD

Classical and DL approaches consider change information at pixel level i.e. pixel to pixel change either by comparing the corresponding pixels alone or with their local neighborhood pixels. Therefore, identification of features for every pixel that relate the most significant information of the whole HSI-CD data in a simple and an efficient way to detect changes effectively is the need of the hour. Therefore, an endmember related feature extraction is

proposed for HSI-CD. ATGP algorithm is adapted to extract endmembers to identify sub-pixel level or endmember related features to detect changes from experimental CD sets. Proposed endmember related features are then explored with classical CD techniques as well as DL based CD models in detecting changes. Therefore, proposed Cd technique is named as ATGP-CD.

6.1.1 ATGP-CD

The main contribution of this work involves in extracting the more meaningful features that are simple yet effective to relate each pixel with the most significant information present in the image. Since endmembers are the most significant information with which whole HSI can be represented, it is considered that exploring the endmembers related information may help in CD related tasks. Therefore, in this work an endmember based feature extraction is explored in detecting changes from HSI CD data sets. The primary objective of this work is to estimate the number of endmembers present in the data and to identify them by means of suitable endmember extraction algorithm. Then, the relationships of the extracted endmembers with each pixel is measured with commonly used spectral matching algorithm so that the changes can be detected with an ease considerably to the good amount. The measured spectral similarity values are considered as endmember based features for change detection.

Proposed Methodology

This figure 6.1 illustrates a comprehensive flowchart delineating the essential steps of the proposed methodology, ATGP-CD. It highlights the methodology's primary emphasis on identifying nuanced sub-pixel features that go beyond simple characteristics. The estimation of the number of endmembers in the data employs the Virtual Dimensionality (VD) algorithm Chang and Du (2004). Subsequently, the ATGP algorithm is employed to extract the required number of endmembers. The methodology further explores various similarity measures, including ED Gower (1985), SAM Kruse et al. (1993), SCM De Carvalho and Meneses (2000), SID Chang (1999), PC Erturk and Erturk (2006), DSSC Kumar et al. (2021) and GSSM Yadav et al. (2021) are explored to extract endmember-based features and also to study their effectiveness to explore further in CD tasks. All the similarity values measured by SMAs are normalized from 0 to 1. Thereafter, the classical CD techniques like CVA and SFA are explored on extracted endmember based features to detect the changes. The

proposed CD algorithms are called as ATGP-CVA and ATGP-SFA. SFA, CVA and DL based algorithms like GETNET and TDSSC are implemented to compare the results.

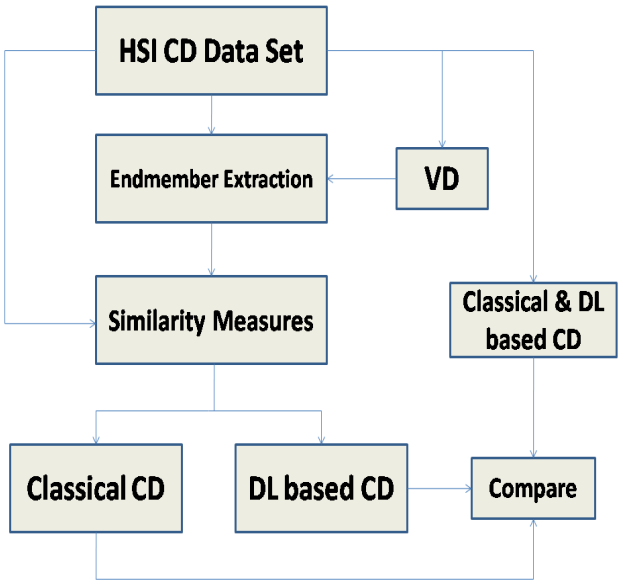

Figure 6.1: Methodology Overview: ATGP-CD for Sub-Pixel Feature Discernment

Experimental Results

Farmland and USA data set ground-truths contain six types of earth surfaces in each. Therefore, VD for them is considered as six. In river data set, there is no such information is available in the ground truth. Therefore, the number of endmembers to be extracted by ATGP is estimated by VD algorithm as thirteen. The endmembers extracted from time-1 data set are considered as endmembers for time-2 data set also to extract endmember related features using the similarity measures.

Primarily, the quality of proposed endmembers based features are tested with that's of original features using classical HSI-CD algorithms like SFA and CVA. Later, the quality of ATGP endmembers based features are compared with the quality of deep features extracted by DL based algorithms in CD. For this purpose, ATGP endmembers based features are fed to the DL models by avoiding deep feature extraction blocks (i.e. initial convolution layers) and preserving the change detection criterion. Performance of the CD algorithms are mentioned in terms of overall accuracy in percentage. In addition, influence of the VD on proposed ATGP-CVA in CD task is studied by considering different values for VD or varying VD from it's estimated value.

ATGP Endmembers based Features vs Original Features

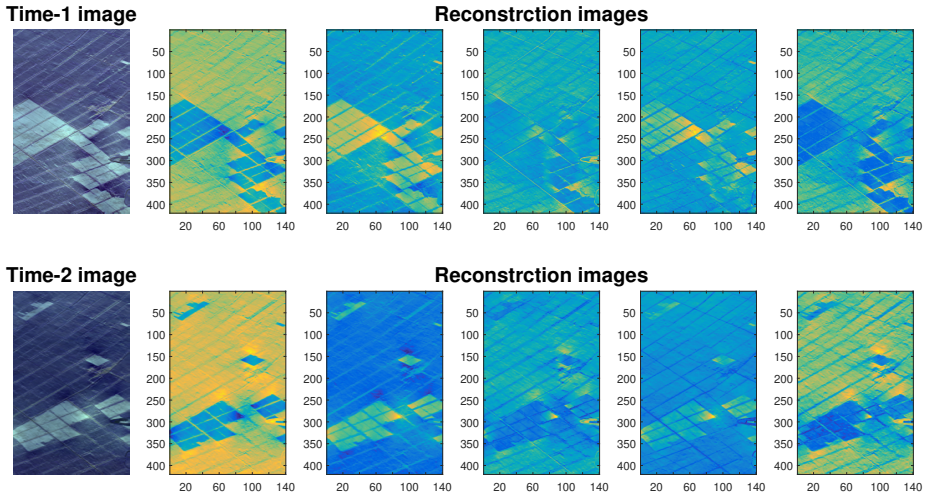

(a) Farmland Data Set: Time-1 (First Row) and Time-2 (Second Row)

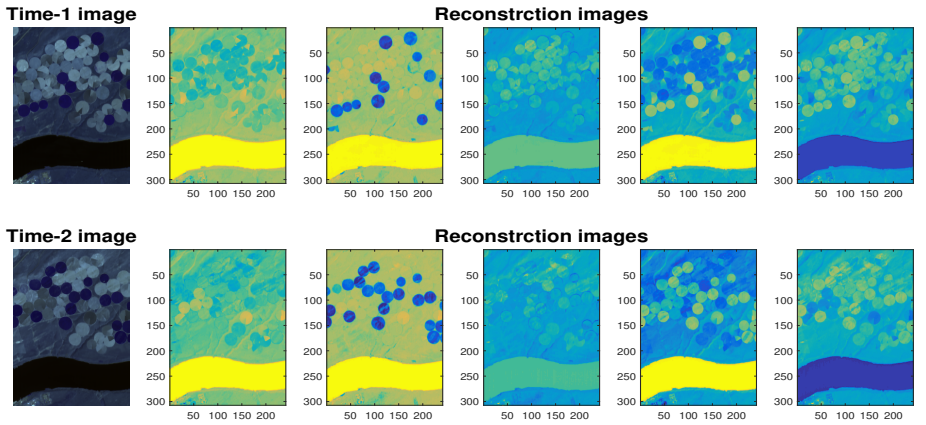

(b) USA Data Set: Time-1 (First Row) and Time-2 (Second Row)

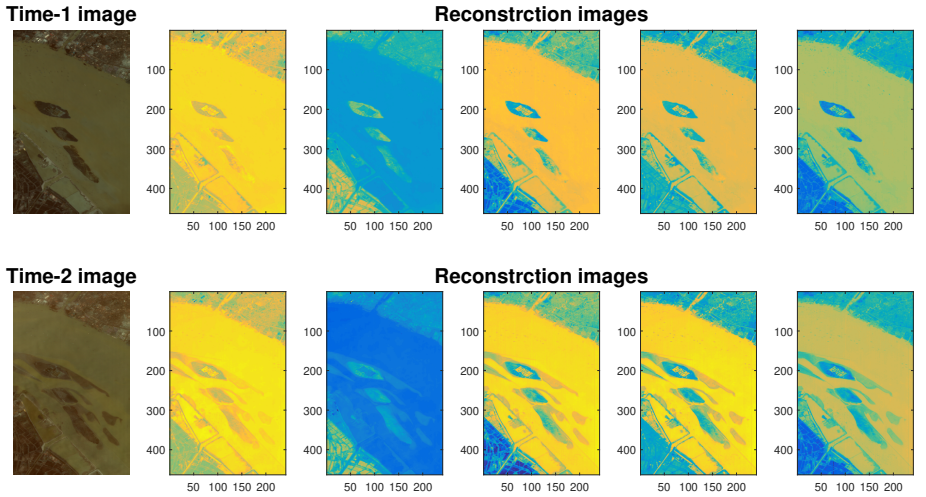

(c) River Data Set: Time-1 (First Row) and Time-2 (Second Row)

Figure 6.2: ATGP Endmember Features Utilizing ED Metric for CD Data set Reconstruction

The ATGP endmember related features identified using ED metric for reconstructing the CD data sets are shown in Figure 6.2. From Figure 6.2, it is clear that proposed endmember related features are able to represent the Time-1 and Time-2 CD data sets with the latent information significant to detect changes from them. Therefore, it is understood that proposed endmember related features are qualitative to reconstruct the CD data sets to analyze them further on final CD accuracy, quantitatively.

Table 6.1: Performance Comparison of ATGP-CD using Endmember-Based Features vs Original Features in HSI-CD

(a) ATGP-SFA

Features	Farmland	USA	River
(ED)	68.61	77.47	91.30
(SAM)	67.71	77.05	91.30
(SCM)	69.00	76.92	91.30
(PC)	68.67	77.02	90.84
(DSSC)	68.74	77.33	91.30
(GSSM)	81.00	82.37	89.87
SFA	64.69	77.35	91.3
DSFA	60.00	61.00	89.00
GETNET	93.15	90.44	96.86
TDSSC	95.25	96.49	97.17

(b) ATGP-CVA

Features	Farmland	USA	River
ED	88.74	93.53	95.52
SAM	87.21	74.96	94.38
SCM	86.85	88.74	94.64
PC	89.85	90.26	77.78
DSSC	87.46	79.09	93.81
GSSM	87.92	62.40	75.28
CVA	87.55	92.02	92.53
DSFA	60.00	61.00	89.00
GETNET	93.15	90.44	96.86
TDSSC	95.25	96.49	97.17

ATGP-SFA

Based on the results presented in Table 6.1a, it is clear that SFA with ATGP endmembers based features extracted by different similarity measures able to detect changes reasonably better than that of original features. Therefore, it is deduced that ATGP endmember based features extracted by different similarity measures are reasonably good as that of original features.

ATGP-CVA

Table 6.1b shows that CVA with ATGP endmember based features extracted by different similarity measures able to detect changes better than that of CVA with original features. In addition, performance of ATGP-CVA especially with ED features is better than DSFA-NET

and reasonably good as that's of GETNET and TDSSC. Performance of CVA is better than SFA and same can be observed on comparing Table 6.1a and Table 6.1b. Overall performance of ATGP-CVA is satisfactory with reasonably good accuracy.

ATGP Endmembers based Features vs Deep Features

The quality of ATGP endmembers based features are studied with that's of deep features extracted by DL based CD algorithms. Initially DL models like GETNET and TDSSC are implemented as it is with the original features. Then, the DL models with suitable modifications are implemented on ATGP endmembers based features to detect changes. Therefore, the block (first few convolutional layers) that is responsible for extracting deep features is removed from original architecture of TDSSC. In this work, we considered GETNET without unmixing architecture for implementation. The affinity matrix required for GETNET is calculated form the ATGP endmembers based features. Since size of the affinity matrix is reduced with the ATGP endmembers based features, GETNET is implemented with the reduced number of convolutional layers (2,4,8 16, 128 and 2) and reduced kernel size (2×2) by removing first two Max-Pooling layers.

Table 6.2: Performance Comparison of ATGP-CD using Endmember-Based Features vs Deep Features in HSI-CD

Features	**GETNET**			**TDSSC**		
	Farmland	**USA**	**River**	**Farmland**	**USA**	**River**
ED	93.14	95.53	95.95	91.63	94.90	95.50
SAM	92.52	89.92	94.99	92.30	90.50	94.21
SCM	92.17	90.84	94.78	91.53	91.07	94.88
PC	90.23	93.17	92.42	90.49	90.25	93.51
DSSC	93.57	88.30	96.13	92.11	94.52	95.70
GC	92.50	89.36	91.87	91.86	89.47	93.39
Deep	93.15	90.44	96.86	95.25	96.49	97.17

Table 6.2 presents that ATGP endmembers based features are as good as that of deep features extracted by DL models in CD tasks. Careful observation of results presented in Table 6.2 and Table 6.1 reveal that performance on ATGP endmembers based features is improved with the change detection criterion considered in the DL based CD algorithms than

with the ATGP-CVA approach. Therefore, it is concluded that proposed ATGP endmembers based features for detecting changes are as good as that of deep features extracted by DL based CD algorithms.

Influence of VD in ATGP-CVA based CD

ATGP-CVA needs VD to be estimated to extract endmembers and their related features. VD is not available with the ground-truth. Availability of ground-truth for the CD tasks is rare in general and therefore VD is unknown in most of the times. In addition, VD estimation is parametric dependent and varies from user to user based on the implementation. Therefore, there is a need for studying the influence of VD on proposed ATGP-CVA in CD task by considering different values for VD or varying VD from it's estimated value. Our implementation of VD on the China, USA and river data sets resulted 13, 4 and 4 respectively. Hence, VD is varied from 4 to 15 to test the performance of CD using different number of features.

The Figure 6.3 illustrates that ED features are not only more effective but also showed better consistency than other features in CD task when VD is varied from 4 to 15. And, the variation in CD accuracy is around 1 percent almost in all the cases and same can be observed in Figure 6.3. From this it is concluded that not only endmember related features are effective but also very less number around 5 features also sufficient to achieve good results in CD.

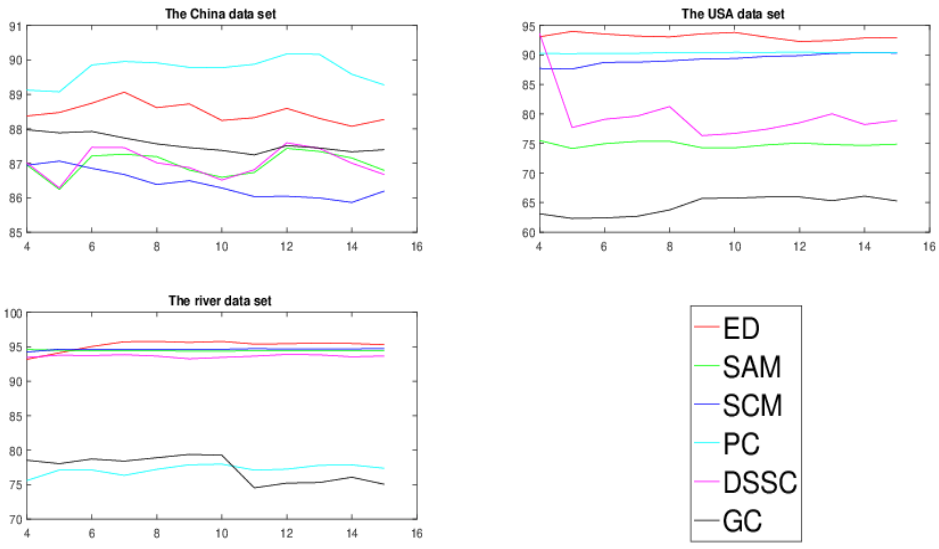

Figure 6.3: Influence of VD in ATGP-CVA based CD

The ATGP-CVA (using ED features) obtained change maps for the experimented CD data sets are presented in Figure 6.4 shows that proposed endmember related features are able to detect changes effectively. The false changes shown by ATGP-CVA in Figure 6.4 might be the insignificant changes that might not labelled in the ground-truth CD maps. Overall, the proposed endmember related features are effective in detecting changed and unchanged pixels and able to generate high quality change maps from the CD data sets.

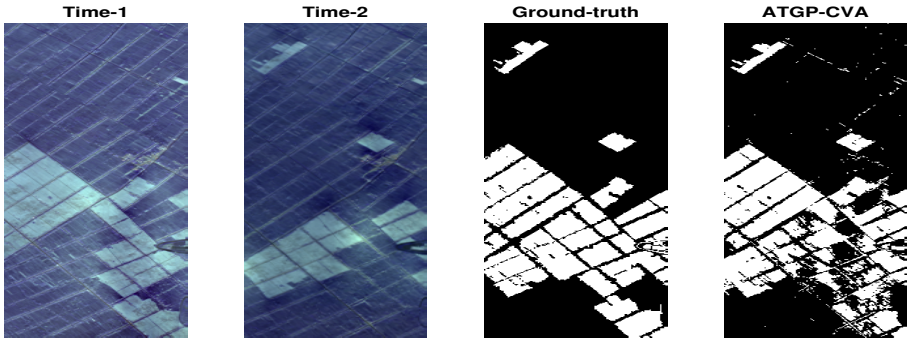

(a) Farmland Data Set

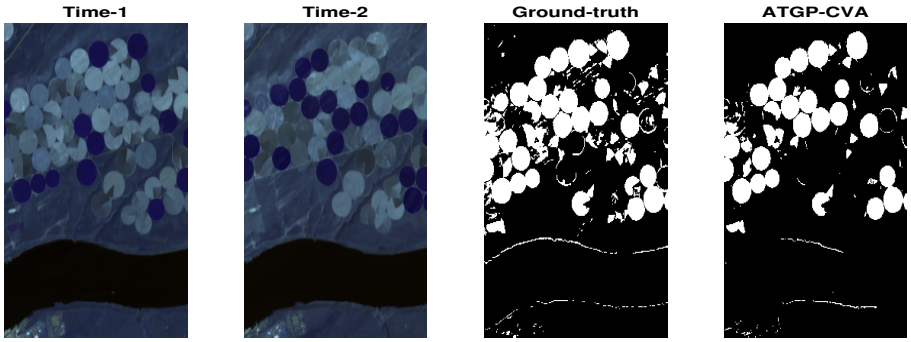

(b) USA Data Set

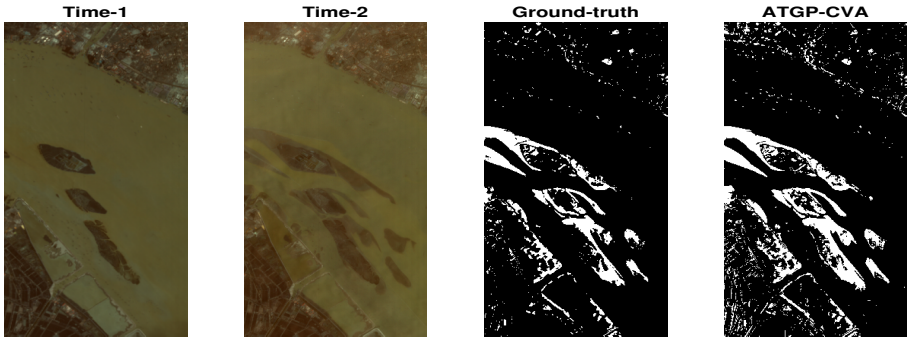

(c) River Data Set

Figure 6.4: Proposed ATGP-CD in Detecting Changes from HSI-CD Data Sets: Time-1 (First Column), Time-2 (Second Column), Ground Truth Change Map (Third Column), and ATGP-CVA Change Map (Fourth Column)

Inferences

Considering all the experimental results, it is inferred that ATGP endmembers based features extracted by different similarity measures are better than original features and also reasonably as good as that of deep features extracted by DL based CD algorithms. Experiments also suggest that ED is reasonably better choice to explore in ATGP based CD. Therefore, it is concluded that ATGP based CD algorithms, especially ATGP-CVA, can be utilised as the pre-detection technique for DL based CD and other algorithms those in need of prior knowledge on changed and unchanged samples from CD data sets.

6.2 Mineral Classification

Due to lack of training samples and sufficient data with ground truth to be tested, DL models not explored much in mineral classification so far. To overcome this, a virtual sample generation to be able to generate more training samples that provide a chance to explore DL models which need variations in training samples in mineral classification is proposed. Further, 1-D CNN model, trained on training samples generated by virtual sample generation, designed to classify minerals performed well in classifying the tested mineral classes with high accuracy.

6.2.1 Virtual Sample Generation

At present deep learning (DL) based models have become a best choice to address the issues and provide better solutions in many fields including remote sensing data analysis. Due to very subtle differences exhibited by mineral signatures and also lack of sufficient training samples, Geo-science and remote sensing research community has not much explored the DL techniques in analyzing mineral data. Therefore, in this paper, a virtual sample generation technique using vector rotation is proposed to increase the mineral data for training DL models. The proposed virtual sample generation technique is explored on a spectral library of 5 minerals that is formed from Cuprite scene, a benchmark mineral data set. The quality of the mineral samples generated are assessed using visual inspection as well as a relative spectral discriminating power of target minerals with respect to non-target or remaining minerals.

Proposed Methodology

Image classification tasks like object detection using DL models involves data augmentation techniques. Formerly developed data augmentation techniques create modified versions of already available not so sufficient training data using operations like random rotation, vertical and horizontal flipping, translation and etc. Spectral signatures are generally considered as vectors or random variables to discriminate them with one another using spectral matching algorithms. Therefore, a vector rotation operation is adapted to generate mineral signatures virtually. A significant degree of resemblance/similarity can be said to exist among spectral signatures when the value of the spectral angle is smaller than 17.2° Tan et al. (2020). Therefore, the angle of rotation for generating virtual samples from proposed method is chosen to be 12.0° at max with an interval of 4.0° so that maximum similarity can be achieved.

Initially, the reflectance values are scaled to match the range of number of bands for making the rotation of spectral signatures reasonable. Since HSIs contain few hundreds of bands, reflectance values which are usually in the range of few thousands (at max ten thousand) are scaled down to within the range of hundred. Then the vector rotation operation is applied only on reflectance values (y-axis) not on their wavelength values or band numbers (x-axis). But, the rotation operation is performed with respect to wavelength (band number) axis (x-axis). After the rotation operation, the reflectance values are re-scaled back to their original range.

Performance Evaluation

The quality of the mineral samples generated are assessed using visual inspection as well as a relative spectral discriminating power of target minerals with respect to non-target or remaining minerals. SAM is used to measure similarity between mineral endmembers and all the training samples. Then the box plot is plotted, as mentioned in Adep et al. (2017a), to present the SAM values for target versus non-target class mineral samples for all the five minerals under study.

The PPI method is considered to extract endmembers from the spectral library to measure target vs non-target SAM values for the corresponding minerals. Then the PPI endmembers are segmented using convex hull to identify diagnostic features. Different minerals have different number of segments based on the spectral profile i.e absorption features. These details are clearly described in Adep et al. (2017a). To evaluate the performance of proposed

virtual sample generation method, box plots are plotted only for spectral library samples and for generated virtual samples.

Mineral Sample Generation

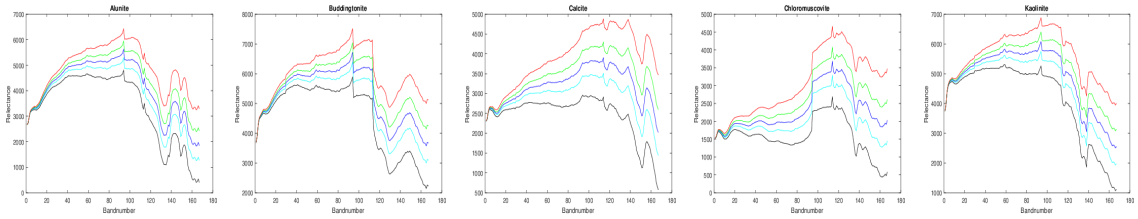

(a) (b) (c) (d) (e)

Figure 6.5: Spectral Profiles of Virtual Mineral Samples Generated through Vector Rotation Operation at Different Angles

Figure 6.5 shows the virtual mineral samples generated with the angle of deviations -8.0° (Black), -4.0° (Cyan), 0.0°, (Blue), 4.0° (Green) and 8.0° (Red) respectively. Text in the bracket refers to the colors used to plot the generated mineral samples. The quality of virtual mineral samples generated can be perceived/observed from the Figure 6.5. And, it is clear that spectral profiles of generated mineral samples are exactly resembling that of the original spectral library samples of corresponding minerals.

Quality of Generated Target vs Non-Target Samples

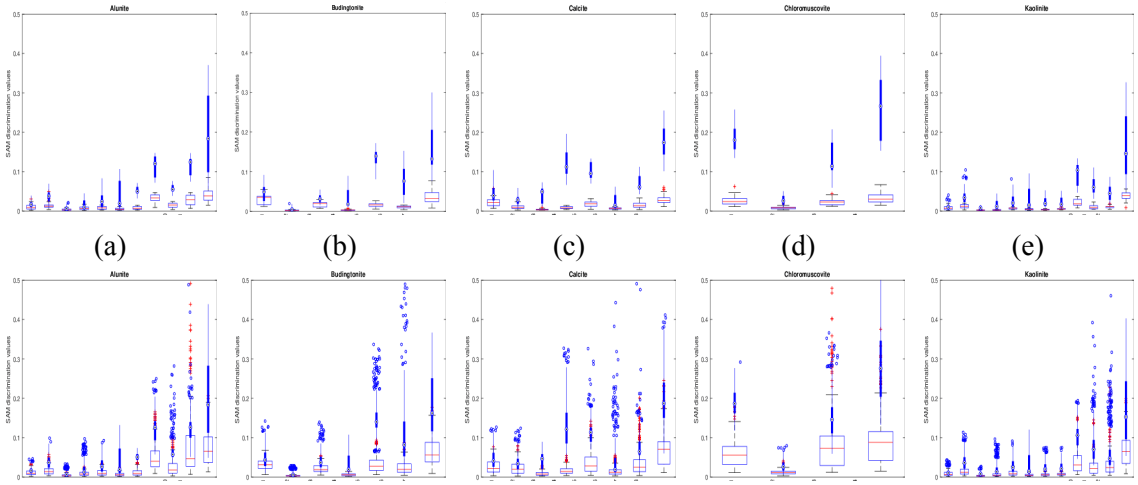

(a) (b) (c) (d) (e)

(f) (g) (h) (i) (j)

Figure 6.6: Comparative Analysis of SAM Values in Distinguishing Target from Non-Target Mineral Classes: Spectral Library Samples (First Row) vs. Virtual Mineral Samples (Second Row)

Visual inspection from the Figure 6.5 depicts that the generated mineral samples are of high quality. Since, all the spectral library samples are rotated using the same set of angles of deviations, there is a high chance for confusion between intra and inter class variations. Therefore, box plot for SAM values of target vs non-target samples are presented in the Figure 6.6 (values within the box are SAM values of corresponding target minerals and outliers or outside box are belongs to SAM values of non-target minerals. From the Figure 6.6, it is clear that box plots for target vs non-target samples of corresponding minerals from spectral library and proposed virtual sample generation are look alike giving hint that the diagnostic features of virtual mineral samples are similar as that of spectral library minerals. Therefore, it is clear that the outliers which are SAM values of non-target minerals make the discrimination of generated target samples easy from the non-target mineral samples. From this, it is clear that proposed method useful to generate additional training samples that have clear inter class variations.

Considering both the qualitative and quantitative analysis on generated mineral samples with respect to the spectral library samples, of their corresponding minerals, the proposed virtual sample generation method can be treated as a reasonably good option for hyperspectral mineral sample generation where there is a lack of training samples. Additionally, the ability of deep learning models in capturing diagnostic features of spectral signatures of different minerals can be explored in the hyperspectral mineral data analysis with the help of the proposed method.

6.2.2 1-D CNN For Mineral Classification

In this work, one dimensional (1-D) CNN model is proposed to classify hyperspectral mineral data. Proposed CNN model is a simple network of 3 convolutional layers activated with ReLu, a flattening layer and a dense layer. convolutional layers contain 8,4 and 2 filters, kernel sizes of 7,5 and 3 and strides of 4,3 and 2 respectively. Output dense layer contains the nodes equal the number of mineral classes in the training data set. A spectral library of five minerals formed referring to USGS library has been adapted to train and test the proposed model. spectral library contains Alunite (Al), Buddingtonite (Bu), Calcite (Ca), Chloromuscovite (Cm) and Kaolinite (Ka). The number of samples in each class is 53, 14, 39, 37 and 24 respectively. Performance of the proposed CNN model is compared with the performance of SAM classifier and ExHype classifier.

Table 6.3: Performance Evaluation of 1-D CNN in Mineral Classification

(a) Confusion Matrix for 5 Minerals

	Al	**Bu**	**Ca**	**Cm**	**Ka**
Al	49	3	0	0	1
Bu	0	14	0	0	0
Ca	0	0	39	0	0
Cm	0	0	0	37	0
Ka	0	0	0	0	24

(b) Performance Assessment of Mineral Classifiers on Test Data

Classifier	**SAM**	**ExHype**	**Proposed 1-D CNN**
OA	71.86	94.01	97.60

Experimental results presented in Table 6.3a are analyzed for classifying a test data set contains five minerals under study showed that proposed 1-D CNN model outperformed the ExHype in classifying all the five mineral classes. Proposed method is able to get an accuracy of 97.60 percent that is higher than SAM and ExHype classifier (see Table 6.3b).

Summary:

This chapter presents research work on change detection and mineral classification. Endmembers extracted by ATGP algorithm that represent whole HSI are explored to identify sub-pixel level features to use instead of simple features to address change detection is presented. Effectiveness of proposed endmember related features are studied in comparison to original as well as deep features in change detection using the proposed ATGP-CD is discussed. A virtual sample generation that generates more training samples and 1-D CNN model designed to classify hyperspectral mineral data is presented.

The next chapter presents concluding remarks and future scope regarding experimental results obtained from this research work.

Chapter 7

Conclusions and Future Directions

> Highest pleasure is the pleasure of love.
> Love is the process of being conquered and to conquer.
> If you love KRISHNA, DEVOTEES will love you, if you love DEVOTEES, KRISHNA will love you!
>
> Radhanath Swami

Introduction

This chapter presents concluding remarks on experimental results obtained from the research carried out on the objectives identified. Additionally, the future directions to carry this research work also included.

Endmember Extraction: Experimental results on proposed EEAs showed the applicability of SMAs in extracting spectrally distinct signatures as the endmembers and hinted the importance of endmember initialization. In the further investigation, the darkest pixel is identified as a TPOI. Results illustrate that the darkest pixel is not only a potential TPOI but also improved the performance of ATGP significantly in four out of five cases. Besides that, the experiments results clearly depict non suitability of maximum distance algorithm MDA in identifying all the vertices of geometrical shapes from pentagon to decagon in 2-D, therefore mutually distinct signatures as well. CDIC appears to perform better in EE by identifying the corner pixels as the clusters.

Measuring similarity/correlation using spectral matching in higher dimensional (n-D) space enables the extraction of higher-order features that might be crucial for discriminating between subtle spectral differences. This can contribute to improved accuracy in applications

like endmember extraction, spectral matching, and classification. Extending TPOIs strategies to operate at multiple resolutions can enhance its applicability across diverse hyperspectral datasets. This involves investigating how TPOIs strategies perform when applied to different spatial resolutions. CDIC-identified endmember class samples can be further used as the training samples for HSI applications like unsupervised classification and mineral identification tasks across multiple data sets to investigate the applicability and robustness of CDIC.

Spectral Matching: Proposed GSSM was not only able to highlight diagnostic features of target signatures but also showed it's effectiveness in discriminating spectrally distinct target signatures better than other SMAs. Further study on GC incorporated showed improved discrimination power with geometrical SMAs. The noise inherited in the HSI becomes a limitation for the broad applications of GS in HSI analysis. The proposed RSDPW appears to be more meaningful in discriminating endmembers and obtaining the range of RSDPW values for different levels of discrimination than the former one.

Identifying bands with substantial spectral gradients can enhance the discriminative power of the data, allowing for better characterization of different land cover or material classes. Therefore, GS can be further explored in identifying unusual/anomalous spectral patterns, DR through band selection. GS can also be explored in distinguishing between similar classes, such as different types of vegetation or minerals. Emphasizing or giving more weightage to the bands with high spectral gradients can lead to more accurate results in unmixing and classification-related tasks (including HSI-CD). A more in-depth exploration could be undertaken to formulate the RSDPW in a manner that adequately accommodates the multidimensional nature of spectral data.

Change Detection: The experimental results on three benchmark HSI CD data sets show that proposed ATGP based CD algorithms not only perform better than classical CD algorithms but also able to reach the performance of DL based CD algorithms. The experimental results demonstrated that ATGP endmembers-based features extracted by different similarity measures are better than original features and also reasonably as good as that of deep features extracted by DL models in CD tasks. Additionally, even a minimum number of features around three to five (3-5) also good enough to get high accuracy as that of DL models. A better endmember extraction or a better pseudo-training sample extraction could improve the performance in detecting changes.

Mineral Classification: The ability of proposed virtual sample generation to be able to generate more training samples provide a chance to explore DL models that need variations in training samples in mineral classification. Proposed 1-D CNN perform well in classifying the tested mineral classes with high accuracy.

Exploration of CDIC, an unsupervised training samples extraction technique, to identify samples for mineral classes present in the hyperspectral data, facilitates further exploration of DL-based models in mineral classification and thereby can be stepped towards designing an expert system for automatic mineral identification.

Bibliography

Adams, J. B., Smith, M. O., and Johnson, P. E. (1986). Spectral mixture modeling: A new analysis of rock and soil types at the viking lander 1 site. *Journal of Geophysical Research: Solid Earth*, 91(B8):8098–8112.

Adep, R. N., Ramesh, H., et al. (2017a). Exhype: A tool for mineral classification using hyperspectral data. *ISPRS Journal of Photogrammetry and Remote Sensing*, 124:106–118.

Adep, R. N., shetty, A., and Ramesh, H. (2017b). Exhype: A tool for mineral classification using hyperspectral data. *ISPRS Journal of Photogrammetry and Remote Sensing*, 124:106 – 118.

Adep, R. N., Vijayan, A. P., Shetty, A., and Ramesh, H. (2016). Performance evaluation of hyperspectral classification algorithms on aviris mineral data. *Perspectives in Science*, 8:722–726.

Agrawal, N. and Govil, H. (2023). A deep residual convolutional neural network for mineral classification. *Advances in Space Research*, 71(8):3186–3202.

Angelopoulou, E., Lee, S. W., and Bajcsy, R. (1999). Spectral gradient: a material descriptor invariant to geometry and incident illumination. In *Proceedings of the Seventh IEEE International Conference on Computer Vision*, volume 2, pages 861–867. IEEE.

Asner, G. and Lobell, D. (2000). Autoswir: A general spectral unmixing algorithm based on 2000-2400 nm endmember datasets and monte carlo analysis. In *Proceedings of the 9th Annual JPL Airborne Earth Science Workshop, Pasadena*.

Ayhan, B. and Kwan, C. (2019). A new approach to change detection using heterogeneous images. In *2019 IEEE 10th Annual Ubiquitous Computing, Electronics & Mobile Communication Conference (UEMCON)*, pages 0192–0197. IEEE.

Bai, T., Wang, L., Yin, D., Sun, K., Chen, Y., Li, W., and Li, D. (2023). Deep learning for change detection in remote sensing: a review. *Geo-spatial Information Science*, 26(3):262–288.

Baisantry, M., Negi, D., and Manocha, O. (2012). Change vector analysis using enhanced pca and inverse triangular function-based thresholding. *Defence Science Journal*, 62(4):236–242.

Bannon, D. (2009). Hyperspectral imaging: Cubes and slices. *Nature photonics*, 3(11):627.

Berman, M., Kiiveri, H., Lagerstrom, R., Ernst, A., Dunne, R., and Huntington, J. F. (2004). Ice: A statistical approach to identifying endmembers in hyperspectral images. *IEEE transactions on Geoscience and Remote Sensing*, 42(10):2085–2095.

Bilgin, G., Erturk, S., and Yildirim, T. (2011). Segmentation of hyperspectral images via subtractive clustering and cluster validation using one-class support vector machines. *IEEE Transactions on Geoscience and Remote Sensing*, 49(8):2936–2944.

Bioucas-Dias, J. M. (2009). A variable splitting augmented lagrangian approach to linear spectral unmixing. In *2009 First workshop on hyperspectral image and signal processing: Evolution in remote sensing*, pages 1–4. IEEE.

Bioucas-Dias, J. M. and Nascimento, J. M. (2008). Hyperspectral subspace identification. *IEEE Transactions on Geoscience and Remote Sensing*, 46(8):2435–2445.

Boardman, J. W. (1989). Inversion of imaging spectrometry data using singular value decomposition. In *12th Canadian Symposium on Remote Sensing Geoscience and Remote Sensing Symposium,*, volume 4, pages 2069–2072. IEEE.

Boardman, J. W., Kruse, F. A., and Green, R. O. (1995). Mapping target signatures via partial unmixing of aviris data.

Brown, A. J. (2006). Spectral curve fitting for automatic hyperspectral data analysis. *IEEE Transactions on Geoscience and Remote Sensing*, 44(6):1601–1608.

Brown, A. J., Cudahy, T. J., and Walter, M. R. (2006). Hydrothermal alteration at the panorama formation, north pole dome, pilbara craton, western australia. *Precambrian Research*, 151(3-4):211–223.

Brown, A. J., Hook, S. J., Baldridge, A. M., Crowley, J. K., Bridges, N. T., Thomson, B. J., Marion, G. M., de Souza Filho, C. R., and Bishop, J. L. (2010). Hydrothermal formation of clay-carbonate alteration assemblages in the nili fossae region of mars. *Earth and Planetary Science Letters*, 297(1-2):174–182.

Cavalli, R. M., Fusilli, L., Pascucci, S., Pignatti, S., and Santini, F. (2008). Hyperspectral sensor data capability for retrieving complex urban land cover in comparison with multispectral data: Venice city case study (italy). *Sensors*, 8(5):3299–3320.

Chan, T.-H., Chi, C.-Y., Huang, Y.-M., and Ma, W.-K. (2009). A convex analysis-based minimum-volume enclosing simplex algorithm for hyperspectral unmixing. *IEEE Transactions on Signal Processing*, 57(11):4418–4432.

Chan, T.-H., Ma, W.-K., Ambikapathi, A., and Chi, C.-Y. (2011). A simplex volume maximization framework for hyperspectral endmember extraction. *IEEE Transactions on Geoscience and Remote Sensing*, 49(11):4177–4193.

Chang, C.-I. (1999). Spectral information divergence for hyperspectral image analysis. In *Geoscience and Remote Sensing Symposium, 1999. IGARSS '99 Proceedings. IEEE 1999 International*, volume 1, pages 509–511 vol.1.

Chang, C.-I. and Du, Q. (2004). Estimation of number of spectrally distinct signal sources in hyperspectral imagery. *IEEE Transactions on geoscience and remote sensing*, 42(3):608–619.

Chang, C.-I. and Plaza, A. (2006). A fast iterative algorithm for implementation of pixel purity index. *IEEE Geoscience and Remote Sensing Letters*, 3(1):63–67.

Chang, C.-I., Wu, C.-C., Liu, W., and Ouyang, Y.-C. (2006). A new growing method for simplex-based endmember extraction algorithm. *IEEE Transactions on Geoscience and Remote Sensing*, 44(10):2804–2819.

Chaudhry, F., Wu, C.-C., Liu, W., Chang, C.-I., and Plaza, A. (2006). Pixel purity index-based algorithms for endmember extraction from hyperspectral imagery. *Recent advances in hyperspectral signal and image processing*, 37(2):29–62.

Chauhan, H. and Mohan, B. K. (2014). Effectiveness of spectral similarity measures to develop precise crop spectra for hyperspectral data analysis. *ISPRS Annals of Photogrammetry, Remote Sensing & Spatial Information Sciences*, 2(8).

Chen, G., Krzyzak, A., and Qian, S.-E. (2022). A new endmember extraction method based on least squares. *Canadian Journal of Remote Sensing*, 48(2):316–326.

Cheng, F., Chen, N., Wang, C., Wang, Q., and Du, B. (2023). A global-to-local evolutionary algorithm for hyperspectral endmember extraction. *IEEE Transactions on Geoscience and Remote Sensing*, 61:1–17.

Cheng, X., Cai, Z., Li, J., Wen, M., Wang, Y., and Zeng, D. (2021). A spatial-spectral clustering-based algorithm for endmember extraction and hyperspectral unmixing. *International Journal of Remote Sensing*, 42(5):1948–1972.

Chetia, G. S. and Devi, B. P. (2022). Endmember extraction with unknown number of sources for hyperspectral unmixing. In *International Conference on Computer Vision and Image Processing*, pages 567–578. Springer.

Chiu, S. L. (1994). Fuzzy model identification based on cluster estimation. *Journal of Intelligent & fuzzy systems*, 2(3):267–278.

Clark, R. N. and King, T. V. (1987). Automatic continuum analysis of reflectance spectra.

Clark, R. N. and Swayze, G. A. (1995). Mapping minerals, amorphous materials, environmental materials, vegetation, water, ice and snow, and other materials: the usgs tricorder algorithm. In *JPL, Summaries of the Fifth Annual JPL Airborne Earth Science Workshop. Volume 1: AVIRIS Workshop*.

Clark, R. N., Swayze, G. A., Livo, K. E., Kokaly, R. F., Sutley, S. J., Dalton, J. B., McDougal, R. R., and Gent, C. A. (2003). Imaging spectroscopy: Earth and planetary remote sensing with the usgs tetracorder and expert systems. *Journal of Geophysical Research: Planets (1991–2012)*, 108(E12).

Cloutis, E. A. (1996). Review article hyperspectral geological remote sensing: evaluation of analytical techniques. *International Journal of Remote Sensing*, 17(12):2215–2242.

Cochrane, M. (2000). Using vegetation reflectance variability for species level classification of hyperspectral data. *International journal of remote sensing*, 21(10):2075–2087.

Contreras, I., Khodadadzadeh, M., and Gloaguen, R. (2020). Multi-label classification for drill-core hyperspectral mineral mapping. *The International Archives of the Photogrammetry, Remote Sensing and Spatial Information Sciences*, 43:383–388.

Craig, M. D. (1994). Minimum-volume transforms for remotely sensed data. *IEEE Transactions on Geoscience and Remote Sensing*, 32(3):542–552.

Cui, C., Wang, X., Wang, S., Zhang, L., and Zhong, Y. (2023). Unrolling nonnegative matrix factorization with group sparsity for blind hyperspectral unmixing. *IEEE Transactions on Geoscience and Remote Sensing*.

De Carvalho, O. A. and Meneses, P. R. (2000). Spectral correlation mapper (scm): an improvement on the spectral angle mapper (sam). In *Summaries of the 9th JPL Airborne Earth Science Workshop, JPL Publication 00-18*, volume 9. JPL Publication Pasadena, CA.

De Kerf, T., Pipintakos, G., Zahiri, Z., Vanlanduit, S., and Scheunders, P. (2022). Identification of corrosion minerals using shortwave infrared hyperspectral imaging. *Sensors*, 22(1):407.

De La Rosa, R., Khodadadzadeh, M., Tusa, L., Kirsch, M., Gisbert, G., Tornos, F., Tolosana-Delgado, R., and Gloaguen, R. (2021). Mineral quantification at deposit scale using drill-core hyperspectral data: A case study in the iberian pyrite belt. *Ore Geology Reviews*, 139:104514.

Deng, C., Zhang, S., Wang, S., Tian, W., and Wu, Z. (2014). Sparse hyperspectral unmixing based on smoothed ł0 regularization. *Infrared Physics & Technology*, 67:306–314.

Deng, K., Zhao, H., Li, N., and Wei, W. (2021). Identification of minerals in hyperspectral imagery based on the attenuation spectral absorption index vector using a multilayer perceptron. *Remote Sensing Letters*, 12(5):449–458.

Dong, X., Jakobi, M., Wang, S., Köhler, M. H., Zhang, X., and Koch, A. W. (2019). A review of hyperspectral imaging for nanoscale materials research. *Applied Spectroscopy Reviews*, 54(4):285–305.

Du, B., Ru, L., Wu, C., and Zhang, L. (2019a). Unsupervised deep slow feature analysis for change detection in multi-temporal remote sensing images. *IEEE Transactions on Geoscience and Remote Sensing*, 57(12):9976–9992.

Du, B., Wei, Q., and Liu, R. (2019b). An improved quantum-behaved particle swarm optimization for endmember extraction. *IEEE Transactions on Geoscience and Remote Sensing*, 57(8):6003–6017.

Du, Y., Chang, C.-I., Ren, H., Chang, C.-C., Jensen, J. O., and D'Amico, F. M. (2004). New hyperspectral discrimination measure for spectral characterization. *Optical Engineering*, 43:1777–1786.

Elmore, A. J., Mustard, J. F., Manning, S. J., and Lobell, D. B. (2000). Quantifying vegetation change in semiarid environments: precision and accuracy of spectral mixture analysis and the normalized difference vegetation index. *Remote sensing of environment*, 73(1):87–102.

Erturk, A. and Erturk, S. (2006). Unsupervised segmentation of hyperspectral images using modified phase correlation. *IEEE Geoscience and Remote Sensing Letters*, 3(4):527–531.

Fernandez-Beltran, R., Pla, F., and Plaza, A. (2020). Endmember extraction from hyperspectral imagery based on probabilistic tensor moments. *IEEE Geoscience and Remote Sensing Letters*, 17(12):2120–2124.

Gan, Y., Hu, B., Liu, W., Wang, S., Zhang, G., Feng, X., and Wen, D. (2018). Endmember extraction from hyperspectral imagery based on qr factorisation using givens rotations. *IET Image Processing*, 13(2):332–343.

Gan, Y., Hu, B., Liu, W., Wang, S., Zhang, G., Feng, X., and Wen, D. (2019). Endmember extraction from hyperspectral imagery based on qr factorisation using givens rotations. *IET Image Processing*, 13(2):332–343.

Gomez, C., Rossel, R. A. V., and McBratney, A. B. (2008). Soil organic carbon prediction by hyperspectral remote sensing and field vis-nir spectroscopy: An australian case study. *Geoderma*, 146(3-4):403–411.

Gower, J. (1985). Properties of euclidean and non-euclidean distance matrices. *Linear Algebra and its Applications*, 67:81 – 97.

Gu, J., Yang, B., and Wang, B. (2021). Nonlinear unmixing for hyperspectral images via kernel-transformed bilinear mixing models. *IEEE Transactions on Geoscience and Remote Sensing*, 60:1–13.

Guerra, R., Santos, L., López, S., and Sarmiento, R. (2015). A new fast algorithm for linearly unmixing hyperspectral images. *IEEE Transactions on Geoscience and Remote Sensing*, 53(12):6752–6765.

Guo, Q., Zhang, J., Zhong, C., and Zhang, Y. (2021). Change detection for hyperspectral images via convolutional sparse analysis and temporal spectral unmixing. *IEEE Journal of Selected Topics in Applied Earth Observations and Remote Sensing*, 14:4417–4426.

Gupta, P. and Venkatesan, M. (2020). Mineral identification using unsupervised classification from hyperspectral data. In *Emerging Research in Data Engineering Systems and Computer Communications: Proceedings of CCODE 2019*, pages 259–268. Springer.

Haboudane, D., Miller, J. R., Pattey, E., Zarco-Tejada, P. J., and Strachan, I. B. (2004). Hyperspectral vegetation indices and novel algorithms for predicting green lai of crop canopies: Modeling and validation in the context of precision agriculture. *Remote sensing of environment*, 90(3):337–352.

Harsanyi, J. C. and Chang, C.-I. (1994). Hyperspectral image classification and dimensionality reduction: An orthogonal subspace projection approach. *IEEE Transactions on geoscience and remote sensing*, 32(4):779–785.

Heinz, D. C. et al. (2001). Fully constrained least squares linear spectral mixture analysis method for material quantification in hyperspectral imagery. *IEEE transactions on geoscience and remote sensing*, 39(3):529–545.

Hou, Z., Li, W., Li, L., Tao, R., and Du, Q. (2021). Hyperspectral change detection based on multiple morphological profiles. *IEEE Transactions on Geoscience and Remote Sensing*, 60:1–12.

Huadong, G., Jianmin, X., Guoqiang, N., and Jialing, M. (2001). A new airborne earth observing system and its applications. In *IGARSS 2001. Scanning the Present and Resolving the Future. Proceedings. IEEE 2001 International Geoscience and Remote Sensing Symposium (Cat. No. 01CH37217)*, volume 1, pages 549–551. Ieee.

Huang, A. (2008). Similarity measures for text document clustering. In *Proceedings of the sixth new zealand computer science research student conference (NZCSRSC2008), Christchurch, New Zealand*, pages 49–56.

Ifarraguerri, A. and Chang, C.-I. (1999). Multispectral and hyperspectral image analysis with convex cones. *IEEE transactions on geoscience and remote sensing*, 37(2):756–770.

Imai, F. H., Rosen, M. R., and Berns, R. S. (2002). Comparative study of metrics for spectral match quality. In *Conference on colour in graphics, imaging, and vision*, volume 2002, pages 492–496. Society for Imaging Science and Technology.

Iordache, M.-D., Bioucas-Dias, J. M., and Plaza, A. (2011). Sparse unmixing of hyperspectral data. *IEEE Transactions on Geoscience and Remote Sensing*, 49(6):2014–2039.

Jasmine, G. and Pattabiraman, V. (2015). Hyperspectral image analysis using end member extraction algorithm. *Int. J. Pure Appl. Math*, 101:809–829.

Jiang, H., Peng, M., Zhong, Y., Xie, H., Hao, Z., Lin, J., Ma, X., and Hu, X. (2022a). A survey on deep learning-based change detection from high-resolution remote sensing images. *Remote Sensing*, 14(7):1552.

Jiang, X., Zhao, Y., Gong, M., Zhan, T., and Zhang, M. (2022b). A vertex-directed evolutionary algorithm for multiobjective endmember estimation. *IEEE Transactions on Geoscience and Remote Sensing*, 60:1–13.

Keshava, N. and Mustard, J. F. (2002). Spectral unmixing. *IEEE signal processing magazine*, 19(1):44–57.

Khan, M. J., Khan, H. S., Yousaf, A., Khurshid, K., and Abbas, A. (2018). Modern trends in hyperspectral image analysis: A review. *Ieee Access*, 6:14118–14129.

Kodama, H. (1979). Clay minerals in canadian soils: Their origin, distribution and alteration. *Canadian Journal of Soil Science*, 59(1):37–58.

Koerting, F., Rogass, C., Kaempf, H., Lubitz, C., Harms, U., Schudack, M., Kokaly, R., Mielke, C., Boesche, N., and Altenberger, U. (2015). Drill core mineral analysis by means of the hyperspectral imaging spectrometer hyspex, xrd and asd in proximity of the mÃ□tina maar, czech republic. *ISPRS - International Archives of the Photogrammetry, Remote Sensing and Spatial Information Sciences*, XL-1/W5:417–424.

Kong, X., Shu, N., Huang, W., and Fu, J. (2010). The research on effectiveness of spectral similarity measures for hyperspectral image. In *Image and Signal Processing (CISP), 2010 3rd International Congress on*, volume 5, pages 2269–2273. IEEE.

Kruse, F., Lefkoff, A., Boardman, J., Heidebrecht, K., Shapiro, A., Barloon, P., and Goetz, A. (1993). The spectral image processing system (sips)—interactive visualization and analysis of imaging spectrometer data. *Remote Sensing of Environment*, 44(2):145 – 163.

Kumar, C., Chatterjee, S., and Oommen, T. (2020). Mapping hydrothermal alteration minerals using high-resolution aviris-ng hyperspectral data in the hutti-maski gold deposit area, india. *International Journal of Remote Sensing*, 41(2):794–812.

Kumar, C., Chatterjee, S., Oommen, T., and Guha, A. (2021). New effective spectral matching measures for hyperspectral data analysis. *International Journal of Remote Sensing*, 42(11):4126–4156.

Kumar, M. N., Seshasai, M. V. R., Prasad, K. S. V., Kamala, V., Ramana, K. V., Dwivedi, R. S., and Roy, P. S. (2011). A new hybrid spectral similarity measure for discrimination among vigna species. *International Journal of Remote Sensing*, 32(14):4041–4053.

Landgrebe, D. (1999). Information extraction principles and methods for multispectral and hyperspectral image data. In *Information processing for remote sensing*, pages 3–37. World Scientific.

Lei, L., Sun, Y., and Kuang, G. (2020). Adaptive local structure consistency-based heterogeneous remote sensing change detection. *IEEE Geoscience and Remote Sensing Letters*.

Li, H., Lee, W. S., Wang, K., Ehsani, R., and Yang, C. (2014). 'extended spectral angle mapping (esam)' for citrus greening disease detection using airborne hyperspectral imaging. *Precision Agriculture*, 15(2):162–183.

Li, H. and Zhang, L. (2011). A hybrid automatic endmember extraction algorithm based on a local window. *IEEE Transactions on Geoscience and Remote Sensing*, 49(11):4223–4238.

Li, J. and Bioucas-Dias, J. M. (2008). Minimum volume simplex analysis: A fast algorithm to unmix hyperspectral data. In *IGARSS 2008-2008 IEEE International Geoscience and Remote Sensing Symposium*, volume 3, pages III–250. IEEE.

Li, Y., Ren, J., Yan, Y., Liu, Q., Petrovski, A., and McCall, J. (2022). Unsupervised change detection in hyperspectral images using principal components space data clustering. In *Journal of Physics: Conference Series*, volume 2278, page 012021. IOP Publishing.

Lin, C.-H., Liu, Y., Chi, C.-Y., Hsu, C.-C., Ren, H., and Quek, T. Q. (2023). Hyperspectral tensor completion using low-rank modeling and convex functional analysis. *IEEE Transactions on Neural Networks and Learning Systems*.

Liu, J. and Zhang, J. (2011). A new maximum simplex volume method based on householder transformation for endmember extraction. *IEEE Transactions on Geoscience and Remote Sensing*, 50(1):104–118.

Liu, R., Wang, P., Du, B., and Qu, B. (2023). Endmember bundle extraction based on improved multi-objective particle swarm optimization. *IEEE Geoscience and Remote Sensing Letters*.

Liu, Z., Li, G., Mercier, G., He, Y., and Pan, Q. (2017). Change detection in heterogenous remote sensing images via homogeneous pixel transformation. *IEEE Transactions on Image Processing*, 27(4):1822–1834.

Lohumi, S., Lee, S., Lee, H., Kim, M. S., Lee, W.-H., and Cho, B.-K. (2016). Application of hyperspectral imaging for characterization of intramuscular fat distribution in beef. *Infrared Physics & Technology*, 74:1–10.

Luo, B., Chanussot, J., Douté, S., and Zhang, L. (2013). Empirical automatic estimation of the number of endmembers in hyperspectral images. *IEEE Geoscience and Remote Sensing Letters*, 10(1):24–28.

Luo, F., Zhou, T., Liu, J., Guo, T., Gong, X., and Ren, J. (2023). Multiscale diff-changed feature fusion network for hyperspectral image change detection. *IEEE Transactions on Geoscience and Remote Sensing*, 61:1–13.

Lv, Z., Huang, H., Li, X., Zhao, M., Benediktsson, J. A., Sun, W., and Falco, N. (2022a). Land cover change detection with heterogeneous remote sensing images: Review, progress, and perspective. *Proceedings of the IEEE*.

Lv, Z., Wang, F., Cui, G., Benediktsson, J. A., Lei, T., and Sun, W. (2022b). Spatial–spectral attention network guided with change magnitude image for land cover change detection using remote sensing images. *IEEE Transactions on Geoscience and Remote Sensing*, 60:1–12.

Ma, W.-K., Bioucas-Dias, J. M., Chan, T.-H., Gillis, N., Gader, P., Plaza, A. J., Ambikapathi, A., and Chi, C.-Y. (2013). A signal processing perspective on hyperspectral unmixing: Insights from remote sensing. *IEEE Signal Processing Magazine*, 31(1):67–81.

Malila, W. A. (1980). Change vector analysis: an approach for detecting forest changes with landsat. In *LARS symposia*, page 385.

Manolakis, D., Pieper, M., Truslow, E., Lockwood, R., Weisner, A., Jacobson, J., and Cooley, T. (2019). Longwave infrared hyperspectral imaging: Principles, progress, and challenges. *IEEE Geoscience and Remote Sensing Magazine*, 7(2):72–100.

Manolakis, D. and Shaw, G. (2002). Detection algorithms for hyperspectral imaging applications. *IEEE signal processing magazine*, 19(1):29–43.

Martínez, P. J., Pérez, R. M., Plaza, A., Aguilar, P. L., Cantero, M. C., Plaza, J., et al. (2006). Endmember extraction algorithms from hyperspectral images.

Miao, L. and Qi, H. (2007). Endmember extraction from highly mixed data using minimum volume constrained nonnegative matrix factorization. *IEEE Transactions on Geoscience and Remote Sensing*, 45(3):765–777.

Mielke, C., Rogass, C., Boesche, N., Segl, K., and Altenberger, U. (2016). Engeomap 2.0—automated hyperspectral mineral identification for the german enmap space mission. *Remote Sensing*, 8(2):127.

Nascimento, J. M. and Dias, J. M. (2005). Vertex component analysis: A fast algorithm to unmix hyperspectral data. *IEEE transactions on Geoscience and Remote Sensing*, 43(4):898–910.

Neville, R. (1999). Automatic endmember extraction from hyperspectral data for mineral exploration. In *International Airborne Remote Sensing Conference and Exhibition, 4 th/21 st Canadian Symposium on Remote Sensing, Ottawa, Canada*.

Ni, L., Xu, H., and Zhou, X. (2020). Mineral identification and mapping by synthesis of hyperspectral vnir/swir and multispectral tir remotely sensed data with different classifiers. *IEEE Journal of Selected Topics in Applied Earth Observations and Remote Sensing*, 13:3155–3163.

Ortega, S., Fabelo, H., Iakovidis, D. K., Koulaouzidis, A., and Callico, G. M. (2019). Use of hyperspectral/multispectral imaging in gastroenterology. shedding some–different–light into the dark. *Journal of clinical medicine*, 8(1):36.

Ou, X., Liu, L., Tu, B., Zhang, G., and Xu, Z. (2022). A cnn framework with slow-fast band selection and feature fusion grouping for hyperspectral image change detection. *IEEE Transactions on Geoscience and Remote Sensing*, 60:1–16.

Ozkan, S., Kaya, B., and Akar, G. B. (2018). Endnet: Sparse autoencoder network for endmember extraction and hyperspectral unmixing. *IEEE Transactions on Geoscience and Remote Sensing*, 57(1):482–496.

Padma, S. and Sanjeevi, S. (2014). Jeffries matusita-spectral angle mapper (jm-sam) spectral matching for species level mapping at bhitarkanika, muthupet and pichavaram mangroves. *ISPRS - International Archives of the Photogrammetry, Remote Sensing and Spatial Information Sciences*, XL-8:1403–1411.

Palacios-Orueta, A. and Ustin, S. L. (1996). Multivariate statistical classification of soil spectra. *Remote Sensing of Environment*, 57(2):108 – 118.

Palla, P. Y., Shetty, A., Raghavendra, B., and Narasimhadhan, A. (2020). Subtractive clustering and phase correlation similarity measure for endmember extraction. *Infrared Physics & Technology*, 110:103452.

Pandey, P. C., Balzter, H., Srivastava, P. K., Petropoulos, G. P., and Bhattacharya, B. (2020). Future perspectives and challenges in hyperspectral remote sensing. *Hyperspectral Remote Sensing*, pages 429–439.

Paoletti, M., Haut, J., Plaza, J., and Plaza, A. (2019). Deep learning classifiers for hyperspectral imaging: A review. *ISPRS Journal of Photogrammetry and Remote Sensing*, 158:279–317.

Penney, G. P., Weese, J., Little, J. A., Desmedt, P., Hill, D. L., et al. (1998). A comparison of similarity measures for use in 2-d-3-d medical image registration. *IEEE transactions on medical imaging*, 17(4):586–595.

Plaza, A. and Chang, C.-I. (2006). Impact of initialization on design of endmember extraction algorithms. *IEEE Transactions on Geoscience and Remote Sensing*, 44(11):3397–3407.

Plaza, A., Martínez, P., Pérez, R., and Plaza, J. (2002). Spatial/spectral endmember extraction by multidimensional morphological operations. *IEEE transactions on geoscience and remote sensing*, 40(9):2025–2041.

Plaza, A., Martínez, P., Pérez, R., and Plaza, J. (2004). A quantitative and comparative analysis of endmember extraction algorithms from hyperspectral data. *IEEE transactions on geoscience and remote sensing*, 42(3):650–663.

Plaza, J., Hendrix, E. M., García, I., Martín, G., and Plaza, A. (2012). On endmember identification in hyperspectral images without pure pixels: A comparison of algorithms. *Journal of Mathematical Imaging and Vision*, 42(2-3):163–175.

Rasti, B., Koirala, B., and Scheunders, P. (2022). Hapkecnn: Blind nonlinear unmixing for intimate mixtures using hapke model and convolutional neural network. *IEEE Transactions on Geoscience and Remote Sensing*, 60:1–15.

Ren, H. and Chang, C.-I. (2003). Automatic spectral target recognition in hyperspectral imagery. *IEEE Transactions on Aerospace and Electronic Systems*, 39(4):1232–1249.

Ren, H., Du, Q., Wang, J., Chang, C.-I., Jensen, J. O., and Jensen, J. L. (2006). Automatic target recognition for hyperspectral imagery using high-order statistics. *IEEE Transactions on Aerospace and Electronic Systems*, 42(4):1372–1385.

Ren, Z., Sun, L., and Zhai, Q. (2020). Improved k-means and spectral matching for hyperspectral mineral mapping. *International Journal of Applied Earth Observation and Geoinformation*, 91:102154.

Richards, J. A. and Richards, J. (1999). *Remote sensing digital image analysis*, volume 3. Springer.

Roberts, D. A., Batista, G. T., Pereira, J. L. G., Waller, E., and Nelson, B. W. (1998). Change identification using multitemporal spectral mixture analysis: Applications in eastern amazonia. *Remote Sensing Change Detection: Environmental Monitoring Applications, pgs. 137-161*.

Robila, S. A. and Gershman, A. (2005). Spectral matching accuracy in processing hyperspectral data. In *International Symposium on Signals, Circuits and Systems, 2005. ISSCS 2005.*, volume 1, pages 163–166. IEEE.

Rogge, D. M., Rivard, B., Zhang, J., and Feng, J. (2006). Iterative spectral unmixing for optimizing per-pixel endmember sets. *IEEE Transactions on Geoscience and Remote Sensing*, 44(12):3725–3736.

Rogge, D. M., Rivard, B., Zhang, J., Sanchez, A., Harris, J., and Feng, J. (2007). Integration of spatial–spectral information for the improved extraction of endmembers. *Remote Sensing of Environment*, 110(3):287–303.

Schott, J. R., Salvaggio, C., and Volchok, W. J. (1988). Radiometric scene normalization using pseudoinvariant features. *Remote sensing of Environment*, 26(1):1–16.

Seydi, S. T. and Hasanlou, M. (2021). A new structure for binary and multiple hyperspectral change detection based on spectral unmixing and convolutional neural network. *Measurement*, 186:110137.

Shafique, A., Cao, G., Khan, Z., Asad, M., and Aslam, M. (2022). Deep learning-based change detection in remote sensing images: A review. *Remote Sensing*, 14(4):871.

Shah, D. and Zaveri, T. (2021). Hyperspectral endmember extraction using pearson's correlation coefficient. *International Journal of Computational Science and Engineering*, 24(1):89–97.

Shah, D. and Zaveri, T. (2023). Dispersion index based endmember extraction for hyperspectral unmixing. *IETE Journal of Research*, 69(5):2837–2845.

Shah, D., Zaveri, T., and Trivedi, Y. (2021). Convex polygon maximization-based hyperspectral endmember extraction algorithm. *Journal of the Indian Society of Remote Sensing*, 49(2):419–432.

Shah, D., Zaveri, T., Trivedi, Y. N., and Plaza, A. (2020). Entropy-based convex set optimization for spatial–spectral endmember extraction from hyperspectral images. *IEEE Journal of Selected Topics in Applied Earth Observations and Remote Sensing*, 13:4200–4213.

Shanmugam, S. and SrinivasaPerumal, P. (2014). Spectral matching approaches in hyperspectral image processing. *International Journal of Remote Sensing*, 35(24):8217–8251.

Shaw, G. A. and hua K. Burke, H. (2003). Spectral imaging for remote sensing.

Shen, X. and Bao, W. (2019). Hyperspectral endmember extraction using spatially weighted simplex strategy. *Remote Sensing*, 11(18):2147.

Shen, X., Bao, W., and Qu, K. (2020). Spatial-spectral hyperspectral endmember extraction using a spatial energy prior constrained maximum simplex volume approach. *IEEE Journal of Selected Topics in Applied Earth Observations and Remote Sensing*, 13:1347–1361.

Shi, C. and Wang, L. (2014). Incorporating spatial information in spectral unmixing: A review. *Remote Sensing of Environment*, 149:70–87.

Shi, C. and Wang, L. (2016). Linear spatial spectral mixture model. *IEEE Transactions on Geoscience and Remote Sensing*, 54(6):3599–3611.

Shippert, P. et al. (2004). Why use hyperspectral imagery? *Photogrammetric engineering and remote sensing*, 70(4):377–396.

Singh, K. D., Ramakrishnan, D., and Mansinha, L. (2012). Relevance of transformation techniques in rapid endmember identification and spectral unmixing: A hypespectral remote sensing perspective. In *2012 IEEE International Geoscience and Remote Sensing Symposium*, pages 4066–4069. IEEE.

Song, X. and Wu, L. (2019). A novel hyperspectral endmember extraction algorithm based on online robust dictionary learning. *Remote Sensing*, 11(15):1792.

Song, X., Zou, L., and Wu, L. (2020). Detection of subpixel targets on hyperspectral remote sensing imagery based on background endmember extraction. *IEEE Transactions on Geoscience and Remote Sensing*, 59(3):2365–2377.

Strehl, A., Ghosh, J., and Mooney, R. (2000). Impact of similarity measures on web-page clustering. In *Workshop on artificial intelligence for web search (AAAI 2000)*, volume 58, page 64.

Sun, Y., Lei, L., Li, X., Tan, X., and Kuang, G. (2021). Structure consistency-based graph for unsupervised change detection with homogeneous and heterogeneous remote sensing images. *IEEE Transactions on Geoscience and Remote Sensing*.

Tan, K., Niu, C., Jia, X., Ou, D., Chen, Y., and Lei, S. (2020). Complete and accurate data correction for seamless mosaicking of airborne hyperspectral images: A case study at a mining site in inner mongolia, china. *ISPRS Journal of Photogrammetry and Remote Sensing*, 165:1–15.

Tao, X., Cui, T., Plaza, A., and Ren, P. (2020). Simultaneously counting and extracting endmembers in a hyperspectral image based on divergent subsets. *IEEE Transactions on Geoscience and Remote Sensing*, 58(12):8952–8966.

Tao, X., Paoletti, M. E., Han, L., Haut, J. M., Ren, P., Plaza, J., and Plaza, A. (2022). Fast orthogonal projection for hyperspectral unmixing. *IEEE Transactions on Geoscience and Remote Sensing*, 60:1–13.

Tian, M., Feng, J., Rivard, B., and Zhao, C. (2016). A method to compute the n-dimensional solid spectral angle between vectors and its use for band selection in hyperspectral data. *International journal of applied earth observation and geoinformation*, 50:141–149.

Tompkins, S., Mustard, J. F., Pieters, C. M., and Forsyth, D. W. (1997). Optimization of endmembers for spectral mixture analysis. *Remote Sensing of Environment*, 59(3):472–489.

Tou, J. and Gonzalez, R. (1974). Pattern recognition principles. pages 92–94.

Transon, J., d'Andrimont, R., Maugnard, A., and Defourny, P. (2017). Survey of current hyperspectral earth observation applications from space and synergies with sentinel-2. In *2017 9th International Workshop on the Analysis of Multitemporal Remote Sensing Images (MultiTemp)*, pages 1–8. IEEE.

Tsubomatsu, H. and Tonooka, H. (2023). Region expansion of a hyperspectral-based mineral map using random forest classification with multispectral data. *Minerals*, 13(6):754.

Tuşa, L., Khodadadzadeh, M., Contreras, C., Rafiezadeh Shahi, K., Fuchs, M., Gloaguen, R., and Gutzmer, J. (2020). Drill-core mineral abundance estimation using hyperspectral and high-resolution mineralogical data. *Remote Sensing*, 12(7):1218.

Ulhaq, D. and Xu, X. (2008). A new approach to band clustering and selection for hyperspectral imagery.

Van der Meer, F. (2006). The effectiveness of spectral similarity measures for the analysis of hyperspectral imagery. *International journal of applied earth observation and geoinformation*, 8(1):3–17.

Van Der Meer, F. and Bakker, W. (1997). Ccsm: Cross correlogram spectral matching. *International Journal of Remote Sensing*, 18(5):1197–1201.

Veganzones, M. A. and Grana, M. (2008). Endmember extraction methods: A short review. In *International Conference on Knowledge-Based and Intelligent Information and Engineering Systems*, pages 400–407. Springer.

Vignesh, K. M. and Kiran, Y. (2020). Comparative analysis of mineral mapping for hyperspectral and multispectral imagery. *Arabian Journal of Geosciences*, 13(4):160.

Wang, J. and Chang, C.-I. (2006). Applications of independent component analysis in endmember extraction and abundance quantification for hyperspectral imagery. *IEEE Transactions on Geoscience and Remote Sensing*, 44(9):2601–2616.

Wang, L., Wang, L., Wang, Q., and Atkinson, P. M. (2021). Ssa-siamnet: Spectral–spatial-wise attention-based siamese network for hyperspectral image change detection. *IEEE Transactions on Geoscience and Remote Sensing*, 60:1–18.

Wang, Q., Yuan, Z., Du, Q., and Li, X. (2018). Getnet: A general end-to-end 2-d cnn framework for hyperspectral image change detection. *IEEE Transactions on Geoscience and Remote Sensing*, 57(1):3–13.

Wang, Y., Hong, D., Sha, J., Gao, L., Liu, L., Zhang, Y., and Rong, X. (2022). Spectral–spatial–temporal transformers for hyperspectral image change detection. *IEEE Transactions on Geoscience and Remote Sensing*, 60:1–14.

Winter, M. E. (1999). N-findr: An algorithm for fast autonomous spectral end-member determination in hyperspectral data. In *Imaging Spectrometry V*, volume 3753, pages 266–276. International Society for Optics and Photonics.

Wu, C., Du, B., and Zhang, L. (2013). Slow feature analysis for change detection in multispectral imagery. *IEEE Transactions on Geoscience and Remote Sensing*, 52(5):2858–2874.

Wu, C.-C. and Chang, C.-I. (2007). Does an endmember set really yield maximum simplex volume? In *2007 IEEE International Geoscience and Remote Sensing Symposium*, pages 3814–3816. IEEE.

Xingtang, H., Bing, Z., Qingxi, T., Lanfen, Z., Qiao, W., Jianlin, Y., et al. (2004). A new architecture for remote-sensing environmental monitoring system rems: Design and implementation. In *IGARSS 2004. 2004 IEEE International Geoscience and Remote Sensing Symposium*, volume 3, pages 2115–2118. Ieee.

Xu, M., Zhang, L., Du, B., Zhang, L., Fan, Y., and Song, D. (2017). A mutation operator accelerated quantum-behaved particle swarm optimization algorithm for hyperspectral endmember extraction. *Remote Sensing*, 9(3):197.

Xu, M., Zou, X., Liu, S., Sheng, H., and Yang, Z. (2023). Manifold regularized sparse archetype analysis considering endmember variability. *IEEE Geoscience and Remote Sensing Letters*.

Yadav, P. P., Shetty, A., Raghavendra, B., and Narasimhadhan, A. (2020a). Effectiveness of phase correlation spectral similarity measure in distinguishing target signatures for hyperspectral data analysis. In *2020 IEEE 17th India Council International Conference (INDICON)*, pages 1–5. IEEE.

Yadav, P. P., Shetty, A., Raghavendra, B., and Narasimhadhan, A. (2020b). Similarity measures in generating spectrally distinct targets. In *2020 IEEE India Geoscience and Remote Sensing Symposium (InGARSS)*, pages 221–224. IEEE.

Yadav, P. P., Shetty, A., Raghavendra, B., and Narasimhadhan, A. (2021). Gradient based spectral similarity measure for hyperspectral image analysis. In *2021 IEEE India Geoscience and Remote Sensing Symposium (InGARSS)*, page (Accepted). IEEE.

Yager, R. R. and Filev, D. P. (1994). Approximate clustering via the mountain method. *IEEE Transactions on Systems, Man, and Cybernetics*, 24(8):1279–1284.

Yang, L., Sun, X., Peng, L., Yao, X., and Chi, T. (2015). An agent-based artificial bee colony (abc) algorithm for hyperspectral image endmember extraction in parallel. *IEEE Journal of Selected Topics in Applied Earth Observations and Remote Sensing*, 8(10):4657–4664.

Yin, C., Meng, F., and Yu, Q. (2020). Calculation of land surface emissivity and retrieval of land surface temperature based on a spectral mixing model. *Infrared Physics & Technology*, page 103333.

Yousefi, B., Castanedo, C. I., Maldague, X. P., and Beaudoin, G. (2020). Assessing the reliability of an automated system for mineral identification using lwir hyperspectral infrared imagery. *Minerals Engineering*, 155:106409.

Zhan, T., Song, B., Sun, L., Jia, X., Wan, M., Yang, G., and Wu, Z. (2020). Tdssc: A three-directions spectral–spatial convolution neural network for hyperspectral image change detection. *IEEE Journal of Selected Topics in Applied Earth Observations and Remote Sensing*, 14:377–388.

Zhang, C., Qin, Q., Zhang, T., Sun, Y., and Chen, C. (2017). Endmember extraction from hyperspectral image based on discrete firefly algorithm (ee-dfa). *ISPRS Journal of Photogrammetry and Remote Sensing*, 126:108–119.

Zhang, N. and Mahmoud, W. (2023). Convex geometry based endmember extraction for hyperspectral images classification. In *2023 13th International Conference on Information Science and Technology (ICIST)*, pages 451–458. IEEE.

Zhang, X., Wang, Y., and Xue, T. (2022). Quadratic clustering-based simplex volume maximization for hyperspectral endmember extraction. *Applied Sciences*, 12(14):7132.

Zhao, C., Cheng, H., and Feng, S. (2021). A spectral–spatial change detection method based on simplified 3-d convolutional autoencoder for multitemporal hyperspectral images. *IEEE Geoscience and Remote Sensing Letters*, 19:1–5.

Zhu, Q., Guo, X., Li, Z., and Li, D. (2022). A review of multi-class change detection for satellite remote sensing imagery. *Geo-spatial Information Science*, pages 1–15.

List of publications

International Journals

- Palla, Parasuram Yadav, Amba Shetty, B. S. Raghavendra, and A. V. Narasimhadhan. ”A Comprehensive Study on Endmember Initialization in Hyperspectral Image Analysis.” Journal of the Indian Society and Remote Sensing (revision submitted)
- Palla, Parasuram Yadav, Amba Shetty, B. S. Raghavendra, and A. V. Narasimhadhan. ”Can Spectral Matching Algorithms be explored in Endmember Extraction.” (Under communication).
- Palla, Parasuram Yadav, Amba Shetty, B. S. Raghavendra, and A. V. Narasimhadhan. ”Corner Driven Iterative Clustering for Endmember Extraction.” (Under communication).

International Conferences Presentations

- Bobate, Nikhi, Palla Parasuram Yadav, and A. V. Narasimhadhan. ”Fusing Conventional and Deep Learning Features for Hyperspectral Image Change Detection.” In 2022 IEEE International Conference on Electronics, Computing and Communication Technologies (CONECCT), pp. 1-6. IEEE, 2022.
- Yadav, Palla Parasuram, Amba Shetty, B. S. Raghavendra, and A. V. Narasimhadhan. ”A Meaningful Reformulation of Relative Spectral Discrimination ower to Aanalyze Hyperspectral Data.” In 2023 IEEE India Geoscience and Remote Sensing Symposium (InGARSS) (Under communication).
- Yadav, Palla Parasuram, Amba Shetty, B. S. Raghavendra, and A. V. Narasimhadhan. ”1-D CNN for Mineral Classification using Hyperspectral Data.” In 2023 IEEE India Geoscience and Remote Sensing Symposium (InGARSS) (Under communication)

CURRICULUM VITAE

Mr. Palla Parasuram Yadav, born on November 11, 1991, in Kadapa District, Andhra Pradesh, India, completed his secondary education at Vijaya High School, Porumamilla, Andhra Pradesh, in 2006, and his intermediate education at Sri Chaitanya Sai Bharathi Junior College, Vijayawada, Krishna District, Andhra Pradesh, in 2008. He holds a Bachelor's degree in Electronics and Communication Engineering from Dr. MGR Educational and Research Institute, Chennai, Tamilnadu, earned in 2013. Following this, he obtained a Master's degree with a specialization in Signal Processing from Sri Venkateswara University College of Engineering, S V University, Tirupati, in 2016.

Continuing his academic journey, he joined the doctoral research program in the Department of Electronics and Communication Engineering at the National Institute of Technology, Karnataka, Surathkal, in 2016. His research focuses on hyperspectral data analysis and signal processing, with notable contributions published in esteemed international journals and conference proceedings. Beyond academia, he achieved success in extracurricular activities, winning the 3M Video Contest and receiving the prestigious IES-SYPA award at IEEE IECON-2022.

The darling of Vrndavan